REPORT DOCUMENTATION PAGE

Form Approved OMB NO. 0704-0188

1. REPORT DATE (DD-MM-YYYY)	2. REPORT TYPE	3. DATES COVERED (From - To)
20-05-2018	Final Report	1-May-2017 - 28-Feb-2018

4. TITLE AND SUBTITLE	5a. CONTRACT NUMBER
Final Report: Full Duplex Antenna Study	W911NF-17-1-0228
	5b. GRANT NUMBER
	5c. PROGRAM ELEMENT NUMBER 111111
6. AUTHORS	5d. PROJECT NUMBER
	5e. TASK NUMBER
	5f. WORK UNIT NUMBER

7. PERFORMING ORGANIZATION NAMES AND ADDRESSES	8. PERFORMING ORGANIZATION REPORT NUMBER
University of Colorado - Boulder 3100 Marine Street, Room 481 572 UCB Boulder, CO 80303 -1058	
9. SPONSORING/MONITORING AGENCY NAME(S) AND ADDRESS (ES)	10. SPONSOR/MONITOR'S ACRONYM(S) ARO
U.S. Army Research Office P.O. Box 12211 Research Triangle Park, NC 27709-2211	11. SPONSOR/MONITOR'S REPORT NUMBER(S) 69839-EL.1

12. DISTRIBUTION AVAILIBILITY STATEMENT

Approved for public release; distribution is unlimited.

13. SUPPLEMENTARY NOTES

The views, opinions and/or findings contained in this report are those of the author(s) and should not contrued as an official Department of the Army position, policy or decision, unless so designated by other documentation.

14. ABSTRACT

15. SUBJECT TERMS

16. SECURITY CLASSIFICATION OF: a. REPORT	b. ABSTRACT	c. THIS PAGE	17. LIMITATION OF ABSTRACT	15. NUMBER OF PAGES	19a. NAME OF RESPONSIBLE PERSON
UU	UU	UU	UU		Dejan Filipovic
					19b. TELEPHONE NUMBER 303-735-6319

Standard Form 298 (Rev 8/98)
Prescribed by ANSI Std. Z39.18

RPPR Final Report
as of 25-May-2018

Agency Code:

Proposal Number: 69839EL | **Agreement Number: W911NF-17-1-0228**

INVESTIGATOR(S):

Name: Ph.D Dejan Filipovic
Email: dejan.filipovic@colorado.edu
Phone Number: 3037356319
Principal: Y

Organization: **University of Colorado - Boulder**
Address: 3100 Marine Street, Room 481, Boulder, CO 803031058
Country: USA
DUNS Number: 007431505 EIN: 846000555

Report Date: 31-May-2018 Date Received: 20-May-2018
Final Report for Period Beginning 01-May-2017 and Ending 28-Feb-2018
Title: Full Duplex Antenna Study
Begin Performance Period: 01-May-2017 **End Performance Period:** 28-Feb-2018
Report Term: 0-Other

Submitted By: Ph.D Dejan Filipovic Email: dejan.filipovic@colorado.edu
Phone: (303) 735-6319

Distribution Statement: 1-Approved for public release; distribution is unlimited.

STEM Degrees: 0 **STEM Participants:** 1

Major Goals: One of the most difficult challenges for RF electronics is achieving a co-channel isolation > 100dB for simultaneous transmit and receive (STAR) from a single aperture without any time / frequency / polarization / beam-pointing multiplexing. For narrow bandwidth channels and transmitted powers in hundreds of watts the isolation must be > 130dB. To achieve gold-STAR capability, the new front-end topologies that combine multiple layers of analog isolation and digital back-end processing are needed. A carefully designed passive antenna sub-system may provide 20-80dB of gold-STAR isolation thus significantly aiding the actual implementation of full duplex RF systems, and then reducing cost.

The objective of this project was to conduct detailed study of antenna configurations that may yield high gold-STAR self-interference cancellation for a general set of applications of interest for the US Army. To allow some degree of realism and practical relevance for the conducted research, we considered applications such as:

1) high-gain point-to-point microwave links,
2) UAS communications, and
3) handheld radios.

The study identified the fundamental and practical challenges, paths for mitigation thereof, tradeoffs, and most importantly antenna configurations that maximize self-interference cancellation with little to no degradation in their performance.

Accomplishments: In this research, different design approaches for achieving monostatic STAR antenna functionality on platforms of interest for US Army are investigated. Theoretical and computational studies are conducted to bridge the gap between the proposed technical approaches and the fundamental antenna theory. Based on the herein developed systematic antenna/array design approach, several antenna and array prototypes are built and theoretical findings are fully validated with experiments. This research project has clearly demonstrated that the fundamental research on STAR antenna systems is now ready to move into the next step, specifically, practical demonstration of a fully-integrated full-duplex system. The main accomplishments of this work can be summarized as follows:
• Monostatic STAR antenna system with a highly directive reflector antennas of interest for microwave links is demonstrated for the first time. Some specific technical contributions include:
- A coaxial cavity antenna is designed to have an octave bandwidth with VSWR < 2, which is higher than the bandwidth reported in the open literature.
- The influence of geometry, configuration, and roughness of the reflector on the system’s gold STAR isolation are

demonstrated.
- New quasi-monostatic configuration for reflector based STAR is proposed in which system isolation is less sensitive to the imbalances and asymmetries and much wider instantaneous bandwidth is achievable.
- Average measured system isolation of 61 dB is achieved with quasi-monostatic STAR configuration, using COTS BFN components.

• Gold STAR antenna system for handheld device platform is proposed. Some selected technical contributions include:
- Prototype of handheld radio antenna system is fabricated and tested. Isolation of more than 30 dB is measured.
- Omnidirectional patterns with highly correlated beams are measured for M0 and M1.
- Extensive sensitivity study that takes into account impact of the soldier's head and the helmet is performed.
- Simple feedback cancelation layer is seen to achieve even high isolation over a narrow channel bandwidth.

• Gold STAR antenna systems on a UAV are studied, which includes:
- Balanced circulator BFN with dual-polarized patch antenna.
- SRA of four dual-polarized patch elements with two Butler matrix BFNs.

Training Opportunities: Nothing to Report

Results Dissemination: The list of journal papers:
• Prathap Valale Prasannakumar, Mohamed A. Elmansouri, and D. S. Filipovic, “Broadband reflector antenna with high isolation feed for full duplex applications,” IEEE Trans. Ant. Propag., Online ISSN: 1558-2221, Digital Object Identifier: 10.1109/TAP.2018.2814224.

The list of conference proceedings:
• Prathap V Prasannakumar, M. A. Elmansouri, and D. S. Filipovic, "High-directivity broadband simultaneous transmit and receive (STAR) antenna systems," IEEE Int. Symp. Ant. Propag, (APSURSI), 2018, Accepted, and qualified for the Best Student Paper Award among 171 submitted papers.
• Prathap V Prasannakumar, A. H. Abdelrahman, M. Elmansouri, and D. Filipovic, "Simultaneous transmit and receive systems for advanced wireless services," GOMACTech Conf., Mar. 2018.
• Prathap V Prasannakumar, M. A. Elmansouri, and D. S. Filipovic, "Broadband reflector antenna for simultaneous transmit and receive (STAR) applications," 2017 XXXIIe URSI General Assembly and Sci. Symp. (URSI GASS), 2017. (Honorable Mention)
• A. H. Abdelrahman and D. S. Filipovic, "Full duplex antenna subsystem for handheld radios," IEEE Int. Symp. Ant. Propag. (APSURSI), 2017.
• Prathap V Prasannakumar, M. A. Elmansouri and D. S. Filipovic, "Broadband monostatic simultaneous transmit and receive reflector antenna system," IEEE Int. Symp. Ant. Propag. (APSURSI), 2017.

Patents:
• Application No 62/650,159 High-directivity Broadband Simultaneous Transmit and Receive (STAR) Antenna System, by D. Filipovic, P. Vallaleprasannakumar, and M. Elmansouri, was filed on March 29th 2018 with USPO.

Honors and Awards: Student Prathap Valaleprasannakumar was recepient of the Honorable Mention on the 2017 General URSI Assembly in Montreal CA for his paper funded by this project.

Student Prathap Valaleprasannakumar is finalist of the 2018 student paper competition (171 papers) at the 2018 IEEE APS/URSI symposium.

Protocol Activity Status:

Technology Transfer: Application No 62/650,159 High-directivity Broadband Simultaneous Transmit and Receive (STAR) Antenna System, by D. Filipovic, P. Vallaleprasannakumar, and M. Elmansouri, was filed on March 29th 2018 with USPO.

PARTICIPANTS:

Participant Type: PD/PI
Participant: Dejan Sokol Filipovic

Person Months Worked: 1.00 **Funding Support:**
Project Contribution:
International Collaboration:
International Travel:
National Academy Member: N
Other Collaborators:

Participant Type: Postdoctoral (scholar, fellow or other postdoctoral position)
Participant: Ahmed Abdelrahman
Person Months Worked: 7.00 **Funding Support:**
Project Contribution:
International Collaboration:
International Travel:
National Academy Member: N
Other Collaborators:

Participant Type: Postdoctoral (scholar, fellow or other postdoctoral position)
Participant: Jaegeun Ha
Person Months Worked: 3.00 **Funding Support:**
Project Contribution:
International Collaboration:
International Travel:
National Academy Member: N
Other Collaborators:

Participant Type: Graduate Student (research assistant)
Participant: Prathap Valaleprasannakumar
Person Months Worked: 9.00 **Funding Support:**
Project Contribution:
International Collaboration:
International Travel:
National Academy Member: N
Other Collaborators:

ARO W911NF-17-1-0228:

Full Duplex Antenna Study

Final Report

Program Officers: Dr. J.F. Harvey, james.f.harvey.civ@mail.mil
Dr. B. Saddler, brain.m.sadler6.civ@mail.mil

Principal Investigator: Prof. D. Filipovic, UC Boulder
Investigators/Researchers: A. Abdelrahman, UC Boulder
J. Ha, UC Boulder
P. Valale Prasannakumar, UC Boulder

Grant No.: W911NF-17-1-0028

Table of Contents

Chapter 1: Introduction

1.1. Motivation

Advancement in communication technologies and increasing adaptability of wireless devices in commercial wireless and electronic warfare (EW) systems have enabled a greater use of electromagnetic spectrum and thus with the ever-increasing needs of consumers its congestion. The rising demand for spectrum has also resulted in the reallocation of certain tactical bands for consumers, such as Advanced Wireless Services-3 (AWS-3) bands [1]. The AWS-3 cover frequency bands 1.69-1.71 GHz, 1.75-1.78 GHz, and 2.15-2.18GHz [2]. Further, reallocation of the spectrum has also affected the available bandwidth for tactical radio systems. As a consequence, efficient utilization of frequency spectrum is increasingly desired. While conventional radios use either time or frequency duplexing for simultaneous transmit and receive (STAR), STAR wireless system without frequency or time duplexing enables theoretically doubled system throughput and thus the efficient use of spectrum [3]. EW systems with full duplex capability can continuously, without any interruptions, perform an electronic attack and electronic support missions using the same antenna system. To allow full STAR functionality, self-interference between TX and RX channels must be suppressed below the receiver sensitivity, which is extremely challenging. Generally, the required TX-to-RX isolation for STAR system is on the order of >110dB [4]-[6]. The higher the TX power and the lower the RX sensitivity, the higher isolation is required. Such a high level of isolation cannot be achieved in a single domain, rather, multiple cancelations at multiple domains (antenna (propagation), analog, and digital domains) are performed to achieve the desired self-interference cancellation [7]. In this program, the research effort is focused on achieving high isolation in the antenna domain, so that the additional isolation required from analog and digital domains can be reduced and the risk of overloading the receiver's analog and digital subsystems is minimized.

1.2. Background

Different antenna-based cancelation techniques for improving the TX-to-RX isolation have been considered in the open literature. Bistatic antenna configuration relies on the separation between TX and RX antennas. In addition to increasing separation, recessing in an absorber, use of high impedance surface, and use of polarization or beam-squint diversity are often considered to further reduce the coupling [8]-[10]. The main drawback of bistatic configuration is the large separation (often multiple wavelengths) required to achieve high isolation level, which is impractical for many applications. Moreover, it is generally believed that the benefit of STAR over multiple input multiple output (MIMO) systems is lost with bistatic configuration. The use of polarization diversity, while acceptable for many commercial applications, is not acceptable for many military applications, such as electronic attack (EA) and electronic support (ES). When a bi-static configuration is permissible, placing the null in the TX antenna radiation pattern along the direction of the RX antenna has also been considered with realizable isolation >35dB. However, the operation bandwidth is usually narrow [11]. A similar approach based on canceling the near-fields of the TX antennas at the location of the RX antenna has also been proposed where high isolation over the utilized antennas operating bandwidth has been demonstrated [12]-[13]. The main issues include the complexity of the beamforming network (BFN), which increases as the number of TX elements increases, the sensitivity to the feeding network errors, size, and the dissimilarity between the TX and RX radiation patterns which is undesired for some applications.

Over the past years, the ARG researchers have developed or initiated the development of about a dozen different STAR antenna configurations [14] for diverse narrow and wide instantaneous bandwidth applications. Several examples of the proposed and developed topologies and concepts are shown in Fig. 1. Monostatic and bi-static antenna STAR topologies, as well as combinations thereof, have been considered in stand-alone or integrated on a specific platform (such as Coyote UAV as shown in the figure below). Isolation bandwidths of several octaves were achieved with some configurations. Some studies related to the impact of obstacles and asymmetries have also been conducted. These research efforts, funded by the Office of Naval Research, Naval Research Laboratory, and Lockheed Martin has resulted in multiple publications [15-24] and was the starting point for the full-duplex antenna study proposed to be executed here.

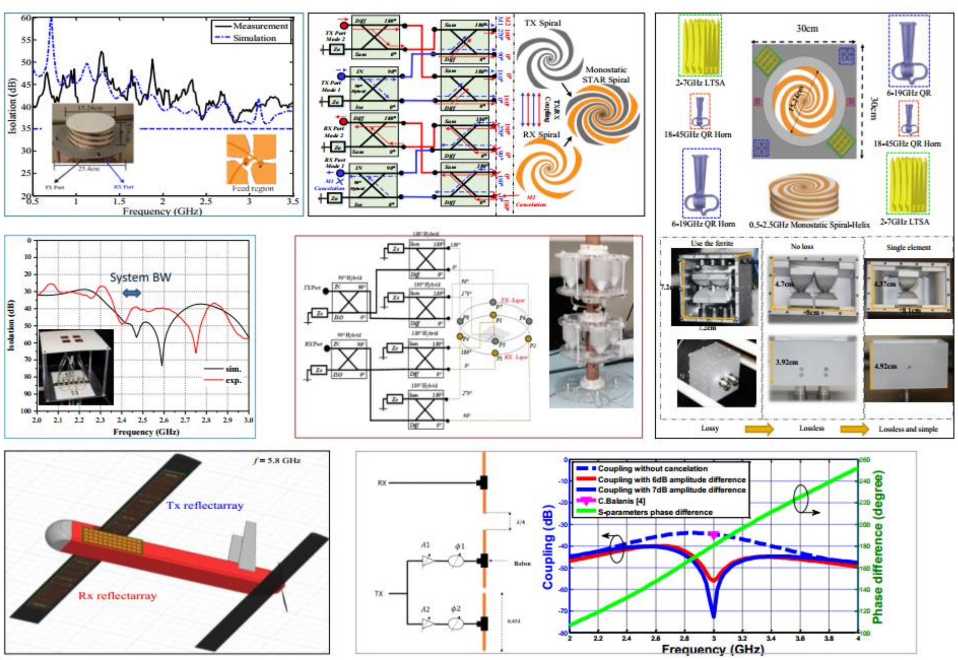

Fig. 1.1: Illustration of several STAR antenna systems developed by the ARG over the past years.

1.3. Objectives

One of the most difficult challenges for RF electronics is achieving a co-channel isolation >100dB for STAR from a single aperture without any time, frequency, polarization, or beam-multiplexing (gold-STAR). For narrow bandwidth channels and transmitted powers in hundreds of watts, the isolation must be > 140 dB. To achieve gold-STAR capability, the new front-end topologies that combine multiple layers of analog isolation and digital back-end processing are needed. A carefully designed passive antenna sub-system can provide 20–80dB of gold-STAR isolation, thus significantly aiding the actual implementation of full duplex RF systems.

The objective of this program is to conduct a detailed study of antenna configurations that may yield high gold-STAR self-interference cancellation for a general set of applications of interest for the US Army. To allow some degree of practical relevance for the conducted research, we considered applications such as high-gain point-to-point microwave links, handheld radios, and UAS communications. This report presents the fundamental and practical challenges, paths for mitigation thereof, tradeoffs, and most importantly, antenna configurations that maximize self-interference cancellation with little to no degradation in their performance.

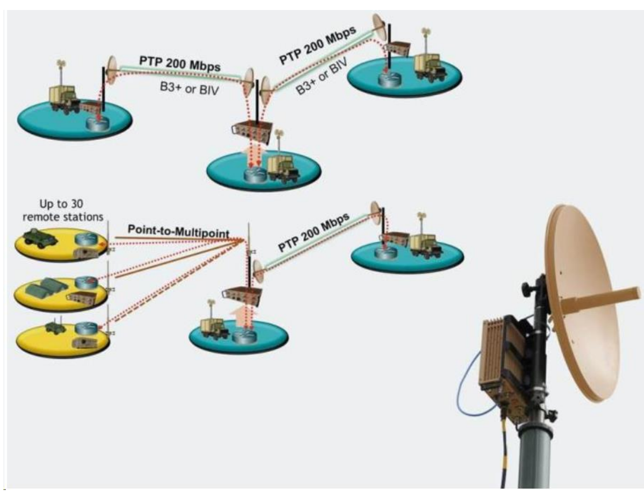

Fig. 1.2: Illustration of the considered application and photo of the antenna in use [25].

1.3.1. Objective 1: Line-of-Sight Microwave Dish Antenna System

The first objective is to research electrically and mechanically robust passive gold-STAR antenna approaches and candidates for applications such as the line-of-sight (LOS) microwave relays illustrated in Fig. 1.2 [25]. This and similar applications rely on quickly deployable high gain reflector antennas and radios, which employs either time or frequency division duplex (TDD/FDD) for simultaneous transmission and reception, thus, not efficiently utilizing the available or assigned electromagnetic spectrum. For easier prototyping and experimental verifications, the antenna system developed herein works over 4–8 GHz band. However, the system can be scaled to operate over other frequency bands. Based on a currently existing systems [26], the goal is to achieve realized gain > 20dBi, front-to-back ratio (FBR) > 25dB, VSWR < 2, and continuous wave (CW) power handling > 150W. Furthermore, the main objective is to maximize the isolation between TX and RX, while preserving same polarization and similar radiation patterns between TX and RX. Specifically, the TX to RX isolation should be at minimum 15dB above that can be obtained by the state-of-the-art commercial-off-the-shelf (COTS) circulators operating in the considered frequency band.

1.3.2. Objective 2: Handheld Radio Antenna System

Tactical handheld radios shall operate over multiple bands and enable simultaneous transmission and reception of voice, data, video, etc. over narrowband and wideband channels nested within the much wider instantaneous bandwidths across VHF through S-band spectrum (and perhaps beyond). For example, THALES AN/PRC C-148B MBITR2 handheld radio, shown in Fig. 1.3, has wideband channels operating over 225-400 MHz, 1250-1390 MHz, and 1750-1850 MHz bands [27]. This radio is chosen as a demonstration platform for our study since single or multiple antenna systems will be needed to enable full-duplex communications.

Fig. 1.3: Illustration of the handheld radio.

The main objective is to research antenna technologies that may have a greater chance to be successfully implemented on handheld radio platforms and facilitate easier practical realization of a true gold-STAR system. The frequency range of interest coincides with the 1750–1850 MHz band. Impact of nearby scatterers including soldiers and ground plane is also investigated. Non-circulator based antenna front-end configurations are considered.

1.3.3. Objective 3: STAR Antenna System for UAS-Raven

Full duplex capability for UASs is of great interest for many reasons including:

- A number of army missions relying on UASs will keep increasing, CONOPS will diversify and perhaps even change while the platform is in the theater.
- They will need to function in highly contested electromagnetic spectrum (EMS) environments.
- When operating in swarms, they will need to share scarce bandwidth resources.

Moreover, size-weight-and-power efficient (SWAP) and low-cost solutions must be sought for. Shown in Fig. 1.4 is an example of a specific UAS platform that is utilized for our study. This platform is chosen for its small physical size which will ensure that the STAR antenna research maintains its focus on highly challenging configurations associated with electrically tight spaces and volumes. The goal is to investigate monostatic antenna configurations operating in 1750–1850MHz band keeping in mind SWAP constraints. Full duplex capability with minimally invasive STAR antenna candidates is researched.

Fig. 1.4: Launch of UAS RQ-11 Raven [28].

1.4. Report Organization

- Chapter 2 presents the design and implementation of highly directive reflector based STAR antenna. First, the approach involving beam forming network and circulators is used to realize monostatic STAR. Next, a quasi-monostatic approach is proposed, which is circulator-less, and less sensitive to imbalances and asymmetries. Further, the design, fabrication, and measurement results of the coaxial cavity (used as feed), the axis-symmetric reflector antenna, and measured isolation of both the STAR configurations are presented.

- Chapter 3 demonstrates the mode multiplexed STAR antenna system for a handheld radio platform. A circular array of four dipoles is the basis for the antenna system, and the mode multiplexing is achieved by BFN. While isolation is theoretically infinite, >30dB isolation is measured over 1750–1850 MHz with the fabricated prototype. Sensitivity analysis is performed on the imbalances of BFN and nearby object, such as soldier's hand and head. Other, possible applications of the proposed system are also discussed.
- Chapter 4 investigates three approaches to implement STAR antenna system on a UAS-Raven platform. First, a balanced circulator BFN with a single dual-pol patch element on Raven's belly is shown to achieve > 20 dB isolation over 1750–1850 MHz. Further, a sequential rotation array (SRA) of four dual-polarized patch elements on Raven's tail fed by two Butler matrix BFNs with expected system isolation > 38 dB over 1750–1850 MHz is considered. It is also demonstrated that the body of Raven can be used as the radiating element based on characteristic mode analysis (CMA). Exciting two orthogonal modes on Raven's body can be used to realize a STAR antenna system, however, no STAR antenna systems are designed.
- Chapter 5 summarizes the contributions of the report.

References

[1] B. Sadler, *Private Communications*, June 2016.

[2] National Telecommunications and Information Administration, Available: https://www.ntia.doc.gov/category/aws-3-transition.

[3] A. Goldsmith, *Wireless Communication*, Cambridge, U.K., 2005.

[4] M. Jain. J. I. Choi, T. M. Kim, D. Bharadia, S. Seth, K. Srinivasan, P. Levis, S. Katti, and P. Sinha, "Practical, real-time, full duplex wireless," *Proc. 17th Int .Conf. Mobile Comp. Netw. (MobiCom'11), 2011.*

[5] D. Bharadia, E. McMilin, and S. Katti, "Full duplex radios," *Proc. ACM SIGCOMM*, 2013.

[6] A. Sabharwal, P. Schniter, D. Guo, D. W. Bliss, S. Rangarajan, and R. Wichman, "In-band full-duplex wireless: challenges and opportunities," *IEEE J. Selected Areas Comm*., Sep. 2014.

[7] H. Krishnaswamy *et al*., "Full-duplex in a hand-held device — from fundamental physics to complex integrated circuits, systems and networks: An overview of the Columbia FlexICoN project," *2016 50th Asilomar Conf. on Signals, Systems and Computers*, 2016.

[8] E. Everett, A. Sahai, and A. Sabharwal, "Passive self-interference suppression for full-duplex infrastructure nodes," *IEEE Trans. Wireless Comm*., Feb. 2014.

[9] P. Valale Prasannakumar, M. A. Elmansouri and D. S. Filipovic, "Wideband dual-polarized bi-static simultaneous transmit and receive antenna system," *2016 IEEE Int. Symp. Ant. Propag. (APSURSI)*, July 2016.

[10] E. Foroozanfard, O. Franek, A. Tatomirescu, E. Tsakalaki, E. de Carvalho, and G. F. Pedesen, "Full-duplex MIMO system based on antenna cencellation technique," *Electronics Letters*, 2014.

[11] J. Choi, M. Jain, K. Srinivasan, P. Levis, and S. Katti, "Achieving single channel, full duplex wireless communications," *Proc. 16th ann. Int. Conf. Mobile Comp. Netw. (MobiCom'10)*, Jul. 2010.

[12] K. E. Kolodziej, P. T. Hurst, A. J. Fenn and L. I. Parad, "Ring array antenna with optimized beamformer for Simultaneous Transmit and Receive," *Proc. of the 2012 IEEE Int. Symp. on Ant. Propag.*, 2012.

[13] W. F. Moulder, B. T. Perry and J. S. Herd, "Wideband antenna array for simultaneous transmit and receive (STAR) applications," *2014 IEEE Ant. Propag. Soc. Int. Symp.*, 2014.

[14] D. S. Filipovic, *STAR Antennas at ARG*, Presentation sent to Dr. B. Sadler, ARL.

[15] E. A. Etellisi, M. A. Elmansouri and D. S. Filipovic, "Wideband multimode monostatic spiral antenna STAR subsytem," *IEEE Trans. Ant. Propag.*, Apr. 2017.

[16] M. A. Elmansouri, A. J. Kee and D. S. Filipovic, "Wideband Antenna Array for Simultaneous Transmit and Receive (STAR) Applications," *IEEE Ant. Wireless Propag. Lett.*, 2017.

[17] M. Elmansouri, E. Etellisi, and D. S. Filipovic, “Ultra-wideband circularly-polarized simultaneous transmit and receive (STAR) antenna system,” *IEEE Ant. Propag. Soc. In. Symp.*, July 2015.

[18] E. Tianang and D. S. Filipovic, “A dipole antenna system for simultaneous transmit and receive,” *IEEE IEEE Ant. Propag. Soc. In. Symp.*, July 2015.

[19] E. Etellisi, M. A. Elmansouri, and D. S. Filipovic, “Wideband simultaneous transmit and receive (STAR) bi-layer circular array,” *IEEE Ant. Propag. Soc. In. Symp.,* July 2015.

[20] M. Elmansouri, P. VPKumar, E. Tianang, E. Etellisi, and D.S. Filipovic, “0.5-45GHz simultaneous transmit and receive (STAR) antenna system for electronic attack,” *Proc. 2016 GOMACTech Conf.*, Mar. 2016.

[21] D. S. Filipovic, M. A. Elmansouri, and E. Etellisi, “On wideband simultaneous transmit and receive (STAR) with a single aperture,” *IEEE Ant. Propag. Soc. In. Symp.*, July 2016.

[22] E. Etellisi, M. A. Elmansouri, and D. S. Filipovic, “Wideband dual-mode monostatic simultaneous transmit and receive antenna system,” *IEEE Ant. Propag. Soc. In. Symp.*, July 2016.

[23] M. A. Elmansouri, and D. S. Filipovic, “Realization of ultra-wideband simultaneous transmit and receive antenna system,” *IEEE Ant. Propag. Soc. In. Symp.*, July 2016.

[24] P. VPKumar, M. A. Elmansouri, and D. S. Filipovic, “Wideband dual-polarized bi-static simultaneous transmit and receive antenna system,” *IEEE Antennas Propag. Soc. In. Symp.*, July 2016.

[25] https://www.thalesgroup.com/en/worldwide/defence/what-we-do-radio-communications-land/tn4100

[26] http://www.antennaexperts.in/product-detail.asp?id=34

[27] http://www.thalescomminc.com/userimages/Documents/Data%20Sheets/Thales_PRC148B_MBITR2.pdf

[28] http://www.army-technology.com/projects/rq11-raven/

Chapter 2: Line-of-Sight STAR System

2.1. Introduction

Point-to-point links rely on high gain antennas for long range and directional communication, often the desired high gain is achieved with reflector antennas. Therefore, a STAR capable reflector antenna can alleviate the challenges imposed by spectrum reallocation in AWS-3 for tactical radio relay. The reallocated spectrum is centered around 1.6 GHz, which covers 3 narrowband channels as mentioned in the introduction (Chapter 1). In this program, an antenna system corresponding to a scaled NATO-III+ (1.35-2.7 GHz) band is fabricated, in order to reduce the size and facilitate the measurement with available resources. Design and analysis of the scaled prototype, which covers the full C-band from 4 GHz to 8 GHz is the focus of this chapter.

The chapter is organized as follows: Architecture and schematic of the monostatic-STAR are explained in Section 2.2. Section 2.3 discusses the operation, design, and performance of the coaxial cavity feed. Section 2.4 describes the design of reflector antenna, influence of struts on the radiation patterns, fabrication, and performance of the antenna. The implementation of proposed STAR configuration, ideal and measured system isolation and impact of imbalances and asymmetries on the system isolation are discussed in Section 2.5. A quasi-monostatic STAR configuration, coupling mechanism, simulated and measured system isolation are discussed in Section 2.6. Conclusions are outlined in Section 2.7.

2.2. STAR Configuration

In this approach, the BFN is arranged to cancel the coupled/leaked signal from the antenna and circulators, by creating 180° phase difference between the TX and RX reflected signals. The realized arrangement results in a theoretically infinite isolation between the TX and the RX [1]-[4]. The schematic and operation of the proposed configuration are further explained in the following paragraphs.

First, the input signals (or the TX signals) are connected to the port 1 of the TX 90° hybrid, HYBD I. Then, the TX signals are split into two signals of equal magnitude and quadrature phase, $\frac{j}{\sqrt{2}}e^{j\varphi}$ and $\frac{1}{\sqrt{2}}e^{j\varphi}$. Further, these signals are routed through Paths I and II, as illustrated in Fig. 2.1. The signals fed to the input of circulators I and II undergo attenuation due to the finite insertion loss (IL) of the circulators. The outputs of circulators are connected to the inputs of 180° hybrids. The 180° hybrids are used to generate two signals with equal magnitude and 180° out of phase, which are required to excite

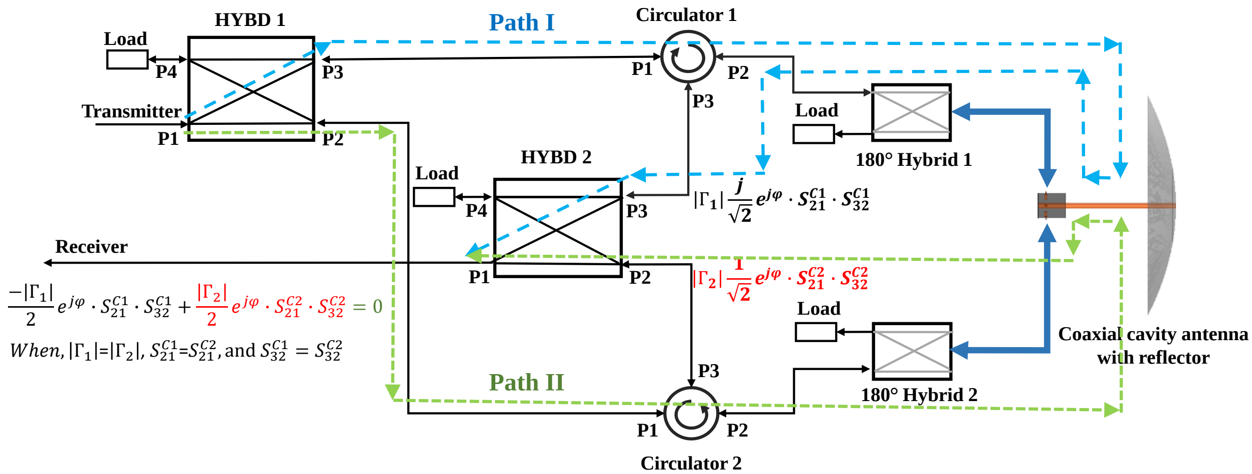

Fig. 2.1: Signal flow diagram of the proposed monostatic STAR system, consisting of circularly polarized reflector antenna, 90° and 180° hybrids, and circulators.

TE_{11} mode in coaxial cavity antenna. Later, the output signals of these 180° hybrids are used to excite the four probes of the coaxial cavity antenna (feed of the reflector). The impedance mismatch of the antenna results in reflected signals (2.1) and (2.2), which travel back to the respective circulators through 180° hybrids, where, S_{21}^{C1} and S_{21}^{C2} are the S_{21} of circulators 1 and 2, respectively.

These signals are further attenuated, due to IL from port 2 to port 3 of circulators, before reaching RX 90° hybrid, HYBD 2. At the HYBD 2, the signals from Path I undergo another 90° phase shift resulting in (2.3), whereas the signals from Path II go through the hybrid without any phase shift (2.4); similarly, the signals from circulators leakage. Thereby, these two signals are combined 180° out of phase at the RX port resulting in theoretically infinite isolation when $|\Gamma_1| = |\Gamma_2|$, $S_{21}^{C1} = S_{21}^{C2}$, $S_{32}^{C1} = S_{32}^{C2}$, and the leakage from circulators 1 and 2 are the same (2.5). However, any asymmetry in the BFN and the antenna geometry will create imbalances in amplitude and phase which results in finite isolation of the system. The signals combined in-phase at the port 4 of HYBD 2 are terminated in a matched load.

The effect of imbalances, asymmetries and practical implementation of the proposed approach is explained in detail in Section 2.5

$$|\Gamma_1|\frac{j}{\sqrt{2}}e^{j\varphi}\cdot S_{21}^{C1} \tag{2.1}$$

$$|\Gamma_2|\frac{1}{\sqrt{2}}e^{j\varphi}\cdot S_{21}^{C2} \tag{2.2}$$

$$|\Gamma_1|\frac{-1}{2}e^{j\varphi}\cdot S_{21}^{C1}\cdot S_{32}^{C1} \tag{2.3}$$

$$|\Gamma_2|\frac{1}{2}e^{j\varphi}\cdot S_{21}^{C2}\cdot S_{32}^{C2} \tag{2.4}$$

$$|\Gamma_1|\frac{-1}{2}e^{j\varphi}\cdot S_{21}^{C1}\cdot S_{32}^{C1}+|\Gamma_2|\frac{1}{2}e^{j\varphi}\cdot S_{21}^{C2}\cdot S_{32}^{C2}=0 \tag{2.5}$$

2.3. Feed Design

The wide use of reflector antennas for long range, satellite communications and radars has resulted in extensive research on the feeds. Various types of antennas are used as feeds for the reflector. Feeds include wide and narrowband horn antennas, circularly polarized antennas such as a helix, cavity-backed sinuous antenna, cross-dipole, and etc. [5]-[8]. Horn antennas can handle high power and can be used to achieve circular polarization (CP) [9]. However, the variation of phase center with frequency can be significant, and the patterns in E and H plane are asymmetric [10]. These two limitations can impact the reflector performance by reducing the directivity and increasing the side lobe level (SLL) [11]. Dual-pol wideband CP antennas such as cavity backed sinuous can have symmetrical radiation patterns. However, the radiation loss of the antenna and power handling can be of concern in high power applications. Coaxial cavity antennas or nested coaxial antennas are the other categories of the antennas that are used as feeds for the reflector antennas, because of their stable phase center, symmetric E and H-plane patterns and low axial ratio [10]. However, the VSWR of the antennas discussed in the literature is often high [12], [13], which is not desired for high power applications, such as the one proposed in this project. Therefore, by performing a parametric study and simple geometrical modifications, the impedance match of the antenna is improved to VSWR < 2 over an octave bandwidth. The design details of the feed are explained in the following sections.

2.3.1. Principle of Operation

The operation principle of the coaxial cavity antenna is analogous to that of an open-ended circular waveguide. The fundamental mode of a circular waveguide is TE_{11}, whereas that of a coaxial waveguide is TEM. The radiation from TEM mode results in null at the boresight, as shown in Fig. 2.2(a), which is not desired for a reflector feed. Hence, the antenna is operated in its first higher order mode, TE_{11}. Radiation from TE_{11} mode results in maximum directivity at the boresight, as shown in the Fig. 2.2(b). The corresponding E-field distribution of TE_{11} at the aperture is shown in Fig. 2.3(a). In the proposed antenna, the TE_{11} mode is realized by exciting two opposite probes with 180° phase shift, as shown in Fig. 2.3(b). Dual polarization, vertical and horizontal can be achieved by using four probes with the excitation illustrated in Fig. 2.4(a). Further, these ports can be excited with ±90° phase progressions to achieve the desired CP operation (RHCP or LHCP), as shown in Fig. 2.4(b).

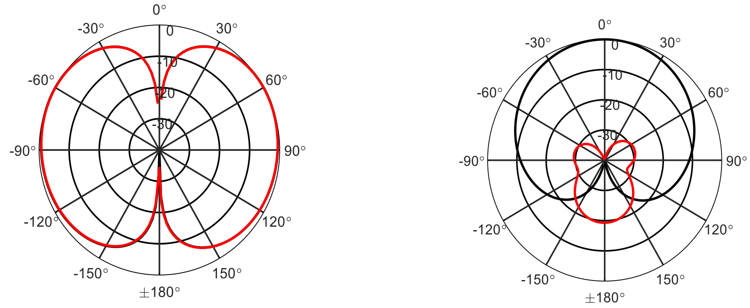

(a) (b)

Fig. 2.2: Simulated Co (black) and cross-pol (red) of coaxial cavity for: (a) TEM mode (b) TE_{11} mode, at 6 GHz.

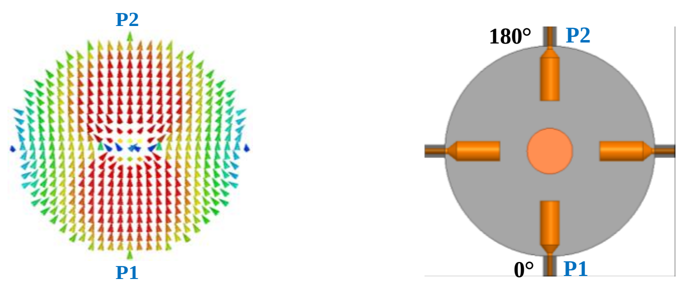

(a) (b)

Fig. 2.3: (a) **E**-field at the aperture for TE_{11} mode (b) excitation for TE_{11} mode.

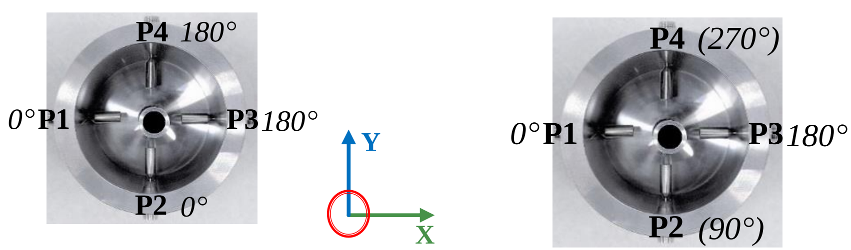

(a) (b)

Fig. 2.4: Probe excitation for: (a) vertical and horizontal polarization (b) circular polarization.

2.3.2. Impedance Match

The impedance seen at the input ports of the antenna, P1, P2, P3, and P4 is primarily dependent on inner to outer conductor diameter ratio, the coupling between the probes, and reactance of the probes. Therefore, first, a parametric study on the ratio of the inner conductor, *b*, to outer conductor diameter, *a*, of an open-ended coaxial waveguide is carried out to achieve reflection coefficient, $|S_{11}| < -10$ dB. The analysis is carried out in FEM (Ansys HFSS) simulation where the open-ended coaxial waveguide is excited by a wave port with the TE_{11} mode. The resulting reflection coefficient of the antenna is shown in Fig. 2.5. The higher b/a ratio deteriorates the impedance match at higher frequencies, and the lower b/a ratio at the lower frequencies, as it can be noticed from the Fig. 2.5. It is found that these results are in accordance with the similar study conducted in [14], [15]. Additionally, the E and H patterns symmetry of the antenna is a function of b/a as mentioned in [14] and observed through our simulations. The symmetry is important for achieving uniform illumination of the reflector surface (in ϕ) and low cross-polarization level, which is an important parameter for the proposed design. Hence, as a compromise between impedance match and pattern symmetry of the feed, b/a =0.23 is selected for the designed antenna.

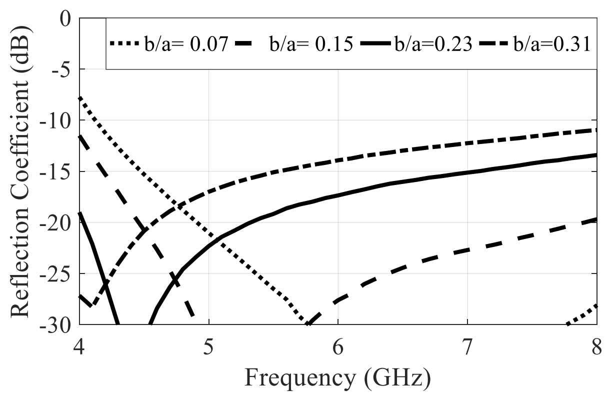

Fig. 2.5: Reflection coefficient of the coaxial cavity antenna for different inner and outer conductor diameter ratios (b/a).

In addition to the cross-section of the aperture/waveguide, the shape and physical dimensions of the exciting probes are critical for impedance match of the antenna. Hence, in step two, the exciting probes are shaped as mono-cones to achieve |S11| < -10 dB for an octave bandwidth. Through parametric analysis, it is found that height of the probes from the bottom of the cavity, h_{probe}, length, l_{probe}, and shape of the probes are critical. Specifically, as shown in Fig. 2.6 a straight probe (probe II) with the diameter of 0.127 cm and length of 1.64 cm has the narrower bandwidth (|S11| < -10 dB) in comparison to the mono-cone shaped probe (probe I). The reduction in the reactance of the input impedance seen by the mono-cone shaped probe is the main reason for this behavior, as illustrated in the Smith charts in Fig. 2.7. Thus, through the above studies, it is found that with proper selection of b/a ratio and probes dimensions, an octave of bandwidth (|S11| < -10 dB) can be achieved from a coaxial cavity antenna. The fabricated antenna has b = 1 cm, a = 4.62 cm and height, h_a = 5.06 cm, shown in Fig. 2.8.

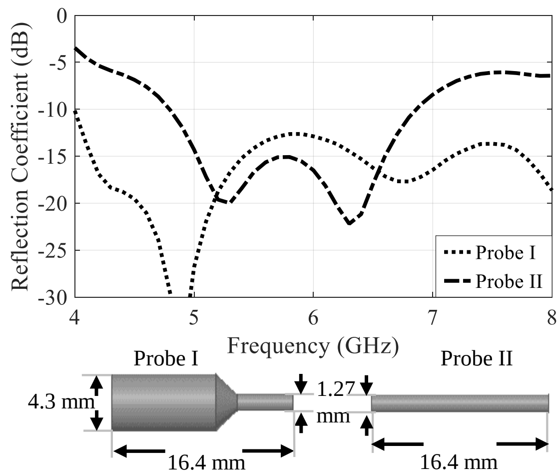

Fig. 2.6: Active reflection coefficient of the coaxial cavity antenna for different probe shapes with dimensions of the considered probes.

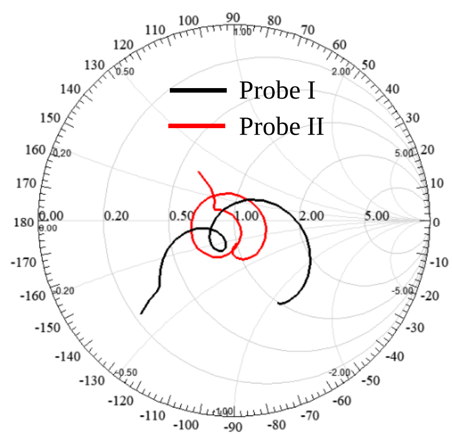

Fig. 2.7: Smith chart showing impedance of coaxial cavity with probe I and probe II.

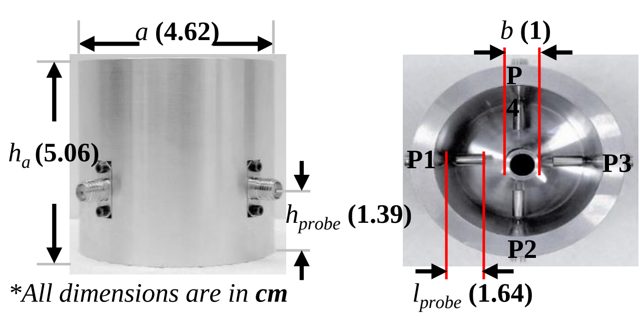

Fig. 2.8: Fabricated coaxial cavity antenna and its dimensions.

The fabricated antenna has measured |S11| < -10 dB over an octave bandwidth as shown in Fig. 2.9. The impedance match of the fabricated and simulated antenna at the antenna ports, and at the inputs of 180° and 90° hybrids are shown in Fig. 2.9(a), (b) and (c), respectively. The 90° hybrids in conjunction with 180° hybrids are used to realize CP, as described in Fig. 2.1. Reflection coefficient at the input of 90° hybrids is < -20 dB since all the reflected signals from the antenna and the 180° hybrids are routed to the unused port of the hybrids, which are terminated in a matched load. It should be noted that all the terminated signals account for the system total loss, and hence it is important to minimize their level.

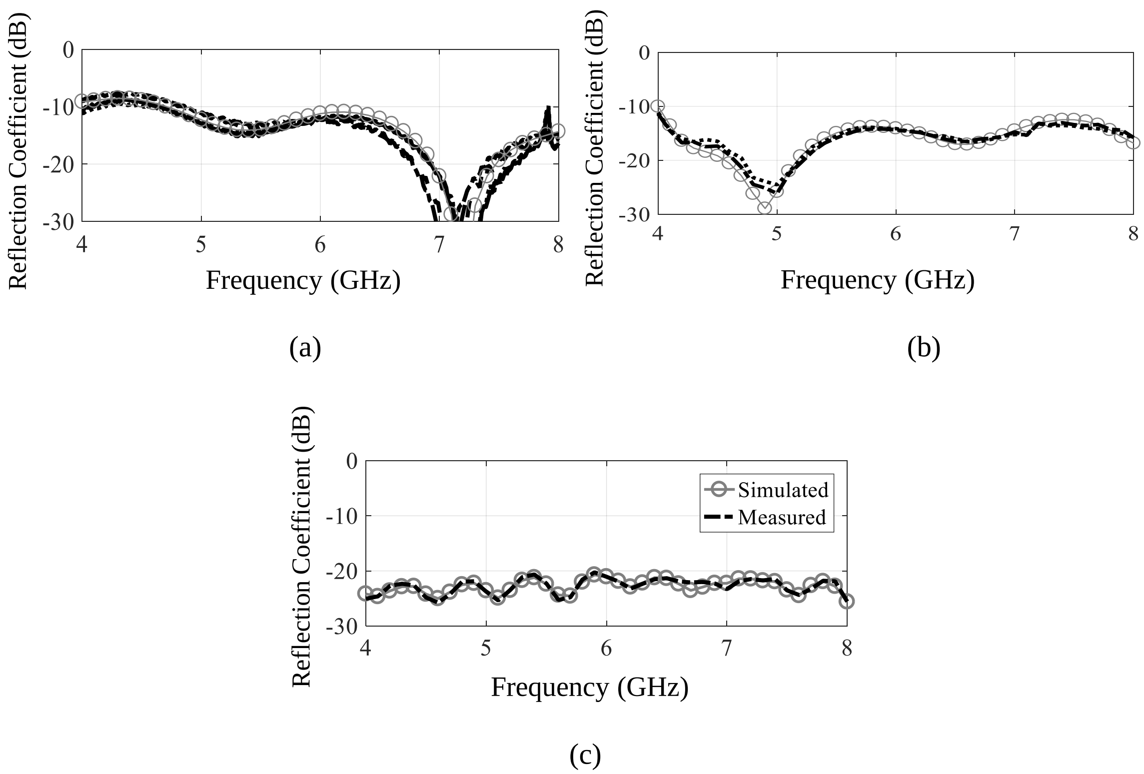

Fig. 2.9: Simulated (grey-circles) and measured (black) active reflection coefficient of the coaxial cavity antenna at inputs of: (a) antenna, (b) 180° hybrids, and (c) 90° hybrids.

2.3.3. Far-field Performance

The proposed coaxial cavity antenna has an excellent far-field performance, which can be observed from the measured and simulated patterns shown in Fig. 2.10. Specifically, the antenna has a gain > 6 dBic, AR < 3 dB for θ = ±30°, over the operating frequencies, as shown in Fig. 2.11. The antenna has aperture efficiency 100 % @ 6 GHz and > 87% (@ 8 GHz) over the band. Good agreement between measurement and simulation can be observed from the presented results herein. The far-field of the antenna is measured in ARG's anechoic chamber.

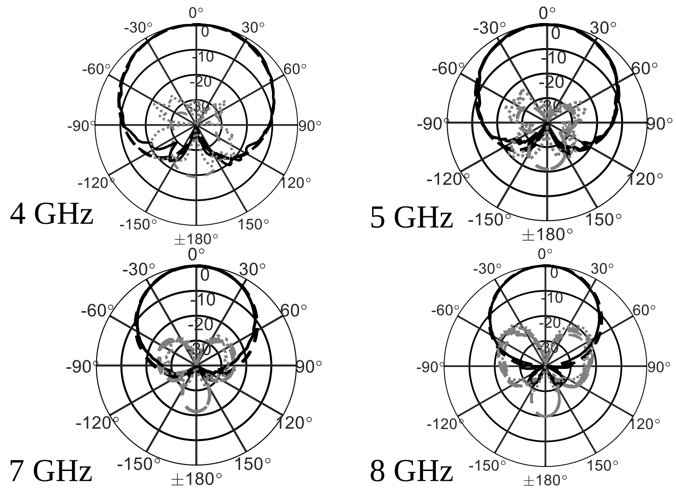

Fig. 2.10: Measured (solid) and simulated (dash) co (LHCP, dark color) and cross-polarized (RHCP, light color) radiation patterns of the proposed coaxial cavity antenna.

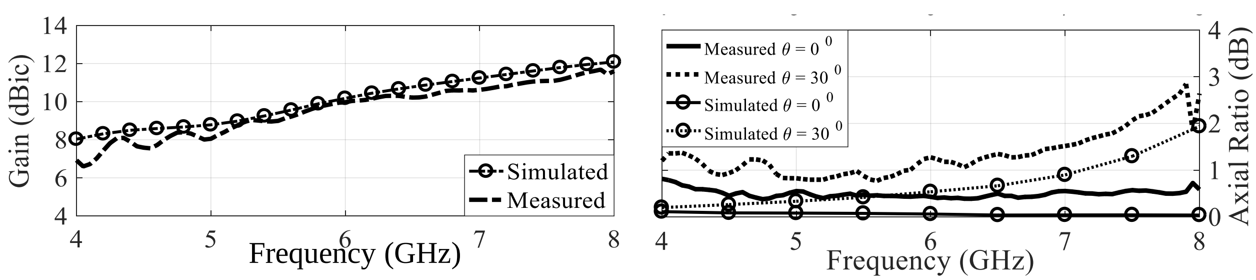

(a) (b)

Fig. 2.11: (a) Meassured and simulated (with circles) broadside gain, and (b) axial ratio at θ = 0 and 30° of the designed coaxial cavity antenna.

Additionally, the designed coaxial cavity antenna has phase center variation < 5% and < 15% for CP and linear polarization operations, respectively for the angular span of 106° in θ (the angle subtended by the designed reflector at the focus), as shown in Fig. 2.12. The reference coordinate system for the calculation of phase center is considered at the aperture of the antenna. The observed relatively stable phase center of the designed antenna makes it an excellent candidate for a reflector feed. The slope method explained in [16] is used in the calculation of the phase center of the antenna.

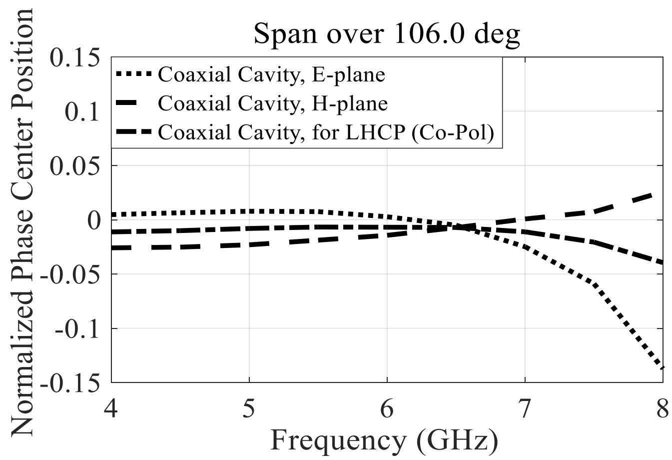

Fig. 2.12: Normalized phase center (w.r.t. wavelength) of the designed coaxial cavity antenna for CP and linear polarization (in E and H planes). Phase center is calculated for the angular span $\theta = \pm 53°$.

2.4. Reflector Antenna Design

A reflector antenna can be realized using various configurations, such as axis-symmetric, offset-feed, and dual-reflector or folded optics configurations [1], [17]. Axis-symmetric reflector is a simple and basic configuration with symmetric radiation patterns and, lower cross-pol level. However, axis-symmetric configuration results in higher aperture blockage and deterioration in the impedance match of the feed due to the reflected fields from the reflector [17], [18]. The later can be noticed from the $|S_{11}|$ response in Fig. 2.13, where the impact of the standing wave between the reflector and the feed is clearly seen.

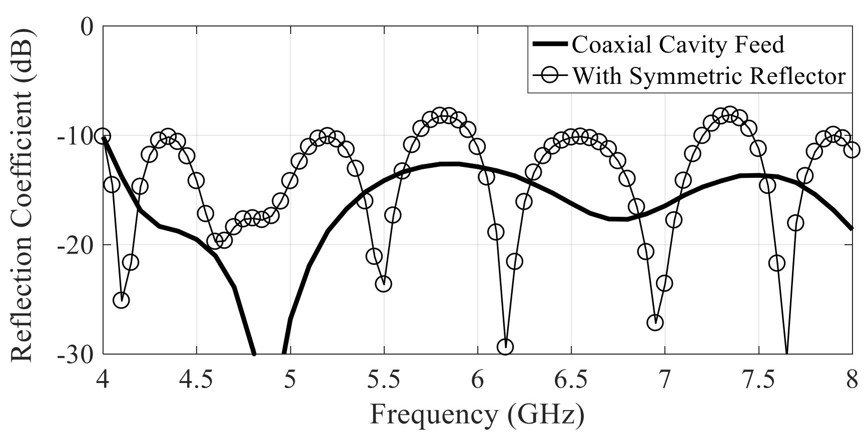

Fig. 2.13: Simulated reflection coefficient of the coaxial cavity feed with and without the axis-symmetric reflector.

Contrarily, an offset-fed reflector can be designed to reduce the feed blockage and to improve the impedance match of the feed [17], [19]. For example, an offset-fed reflector with lower rim offset, H =

4.4 cm has less influence on the impedance match than an axis-symmetric reflector as shown in Fig. 2.14. The value of H is selected such that the topmost point of the feed clears the bottom most point of the reflector, and the corresponding feed orientation angle is calculated using equations in [17], [18]. Additionally, the projected diameter of the offset parabolic reflector is maintained equal to that of the symmetric parabolic reflector. However, the radiation patterns of the offset fed reflector are asymmetric and have higher cross-polarization in comparison to the symmetric reflector as shown in Fig. 2.15. Further, the asymmetry in the antenna geometry and radiation patterns deteriorates the isolation of the proposed system, as shown in Fig. 2.16. Hence, the axis-symmetric configuration is selected for the proposed STAR configuration.

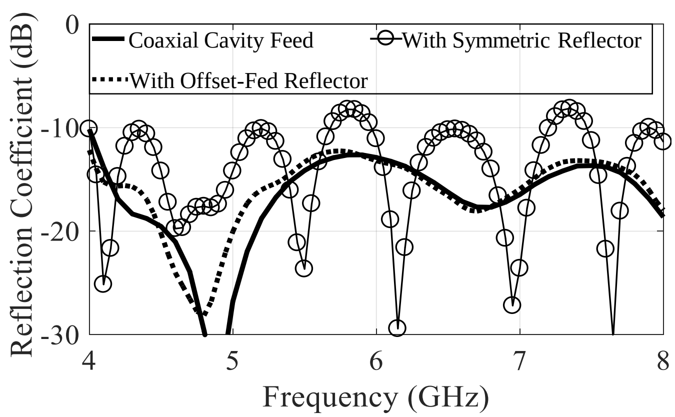

Fig. 2.14: Simulated reflection coefficient of the coaxial cavity feed (standalone) compared to that of symmetric and offset-fed reflector antenna.

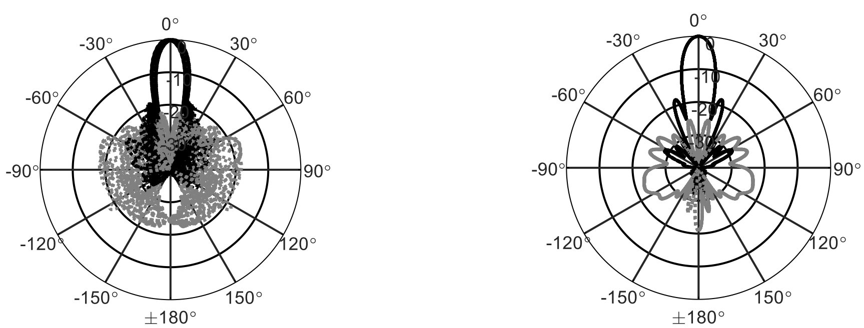

(a) (b)

Fig. 2.15: Co and cross-polarized radiation patterns of (a) offset-fed, and (b) symmetric reflectors @ 4 GHz over several azimuthal cuts from $\phi = 0°$ to 360°.

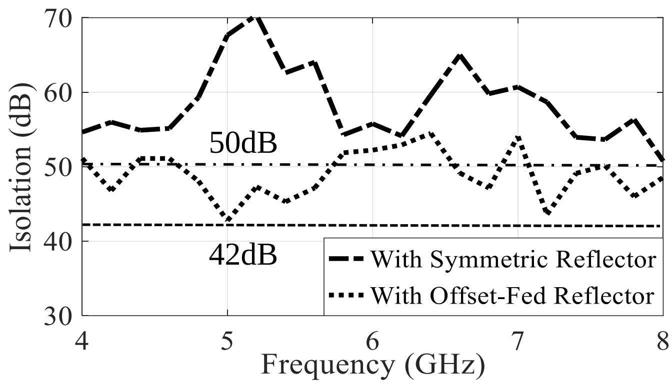

Fig. 2.16: Simulated isolation of the proposed system with symmetric self-supporting and offset-fed reflectors.

2.4.1. Axis-symmetric Reflector

The diameter and the focal length of the reflector are computed through a parametric study conducted in HFSS, to achieve gain > 20 dBi while maintaining low side lobe and cross-polarization level. The designed reflector antenna has the diameter, D = 40 cm, and F/D of 0.495 resulting in the subtended angle of 106° at the feed location or focal point. The CAD model of the system with its dimensions is shown in the Fig. 2.17.

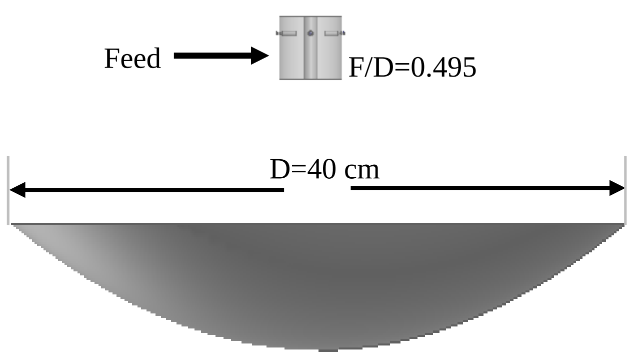

Fig. 2.17: CAD model of the proposed axis-symmetric reflector antenna.

2.4.2. Influence of Reflections

Reflections from the reflector can deteriorate impedance match of the feed, as shown in Fig. 2.13. Therefore, apex matching technique is applied to minimize these effects [20], [21]. In apex matching, a circular disk is placed at the apex of the reflector, and the dimension of the flat metallic plate is selected to create 180° phase difference between the reflected signal from the apex (with plate) and from the rest of the reflector surface at the focal point (or feed) such that they cancel each other. Thus, reducing the effect on the impedance match of the feed. The significance of apex matching can be clearly seen in Fig.

2.18. Further, a Gaussian shaped or cone shaped apex matching can be used to reduce the impact of reflections over wider bandwidth [22]. The flat disk is chosen in the proposed design to minimize the fabrication cost and complexity. Apex matching can have some effect on the far field of the antenna because of the modification in the parabolic surface [21], which is also noticed in the proposed configuration. The designed apex matching reduced the gain by 0.4 dB at 8 GHz. Nonetheless, the antenna has SLL < -16 dB and cross-pol level < -20 dB over the operating frequencies. However, the symmetry in antenna geometry and radiation patterns is maintained.

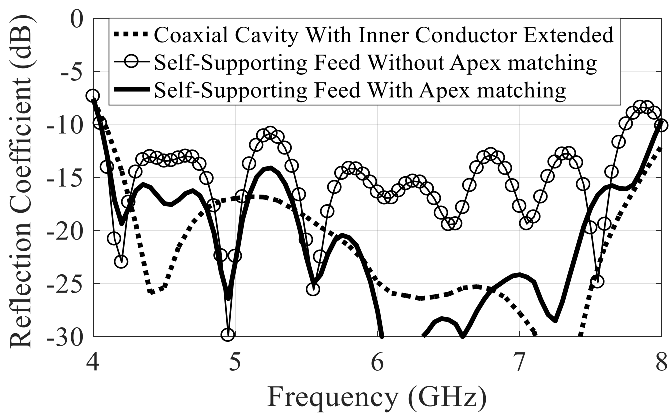

Fig. 2.18: Simulated reflection coefficient of the coaxial cavity antenna with probe extended to support the feed, and reflection coefficient of the self-supporting reflector antenna with and without apex matching.

2.4.3. Design of Struts

The feed of a reflector is supported through struts. Typically, 3 or 4 struts are used in axis-symmetry reflector configuration to hold the feed. These struts increase aperture blockage. Also, the re-radiated currents from the struts contaminate radiation patterns by increasing side lobe levels [23]. Therefore, to avoid the additional supporting struts, the inner conductor of the feed is extended till the apex of the reflector in the proposed antenna. The extended inner conductor improved the impedance match of the feed (standalone) at the mid-band, as shown in Fig. 2.18, which is in accordance with [15], without any noticeable deterioration in the far field performance. The self-supporting feed maintains the symmetry of the antenna structure while eliminating the need for complex struts. The fabricated self-supporting reflector antenna with its dimensions is shown Fig. 2.19.

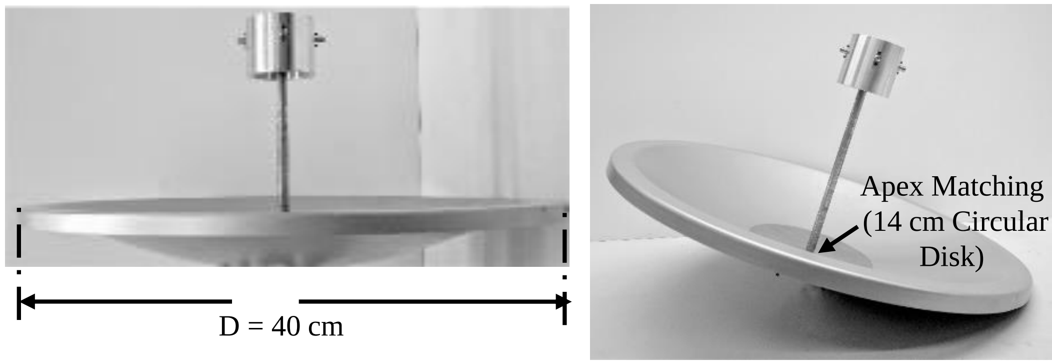

(a) (b)

Fig. 2.19: Picture of fabricated antenna with aperture matching.

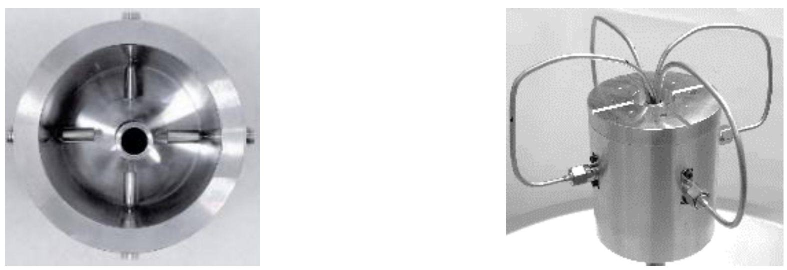

(a) (b)

Fig. 2.20: Picture of fabricated feed: (a) top view, and (b) with feeding cables.

2.4.4. Far-field Performance

The axis-symmetric reflector antenna without any struts has a gain > 21 dBic over the band of operation with a maximum of 28 dBic at 8 GHz, as shown in the Fig. 2.21. Also, aperture efficiency above 60% over 87.5% of the bandwidth with a peak efficiency of 70% is achieved. The radiation patterns are directive and symmetric around ϕ (0° to 360°) as shown in Fig. 2.22, and the HPBW of the antenna is 6° at 8 GHz. Similarly, the radiation patterns of the self-supporting apex matched reflector are symmetric with cross-polarization level < -20 dB, SLL < -16 dB, and gain > 21 dBic over the operating bandwidth, refer Fig. 2.22 and Fig. 2.23.

The observed deviation in the measured directivity with respect to the simulated directivity at higher frequencies (Fig. 2.23) is mainly due to defocusing the feed. Defocusing is caused by the slight variation in the focal and feed point of the fabricated antenna. Specifically, the focal length of the fabricated antenna is 1 cm shorter than the simulated, and the support of feed (or extended inner conductor) is tilted by 2.5°, approx., leading to feed offset of 0.33 cm, 0.83 cm (X, and Y axis, respectively). A drop of 1.79 dB in directivity is also noticed in simulated results on incorporating the offsets in the simulation, as shown in Fig. 2.23.

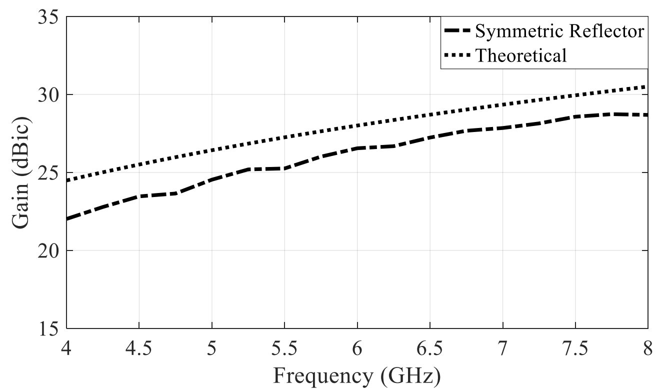

Fig. 2.21: Picture of fabricated feed: (a) top view, and (b) with feeding cables.

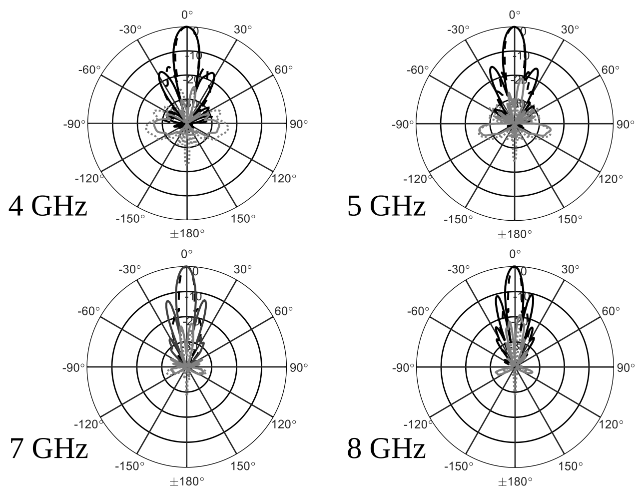

Fig. 2.22: Measured (solid) and simulated (dash) co (LHCP, dark color) and cross-polarized (RHCP, light color) radiation patterns of the self-supporting reflector antenna with apex matching, at $\phi = 0°$.

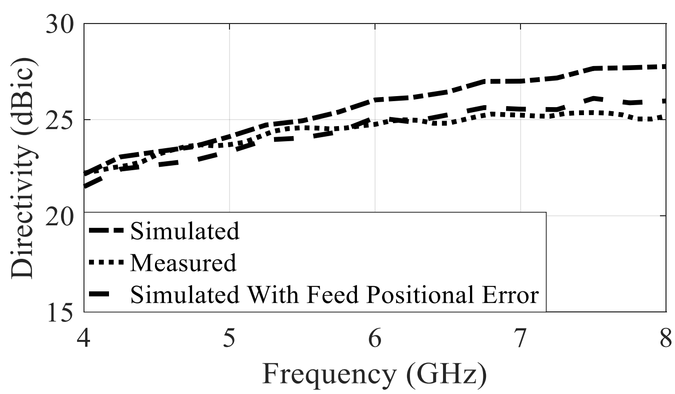

Fig. 2.23: Measured and simulated broadside directivity of the proposed self-supporting reflector antenna. Also shown the simulated directivity with error in feed position.

2.5. STAR Realization

The proposed monostatic STAR relies on rerouting the coupled/leaked signal through the BFN consisting of hybrids and circulators to achieve high isolation between TX and RX, as explained in the introduction, Section 2.2. System isolation of the proposed approach is dependent on the symmetries and imbalances in the antenna geometry and BFN, respectively. Therefore, in this section isolation of the system is computed using ideal case, with amplitude and phase imbalances, and asymmetries in the reflector geometry.

2.5.1. Ideal Case

The S-parameters of the simulated antennas, in HFSS, is combined with the ideal BFN components in AWR Microwave office to realize ideal case. Ideal components refer to the 90, 180 hybrids and circulators without any imbalances in amplitude and phase. Hence, the only asymmetries that are present in this case are the asymmetries resulting from the numerical mesh. System isolation > 60 dB can be achieved from the proposed configuration, as shown in the Fig.2.24. The finite isolation is mainly due to the mesh as mentioned before.

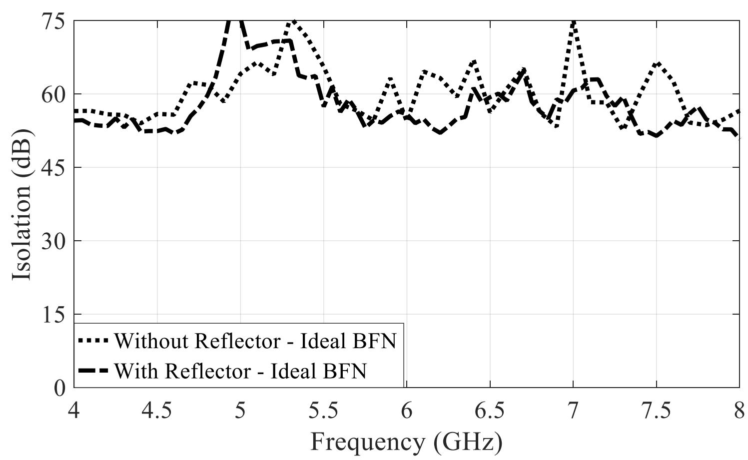

Fig. 2.24: Isolation of the proposed system with and without reflector using simulated antennas and ideal BFN.

2.5.2. Impact of Imbalances

The system isolation is impacted by the imbalances in amplitude and phase of the BFN since the imbalances negatively influence the cancelation process. That is, when frequency independent phase imbalance of ±6° and amplitude imbalance of ±0.4 dB are introduced into the system BFN in circuit simulator (AWR Microwave Office), the achievable system isolation dropped to 30 dB, as shown in Fig. 2.25. It should be noted that though the system isolation is dropped due to the imbalances, the obtained isolation is still higher than the circulator's isolation (ideal circulator with 15 dB isolation is used in this analysis). Importantly, system isolation is less dependent on the isolation of the circulator itself. Therefore, a circulator with low isolation can still lead to high isolation when the imbalances are minimal.

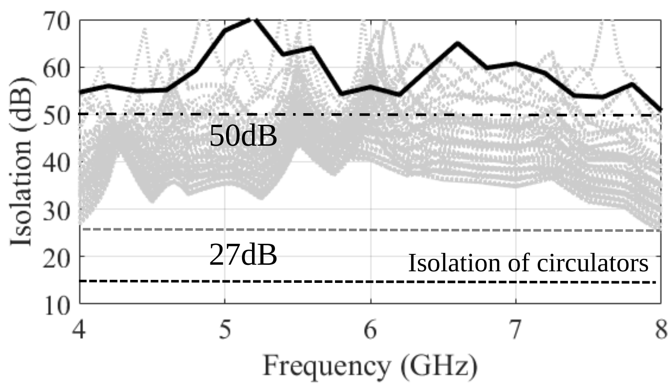

Fig. 2.25: Simulated isolation of the proposed axis-symmetric self-supporting reflector antenna with imbalances in BFN.

2.5.3. Impact of Asymmetries

Reflectors, especially, that are physically large, can develop aberrations or roughness over the time. The roughness or aberrations in the reflector surface create phase errors, and its impact on directivity is well documented in [24]-[26]. In addition to decreasing directivity, asymmetric or random roughness can deteriorate the isolation of the proposed STAR antenna system. Random roughness can be modeled using various statistical models or distributions [25]. Herein, we use a Gaussian distribution with correlation interval comparable to wavelength and root mean square (RMS) height much less than the wavelength [24]. Specifically, the surface roughness with correlation length 10 cm (1.33 λ_{4GHz}) and RMS height of 0.2 cm (0.026 λ4GHz), when projected on XY plane, is considered. The resulting random rough surface (RRS) is shown in Fig. 2.26(a) and (b). The directivity of the antenna with roughness is reduced to 24.9 dB from 25.6 dB and 26.9 dB from 28.2 dB, at 6 GHz and 8 GHz, respectively. Also, roughness has increased the SLL of the antenna by 8 dB, at 8 GHz. Additionally, the roughness in the order of magnitude considered herein can deteriorate isolation up to 14 dB as shown in Fig. 2.27.

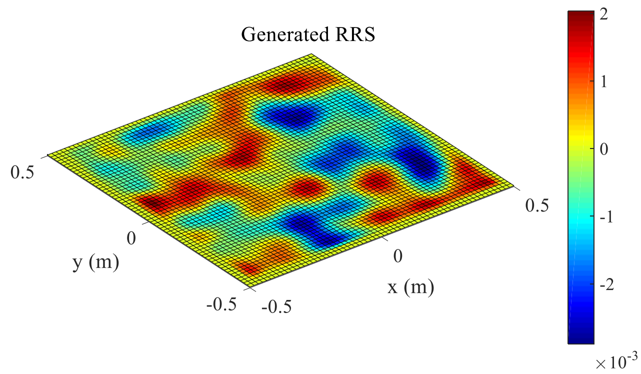

(a)

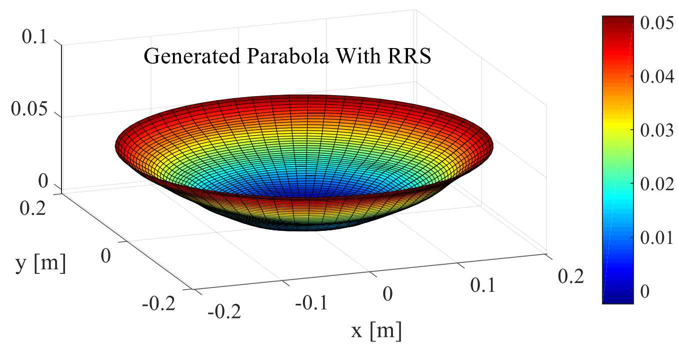

(b)

Fig. 2.26: (a) Generated Gaussian roughness with RMS height = 0.2 cm, (b) parabolic surface with Gaussian roughness.

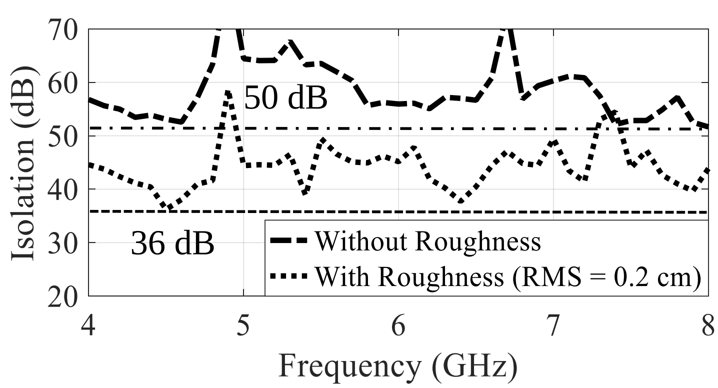

Fig. 2.27: Simulated systems isolation of the proposed system with and without roughness.

2.5.2. Measured Isolation

System isolation > 30dB (refer Fig. 2.28) is achieved with the prototyped STAR system, where COTS hybrids with high amplitude and phase imbalances are used in the BFN. Specifically, the used 180° hybrids have amplitude and phase imbalances of ±0.6 dB and ±10° [27], respectively. Similarly, 90° hybrids have amplitude and phase imbalances of ±0.5 dB and ±3°, respectively [28]. COTS circulators with 20 dB isolation, 0.35 dB IL and VSWR <1.25 are used [29]. Nonetheless, with the proposed approach, an average improvement of 15 dB in isolation is achieved in comparison to the conventional single circulator approach, as demonstrated in Fig. 2.28. The impact of the reflector on isolation is minimal, as seen in measured isolation with and without reflector, which is because of the geometrical symmetry of the self- supporting reflector antenna.

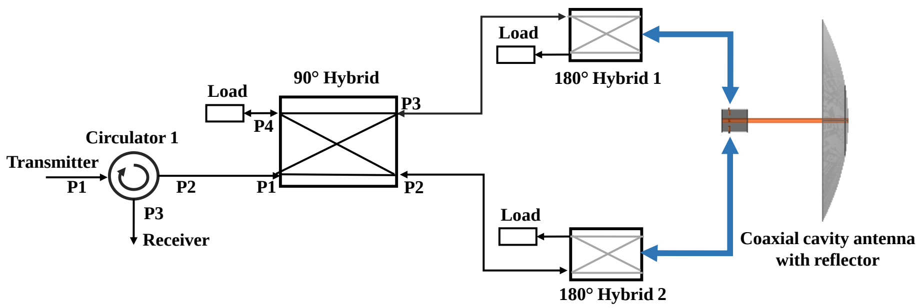

(a)

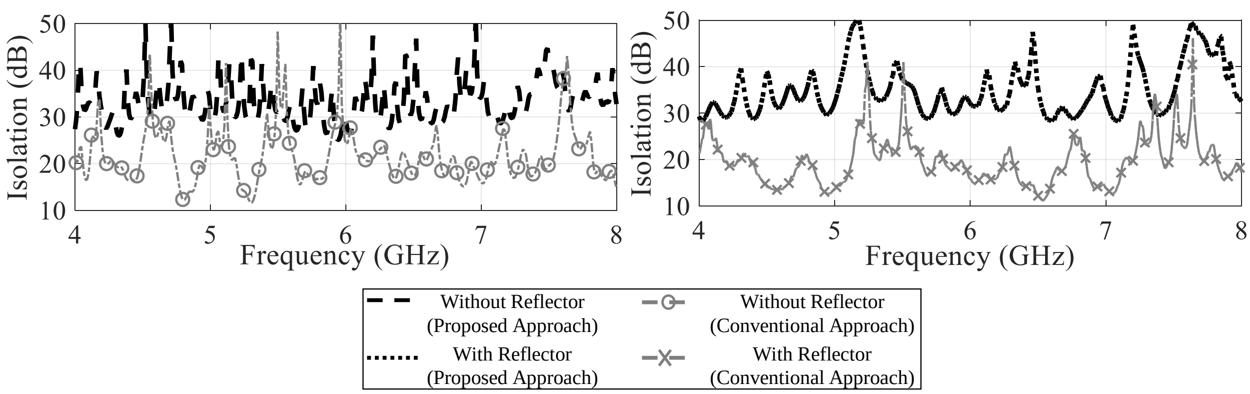

(b) (c)

Fig. 2.28: (a) Schematic diagram of the conventional approach and mmeasured isolation of the coaxial cavity antenna: (a) without reflector, and (b) with reflector, using proposed monostatic approach and the isolation of the full-duplex system for the conventional approach.

2.6. Quasi-monostatic STAR

The monostatic approach discussed in the previous section can achieve theoretically infinite isolation. However, practically achievable isolation is limited by the imbalances of COTS components, as illustrated by measured results. Therefore, to overcome the high dependency of isolation on imbalances a novel reflector-based space and volume-independent bi-static STAR antenna is proposed. The proposed STAR antenna system is realized using the previously designed coaxial cavity feed and center-fed symmetric parabolic reflector antenna. However, an additional coaxial cavity antenna, operating in CP, is mounted behind the TX feed to function as a receiving antenna. The proposed configuration and its operation are shown in Fig. 2. 29. High isolation, i.e. > 70 dB, is achieved with ideal BFN components, which is due to the low back lobe and axial ratio of TX feed and RX antenna. In addition, the antennas are operated in opposite polarization due to the orientation. The presence of reflector ensures that TX and RX subsystems are co-polarized, that is, gold STAR. Thus, the proposed approach eliminates the need of circulators required in the configuration discussed in Section 2.5. Also, the configuration is less sensitive to the imbalances in BFN as demonstrated in the following sections.

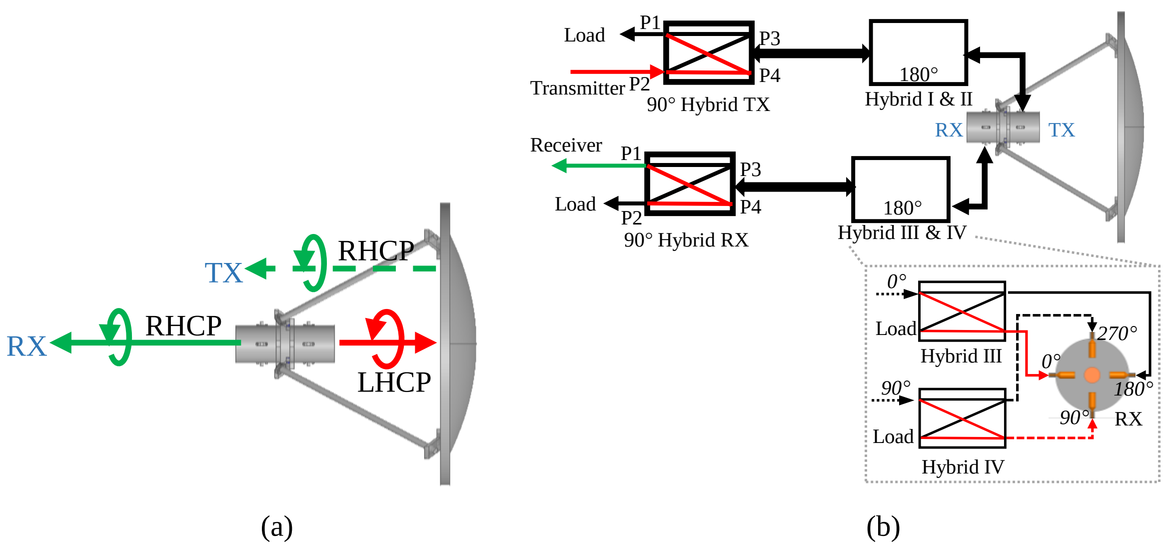

Fig. 2.29: (a) Operational principle of the proposed STAR reflector antenna system, and (a) BFN.

2.6.1. Configuration

The design along with physical dimensions of the proposed STAR antenna system is shown in Fig. 2.30. Two coaxial cavity antennas are mounted back-to-back, where one serves as the feed for the reflector and the other as the RX antenna. Further, each antenna is fed by a BFN consisting of two 180° and one 90° hybrids to excite the desired CP polarization, which is same as the coaxial cavity antenna in

Section 2.3. The feed for the reflector is operated in the left hand (LHCP) whereas the RX is operated in the right hand CP (RHCP), see Fig. 2.29. The reflector flips the polarization of the incident wave from LHCP to RHCP, achieving desired co-polarized STAR operation. The antennas are separated by 1.25 cm thick metal disk which is used to hold the struts. Four identical circular struts of 1 cm diameter are used to support the feed and RX. The struts are rotated by 45° in order to reduce the impact on radiation patterns in principal planes.

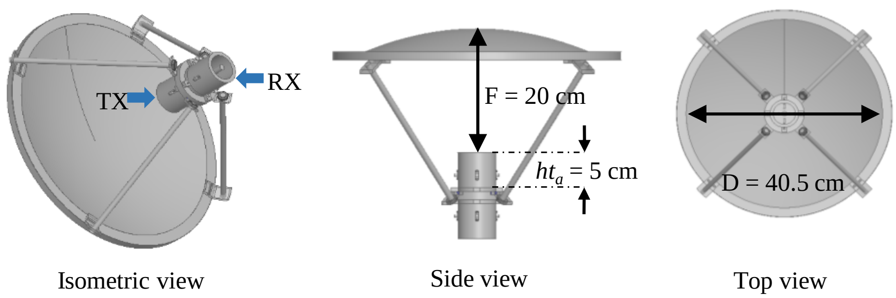

Fig. 2.30: CAD model of the proposed STAR reflector antenna system with dimensions.

2.6.2. Coupling Paths

In the absence of reflector, the main path for coupling between the TX feed and RX antenna is through the back lobe. Therefore, the low back lobe of the proposed antenna results in coupling < -49 dB between the TX and RX probes. Further, when the antennas are excited with mode 1 phase progression (0°, 90°, 180°, and 270°), required for CP operation, the BFN provides additional isolation because of the polarization diversity. This leads to the system isolation > 70 dB between the TX and RX ports (Fig. 2.31).

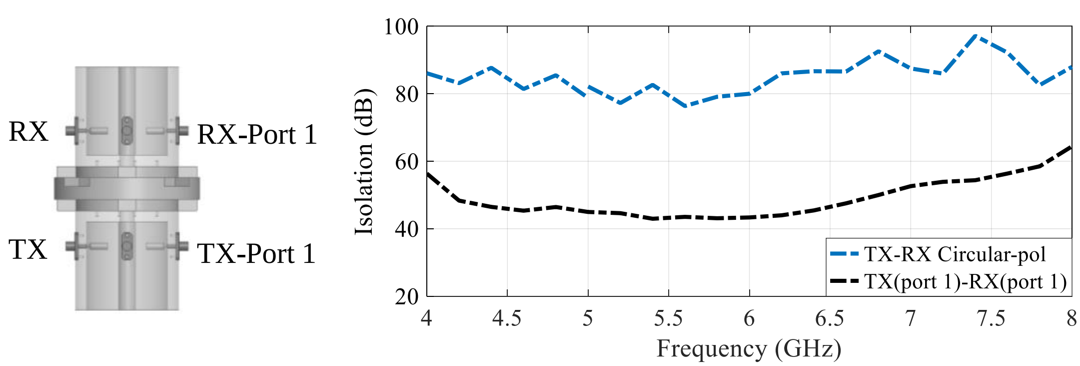

Fig. 2.31: Isolation between TX feed and RX antenna without reflector for circular polarization and linear polarization.

In the presence of the reflector, the antennas couple through the cross polarization as well, thereby, influencing the isolation of the system. Therefore, antennas with high F/B and the low axial ratio (AR) as the utilized coaxial cavity will still maintain high TX/RX isolation. High isolation > 70 dB can be achieved with ideal BFN components as shown in the Fig. 2.32.

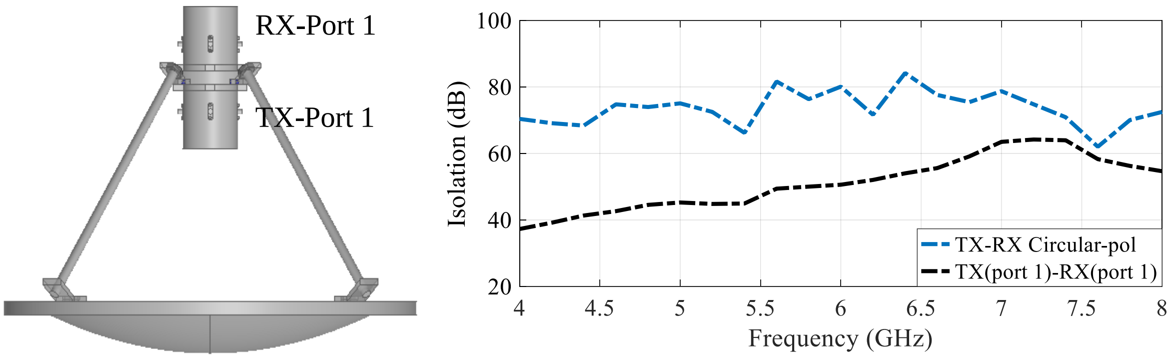

Fig. 2.32: Isolation between TX feed and RX antenna with reflector for circular polarization and linear polarization.

2.6.3. Fabrication and Measurement Results

The designed coaxial cavity antenna has VSWR < 2, directivity > 9 dBic (Fig.2.33) with aperture efficiency > 87.45%, and low AR (< 3dB up to elevation angle of ±35°), which is same as the antenna discussed in Section 2.4. Similarly, the reflector antenna has good impedance match and directivity > 21.9 dBic. In addition, the presence of RX antenna behind the feed and the struts have minimal impact on the directivity of the reflector antenna, as shown in Fig. 2.33. Hence, the proposed approach enables high isolation without influencing the electrical performance of the TX (reflector) and RX (coaxial cavity) antennas.

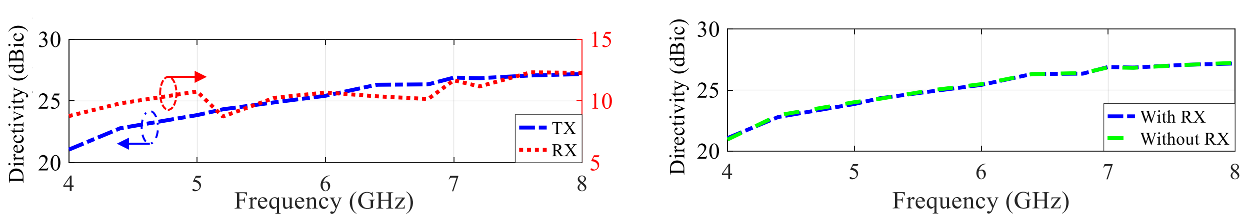

(a) (b)

Fig. 2.33: (a) Simulated directivity of TX and RX, and (b) directivity of TX with and without RX.

The amplitude and phase imbalances in the actual 90° and 180° hybrids increase the cross-polarized and back lobe levels, which degrade the system isolation. That is, when the COTS components from section 2.5 are used in BFN, the isolation has dropped to > 46 dB as shown in Fig. 2.34. Nevertheless, the proposed approach is not crucially sensitive to the BFN's imbalances and has average measured system isolation of 61 dB. Also, it is observed that lower the coupling between TX feed and RX, lower is the influence of imbalances on system isolation, which can be noticed from Fig. 2.34.

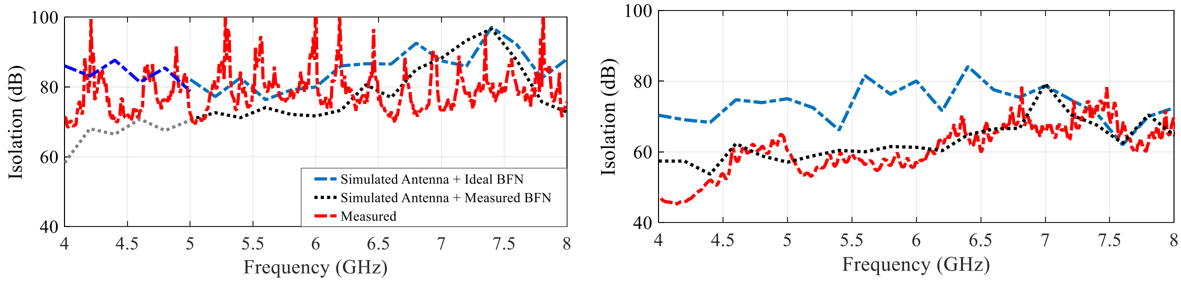

(a) (b)

Fig. 2.34: Simulated and measured TX/RX isolation: (a) without, and (b) with the reflector.

The radiation patterns of the TX and RX subsystems are shown in Fig. 2.35. As expected, the TX and RX patterns are different due to the physical size of the aperture. However, for some applications, it is still beneficial to have simultaneously wide-beam antenna at RX side for a wide field of view sensing and high directivity and power handling TX antenna for long-range transmission or jamming operations. The aperture efficiency of the reflector antenna can be further improved by using a larger reflector with smaller edge taper (~ -12 dB) and reduced spillover.

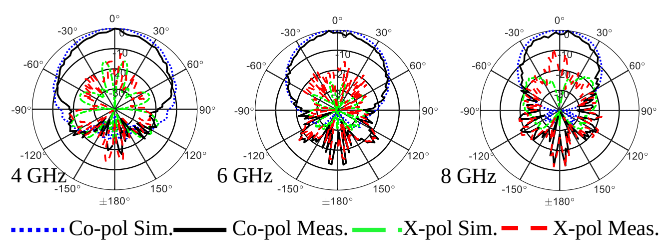

(a)

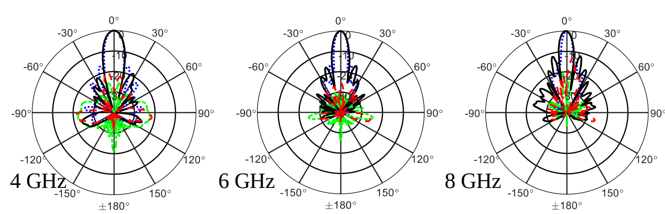

(b)

Fig. 2.35: Simulated and measured radiation patterns of (a) TX and (b) RX, at $\phi = 0°$.

2.7. Conclusions

This chapter discussed two approaches to increase the isolation between the TX and RX channels of a high gain reflector antenna. In the first approach, high isolation in the introduced monostatic STAR approach is achieved by canceling the coupled/leaked signals using the BFN consisting of 90° and 180° hybrids and circulators. Theoretically, it is explained that infinite isolation can be achieved between the TX and RX, through the proposed method. However, it is shown that the asymmetry in the antenna geometry and the BFN can significantly deteriorate the achievable isolation which is demonstrated by considering an offset-fed reflector, surface roughness of the reflector and imbalances in BFN. Using COTS components with noticeable imbalances and more importantly variation between thereof, average isolation > 30 dB is achieved with the fabricated system, which is ~15 dB higher than the isolation achieved with the conventional circulator approach.

In the second approach, a quasi-monostatic high gain reflector based STAR antenna configuration is outlined. High isolation between TX feed and RX is achieved by using high F/B ratio and low cross-pol level coaxial cavity antennas. System isolation > 70 dB is achieved with ideal BFN and average measured isolation of 61 dB is achieved with COTs BFN components. Further, it is shown that the quasi-monostatic approach proposed herein is less sensitive to imbalances and asymmetries in the BFN and antenna geometry, respectively.

References

[1] M. E. Knox, “Single antenna full duplex communications using a common carrier,” *IEEE Wireless Micro. Tech. Conf.*, Apr.2012, pp.1 – 6.

[2] J. R. F. Guy and D. E. N. Davies, "Novel method of multiplexing radio communication antennas using circular-array configuration," *Microw., Optics Ant., IEE Proc. H*, Oct. 1983.

[3] W. G. Lim, W. I. Son, K. S. Oh, W. K. Kim and J. W. Yu, "Compact integrated antenna with circulator for UHF RFID system," *IEEE Ant. Wireless Propag. Lett.*, 2008.

[4] W. G. Lim and J. W. Yu, "Balanced circulator structure with enhanced isolation characteristics". *Microw. Opt. Tech. Lett.*, 2008.

[5] S. K. Sharma, S. Rao, and L. Shafai, *Handbook of reflector antennas and feed systems –Feed Systems*, Vol. II, Boston, MA, USA: Artech House, 2013.

[6] P.S. Kildal, “Some reflector and feed antenna inventions that made a difference: Fundamentals and examples from radio telescopes, satellite communications and radio links,” *Africon*, Pointe-Aux-Piments, 2013.

[7] J. L. Volakis, *Antenna engineering handbook,* 4th ed., NY, USA: McGraw Hill, 2007.

[8] K.A. Abdalmalak *et al.*, "Radio astronomy ultra wideband receiver covering the 2–14 GHz frequency band for VGOS applications," *2016 10th Eur. Conf. Ant. Propag. (EuCAP)*, 2016.

[9] A. Akgiray, S. Weinreb, W. A. Imbriale and C. Beaudoin, “Circular quadruple-ridged flared horn achieving near-constant beam width over multi-octave bandwidth: design and measurements,” *IEEE Trans. Ant. Propag.*, Mar. 2013.
[10] S. L. Johns and A. Prata, "An ultra-wideband nested coaxial waveguide feed for reflector antenna applications," *1999 IEEE Ant. Propag. Soc. Int. Symp.*, 1999.
[11] A. D. Olver, P. J. B. Clarricoats, A. A. Kishk, and L. Shafai, *Microwave horns and feeds,* NY, USA, IEEE Press, 1994, ch. 2.
[12] T. R. Holzheimer, “Applications of the coaxial cavity antenna in time and frequency”, *2004 Antenna Appl. Symp.*, Sep. 2004.
[13] T. R. Holzheimer, “The low dispersion coaxial cavity as an ultra-wideband antenna”, *2002 IEEE Conf. on Ultra-wideband Sys. and Tech.*, May, 2002.
[14] C. Profera, "Improvement of TE11mode coaxial waveguide and horn radiation patterns by incorporation of a radial aperture reactance," *IEEE Trans. Ant. Propag.*, Mar. 1976.
[15] T. Bird, “TE11mode excitation of flanged circular coaxial waveguides with an extended center conductor,” *IEEE Trans. Ant. Propag.*, Dec. 1987.
[16] B. H. Simakauskas, “Phase center stabilization of a horn antenna and its application in a Luneburg lens feed array”, M.S. thesis, Dept. Elect. Comput. and Energy Eng., Uni. Colorado, Boulder, 2015.
[17] T. A. Milligan, *Modern antenna design*. Hoboken, NJ, USA: John Wiley & Sons, 2005, ch. 8.
[18] S. K. Sharma, S. Rao, and L. Shafai, *Handbook of Reflector Antennas and Feed Systems -Theory and design of reflectors*, vol. I, Boston, MA, USA: Artech House, 2013.
[19] C. C. Cutler, "Parabolic-antenna design for microwaves," *Proceedings of the IRE*, Nov. 1947.
[20] A. B. Pippard and N. Elson, "The elimination of standing waves in aerials employing paraboloidal reflectors," *Electrical Engineers - Part IIIA: Radiolocation, J. IEE*, 1946.
[21] E. G. Geterud, J. Yang, T. Ostling and P. Bergmark, "Design and optimization of a compact wideband hat-fed reflector antenna for satellite communications," *IEEE Trans. Ant. Propag.*, Jan. 2013.
[22] G. Wainwright and C. C. Chen, "Low-profile broadband reflector antenna designed for low mutual coupling," *2016 10th Euro. Conf. Ant. Propag. (EuCAP)*, 2016.
[23] L. Shafai, A. Ittipiboon, E. Bridges and F. Hyjazie, "Dual band horn with inherent isolation between its transmit and receive ports," *Microw., Opt. Ant., IEE Proc. H*, June 1984.
[24] C. A. Balanis, *Antenna theory – Analysis and Design* (Third Edition). Hoboken, NJ, USA: John Wiley & Sons, 2005, ch. 15, pp. 924 – 926.
[25] A. W. Love, “Some highlights in reflector antenna development”, *Radio Science*, 1976.
[26] J. Ruze, “The effect of aperture errors on the antenna radiation pattern”, *Nuevo Cimento Suppl.*, 1952.
[27] JSO-04-471/1S, Pulsar microwave corporation, Clifton, NJ. Accessed on: Sep.22, 2017. [Online]. Available: https://www.pulsarmicrowave.com/product/hybrid/JSO-04-471-1S
[28] RFHB04G08GVT, RF-Lambda, Plano, TX. Accessed on: Sep. 22, 2017. [Online]. Available: http://www.rflambda.com/pdf/hybrid/RFHB04G08GVT.pdf
[29] D3C4080, Ditom, Fresno, CA. Accessed on: Sep.22, 2017. [Online]. Available: https://www.ditom.com/cart/product/d3c4080.

Chapter 3: Handheld Radio Antenna System

3.1. Introduction

Simultaneous transmit and receive (STAR) concept attracts growing interest of researchers in the areas of wireless communications and electronic warfare. True STAR systems aim to enable full duplex operation without multiplexing in frequency, time, and polarization. Therefore, leading to the efficient use of frequency spectrum and theoretically doubled system throughput. For practical realization of a STAR system, isolation between transmitter (TX) and receiver (RX) ports in the order of more than 100 dB is desired. This is typically achieved by reducing the self-interferences between the TX and RX at the antenna, analog, and digital cancelation layers [1]-[3]. This work focuses mainly on the antenna system layer implemented on handheld radio platforms.

Different antenna design techniques have been proposed to reduce the self-interference between TX and RX ports and thereby increase the isolation between them. Bistatic STAR configurations rely on using separate antennas for TX and RX, and often take advantages of spatial, polarization, or beam multiplexing [4]-[8] to further reduce the TX/RX coupling. The issue with this approach is the large distance required between TX and RX antennas to achieve an acceptable isolation level. A bistatic spatial filtering in [5] demonstrates an isolation of more than 30 dB over tunable narrowband channels for mobile handsets. In [6], a collocated bistatic TX/RX antennas with orthogonal linear polarizations achieve 50 dB isolation over 6.5% bandwidth. In [7], the coupling between closely-packed antennas is reduced to less than -40 dB, using defective ground structure placed between TX and RX antenna elements. A wideband dual-polarized bistatic STAR antenna system, given in [8], shows the isolation of more than 60 dB over 3:1 bandwidth. Other bistatic STAR antennas rely on near-field cancellation of the TX (RX) antennas along the direction of the RX (TX) antennas [3], [9]-[15]. For example, an isolation of more than 50 dB, between an RX monocone and a TX ring array of eight TEM horns, is achieved in [15], over a decade bandwidth. The main issues of this approach include the complex beamforming network (BFN) required for the large number of TX (RX) elements, the sensitivity to BFN imbalances, and the dissimilarities between TX and RX radiation patterns.

Monostatic STAR configurations aim to use same antennas for both TX and RX, therefore reducing the size of the antenna system which is critical for space-constrained platforms. However, its implementation is quite challenging given the impact of the internal self-leakage of the actual circuit components. Monostatic STAR techniques rely mainly on circulators [16]-[22] or antennas with internal isolation capability [23]-[25]. Isolation of the former approach is limited not only by the circulator internal isolation but also with the reflected signal from the antenna due to mismatch or interactions with nearby scatterers. The later approach includes several configurations, mainly based on system symmetry to provide high isolation levels. In [23], a bi-directional single antenna achieves high isolation of more than 40 dB using a balanced feed network based on quadrature hybrids and circulators. An ultra-wideband monostatic STAR antenna system, presented in [24], demonstrates an isolation of more than 39.5 dB, based on the multi-arm frequency-independent antenna and feed cancelation technique. In [25], an antenna system, composed of a sequential rotation array of four dual-polarized patch antennas and two modified Butler-matrix BFN, achieves isolation higher than 47 dB.

This work presents a monostatic full-duplex antenna system, designed for a typical handheld radio platform, based on a mode multiplexing technique. The antenna structure is a circular array of four identical dipole elements, which are fed in two orthogonal phase modes for TX and RX using BFN. This mode orthogonality can, theoretically, achieve an infinite isolation between TX and RX, provided that the symmetry between antenna elements is maintained. The main challenges associated with the proposed platforms are the asymmetric shape of the handheld device and the impact of nearby objects represented mainly by a soldier holding the radio. Two BFNs are proposed, demonstrating an isolation level of more than 65 dB, assuming ideal BFN components while considering the asymmetric shape of the handheld radio. To illustrate the practical realization of the antenna structure, sensitivity analyses on the impacts of imbalances in realistic BFN, as well as nearby soldier are carefully executed. These analyses demonstrate high isolation level of more than 24 dB over the dedicated frequency band (i.e., 1.75-1.85 GHz). To validate the proposed antenna configuration, a system prototype is fabricated and tested using BFN components. The measurement results show the isolation of more than 30 dB between TX and RX ports. Further improvement in the isolation level, (more than 60 dB), is obtained at narrow bandwidth channels, using the feedback cancellation technique.

3.2. Full-Duplex Antenna System Design

3.2.1. Antenna System Configuration

The proposed antenna structure is a circular array of four symmetrical half-wavelength dipoles placed around a cylindrical metallic mast, as shown in Fig. 3.1. The mast is used to reduce coupling between dipoles and route the BFN. Four microstrip baluns are designed to provide balanced feed for the dipoles. Plastic parts, fabricated using 3D-printing, are used to mechanically support the antenna elements. A BFN feeds the dipoles in two orthogonal phases modes, which ensures high isolation between TX and RX.

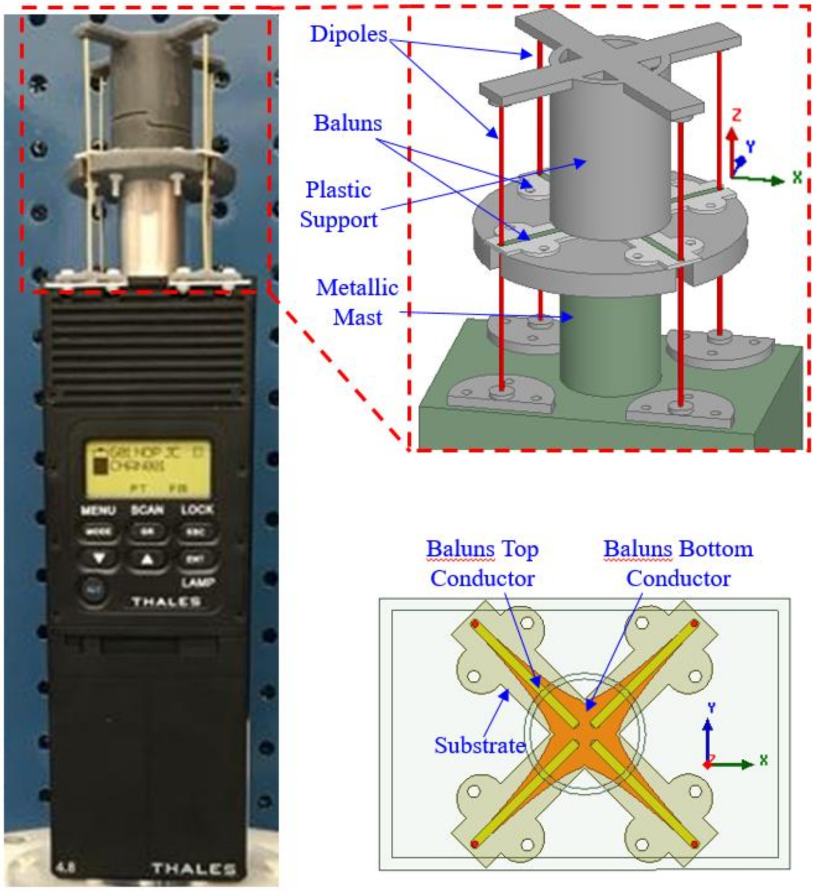

Fig. 3.1: Proposed antenna system for handheld radios.

This antenna configuration is applicable for different types of handheld radios. Specifically, handheld radio THALES AN/PRC-148B MBITR2 [26] is used as an example of a realistic platform implementation of the proposed design. This radio has dimensions of 8.5″ x 2.65″ x 1.75″ (215.9 x 67.3 x 44.5 mm^3) and it operates over three frequency bands, 225-450 MHz, 1250-1390 MHz, and 1750–1850 MHz. The proposed antenna system is designed to cover the upper frequency band of 1750–1850 MHz. The spacing between the dipoles is deliberately selected as 36 mm to fit within the handheld width as shown in Fig. 3.1. The length of the metallic mast is equal to the height of the dipoles, and its diameter is equal to 20 mm, which is tuned for low coupling between the dipoles. The length and diameter of the dipole elements are equal to 64 mm and 1 mm, respectively. A Taconic RF-30 substrate is used for the design of the microstrip baluns.

A full-wave simulation for the whole system is carried out using the commercial software ANSYS HFSS [27]. The S-parameters of one dipole, where the other dipoles are symmetric, are shown in

Fig. 3.2. The simulation results demonstrate good antenna matching and low coupling of less than -16 dB between the dipoles.

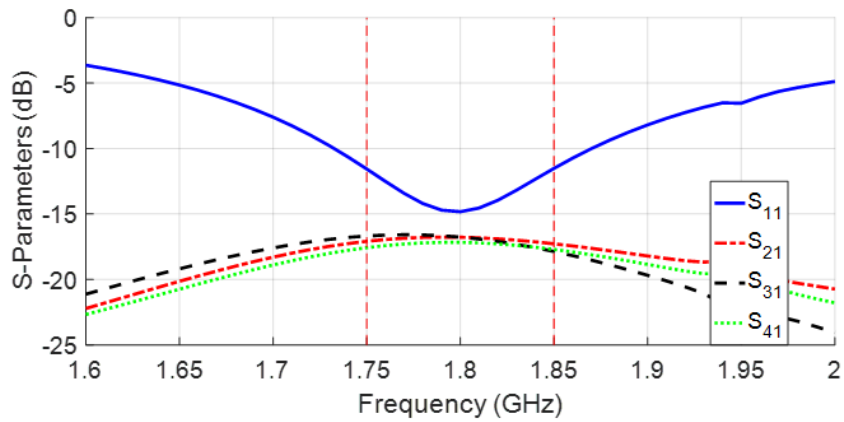

Fig. 3.2: S-parameters of the antenna system.

3.2.2. Beamforming Network (BFN)

A BFN, shown in Fig. 3.3 (a), is used to feed the dipoles in two orthogonal phase modes. Mode 1 (M1), i.e., quadrature phase shift between dipoles, is used for TX path, and mode 0 (M0), i.e., no spatial phase shift between dipoles, is used for RX path. The BFN has a 90° hybrid, two 180° hybrids, and a splitter. This mode multiplexing ideally achieves an infinite isolation and high radiation pattern correlation between TX and RX, in case of maintained symmetry between antenna elements [28]. Nevertheless, the asymmetric shape of the handheld radio, as well as the internal self-leakage of the actual components of BFN may reduce the system isolation. The BFN analysis is performed using the commercial NI AWR [29] software [29], considering both ideal BFN and actual COTS components available in our lab. To determine the impact of the asymmetry in COTS BFN, we studied the case of two identical 180° hybrids and the case where these hybrids are different.

The simulation results, shown in Fig. 3.3 (b) and (c), demonstrate good impedance match and high isolation between TX and RX ports. Isolation greater than 68 dB is achieved over the entire band with the ideal BFN, and greater than 30 dB when actual COTS BFN is considered. The utilized 90° and 180° hybrids are from Werlatone, Inc. with model numbers QH7903 and H7942, respectively, and the splitter, model RFLT2W08025, is from RF-Lambda. M1–M0 topology is less-sensitive to BFN asymmetry, so that only 1.5 dB improvement in isolation is achieved when considering identical 180° hybrids, as shown in Fig. 3.3 (c). Moreover, this enables omnidirectional radiation patterns for both TX and RX, as shown in Fig. 3.4 (a) and (b). As seen, there is a small discrepancy in the radiation pattern of M1 due to the small size of the nearby ground plane, which is represented by the top surface of the

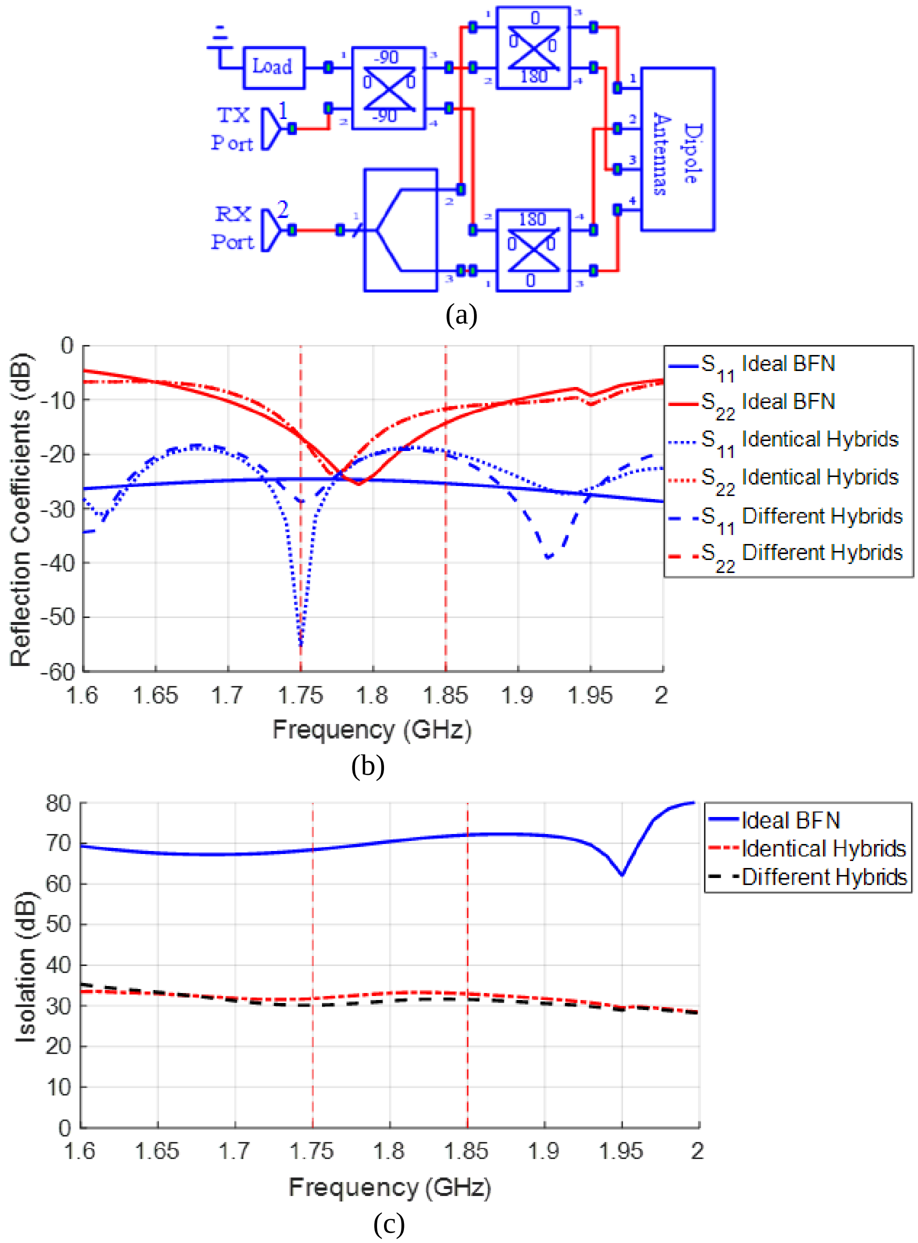

Fig. 3.3: Phase modulation “Mode 1 – Mode 0”; (a) BFN, (b) reflection coefficients, and (c) isolation between TX and RX.

handheld radio. However, the radiation pattern maintains the close similarities between TX and RX patterns, demonstrating an envelope correlation coefficient (ECC) larger than 61 % over the entire frequency band, as shown in Fig. 3.4(c). ECC is an indication of how dependent/independent radiation patterns of two antennas are, considering both polarization and pattern shapes [30].

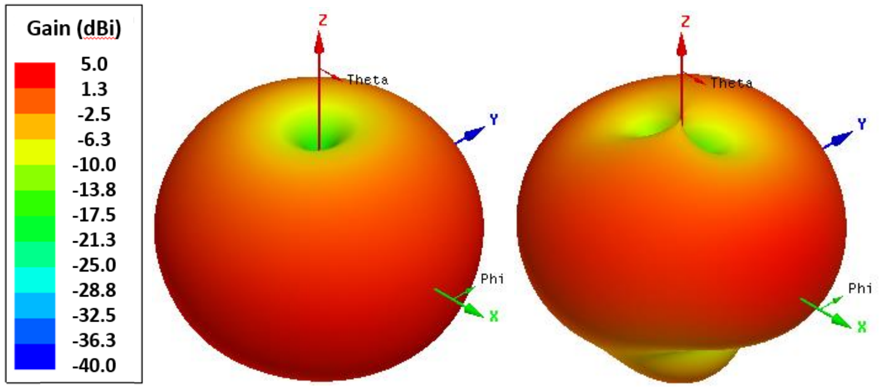

(a) (b)

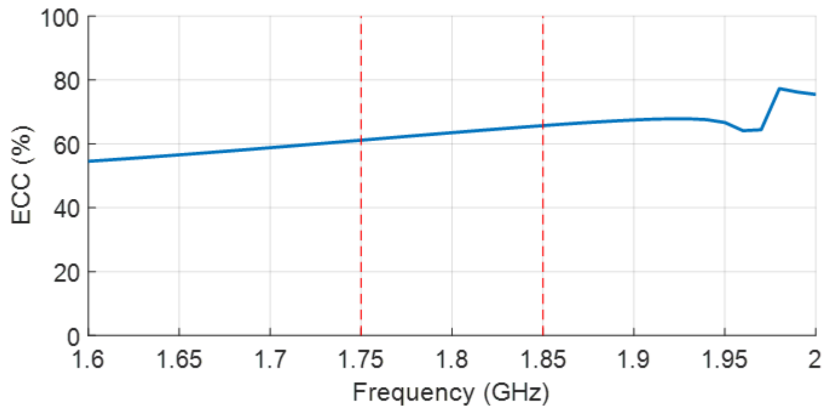

(c)

Fig. 3.4: (a) Gain pattern of mode 0, (b) gain pattern of mode 1, and (c) envelope correlation coefficient between the two patterns.

Further improvement in the isolation between TX and RX ports is achieved by replacing the 90° hybrid of Fig. 3.3 (a) by a 180° hybrid, as shown in Fig. 3.5 (a) and (b). Consequently, the TX signal that flows through the 180° hybrid is divided into two signals equal in magnitude and opposite in phase. This, in turn, makes the self-leakage of the other two 180° hybrids to be opposite in phase, resulting in cancelation at the RX port, and thereby increasing the isolation. This topology feeds the antenna elements in a mixed mode (MM) with phase shifting between the dipoles of either 0°, 0°, 180°, 180° (MM1 in Fig. 3.5 (a)) or 0°, 180°, 180°, 0° (MM2 in Fig. 3.5 (b)). The simulation results of MM–M0 topology demonstrate improvements in isolation, which is > 58 dB when considering identical 180° hybrids and > 43 dB with non-identical hybrids, as shown in Fig. 3.5 (c). The difference between results of MM1 and MM2 is due to the asymmetric shape of the handheld radio. As seen, MM-M0 topology shows high sensitivity to the asymmetry of BFN. Besides, the radiation patterns of the mixed modes are not omnidirectional, demonstrating ECC of around 50 % with mode 0, as shown in Fig. 3.6. Therefore, switching between MM1 and MM2 is needed to compensate for the low pattern correlation with M0.

Based on these results, the proposed mode multiplexing techniques, i.e., M1-M0 and MM-M0, demonstrate high isolation between TX and RX ports over the dedicated frequency band.

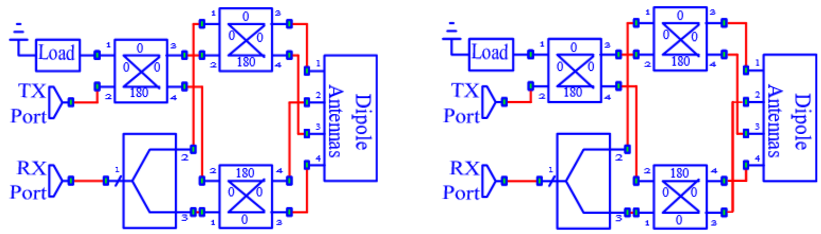

(a) (b)

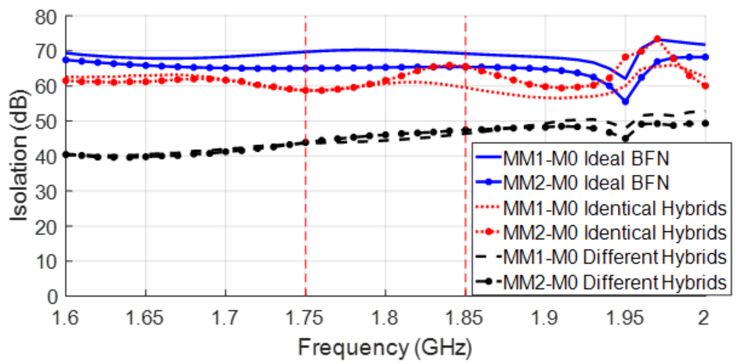

(c)

Fig. 3.5: (a) BFN MM1-M0, (b) BFN MM2-M0, and (c) isolation between TX and RX.

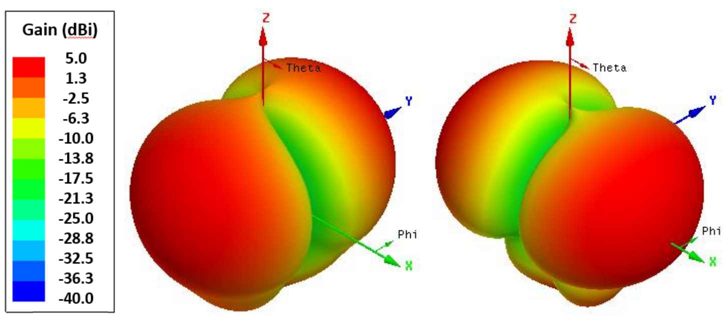

(a) (b)

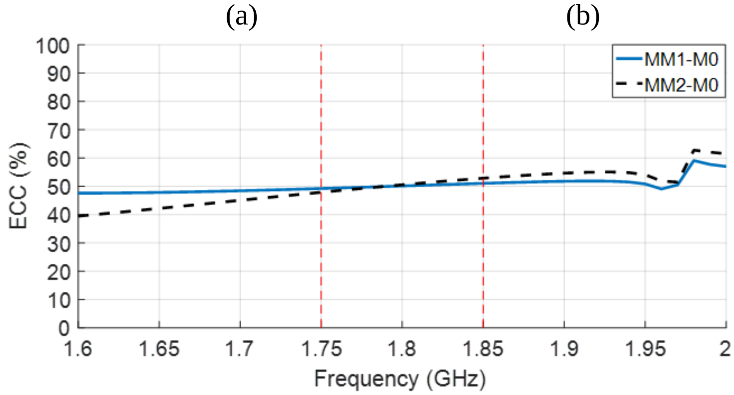

(c)

Fig. 3.6: (a) Gain pattern of Mixed Mode 1, (b) Gain pattern of Mixed Mode 2, and (c) envelope correlation coefficient between mixed modes and mode 0.

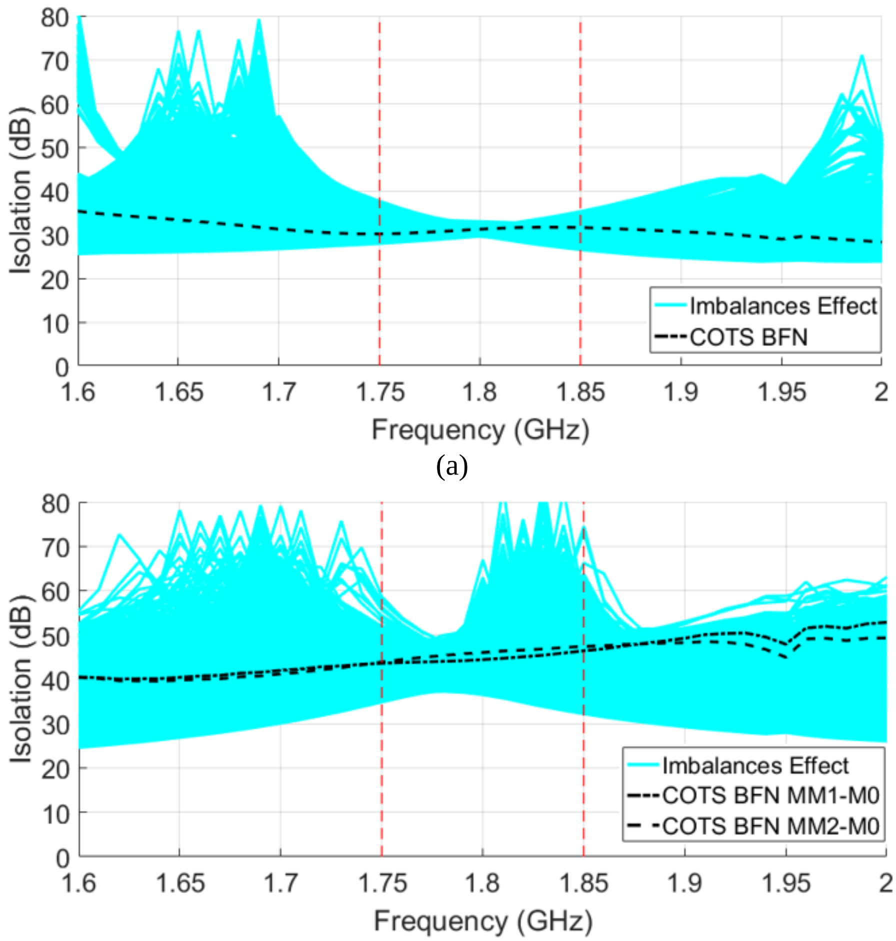

(b)

Fig. 3.7: Impact of BFN imbalances on isolation; (a) M1-M0, (b) MM-M0.

3.2.3. Impact of Amplitude and Phase Imbalances of BFN

As seen from the previous analysis, the isolation between TX and RX ports is limited by the asymmetries in the COTS BFN. Therefore, we have studied the influence of amplitude and phase imbalances on the system isolation. The imbalances used are chosen to be within the actual amplitude and phase variations of the COTS hybrids, which are 0-0.5 dB and ±5°, respectively. The results, shown in Fig. 3.7, illustrate that the M1-M0 BFN is less-sensitive to imbalances in comparison with MM-M0 BFN. However, the later maintains higher isolation levels greater than 32 dB, and the former achieves isolation of more than 26.5 dB over the operational bandwidth. As seen in Fig. 3.7, the isolation values obtained in simulations using the COTS components available in our lab are within the range obtained from this analysis. Based on this analysis, it is seen that the two proposed structures achieve high isolation values while considering amplitude and phase variations of realistic BFN components.

3.3. Fabrication and Measurements

To validate the performance of the proposed antenna system, a prototype of the antenna structure is fabricated and mounted on the top of a dummy handheld radio to be tested, as shown in Fig. 3.8 (a). The dipoles are made of 1 mm diameter brass rods. Polylactic plastic is 3D printed to mechanically support the dipoles, and nylon screws are used to secure the balun substrate and auxiliary plastic parts. To enable measurements, long coaxial cables are used with extended lengths through the metallic mast and the dummy radio. The outer conductors of the four cables are grounded by connecting them to the metallic mast to choke the surface currents. In the actual system, these cables are not needed, and the antenna elements will be connected directly to the BFN inside the metallic mast.

3.3.1. Measurements of Scattering Parameters

Scattering parameters of the four dipoles are measured inside an anechoic chamber, using a vector network analyzer (VNA), to eliminate reflections from the surroundings. As seen from Fig. 3.8 (b), the four dipoles are well matched over the operational bandwidth, and the coupling between dipole elements is less than -14 dB. One cable (i.e., port 2) shows a small notch out of the dedicated band in S22 and the corresponding couplings (i.e., S21, S32, and S42), which is due to soldering errors. Since the antenna symmetry is an important factor to achieve high isolation, we have checked the reflection coefficient phases of the four ports, as shown in Fig. 3.8 (c). As seen, there are some discrepancies in the phases, which are mainly due to an error in cutting equal lengths for the four cables, as well as tolerance in the antenna fabrication and assembly. Differences in reflection coefficient phases correspond to twice the actual phase errors between input ports. Considering the smallest phase value as a reference, the phase errors of the four ports at 1.8 GHz are 0°, 2.1°, 6.6°, and 9.7°, respectively.

3.3.2. Isolation Measurements

As previously discussed, the internal self-leakage and magnitude and phase imbalances of COTS BFN components impact the isolation between TX and RX ports. Therefore, we have measured the system isolation using several COTS components available in our lab, and using different combinations of hybrids. All measurements were conducted in the anechoic chamber to avoid reflections from surroundings. Reflection coefficients of all BFN combinations, shown in Fig. 3.9 (a) and (b), demonstrate good impedance match over the required frequency band. For M1-M0 configuration, measurements of all BFN iterations show system isolation of more than 24 dB over the entire frequency band, as shown in Fig. 3.9 (c). The best iteration achieves an isolation of more than 29.5 dB over the operational bandwidth, which is very close to the simulation results (i.e., > 30 dB) despite the asymmetry in the system prototype.

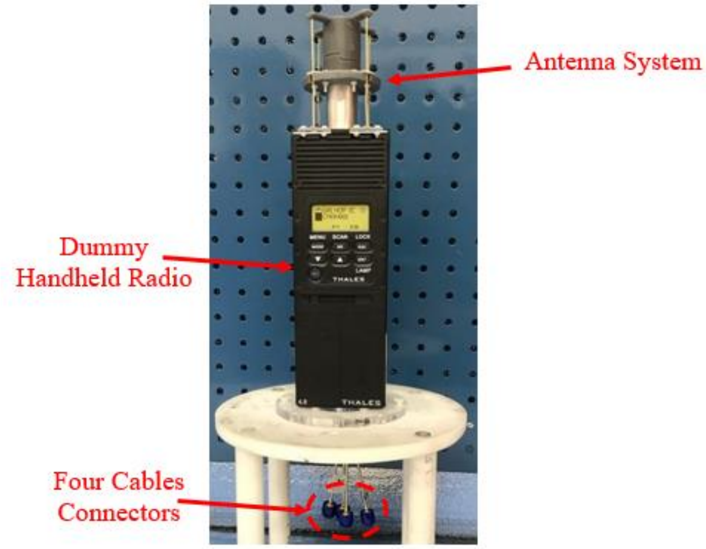

(a)

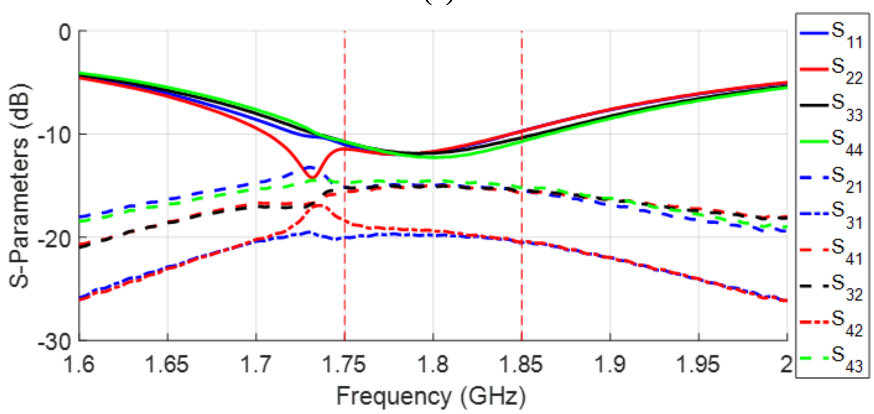

(b)

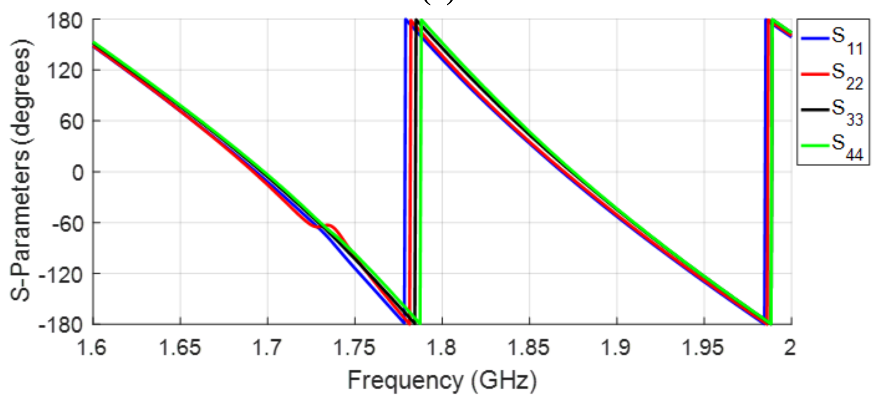

(c)

Fig. 3.8: (a) System prototype, (b) measured magnitudes of S-parameters, and (c) measured phases of reflection coefficients.

To illustrate the effect of the tolerances in fabrication and assembly, the measured S-parameters are imported to the NI AWR software and are connected to an ideal BFN. This study shows a reduction in the theoretical isolation from 68 dB (see Fig. 3.3(c)) to 36 dB (see Fig. 3.9(c)). Moreover, we studied to impact of the long cables by correcting the associated phase errors at 1.8 GHz using NI's AWR. The result shows some improvement in the isolation at narrow band of frequency, as shown in Fig. 3.9(c).

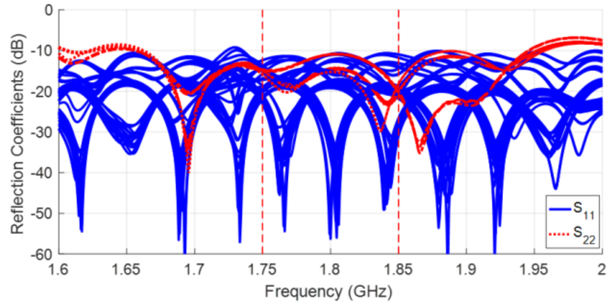

(a)

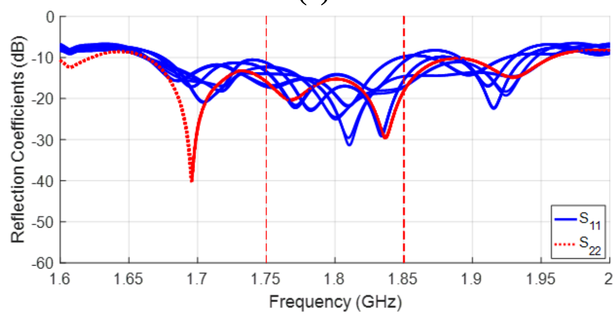

(b)

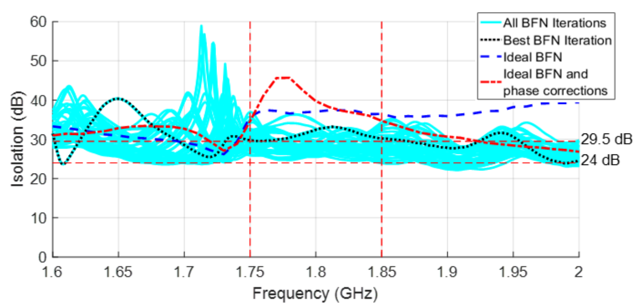

(c)

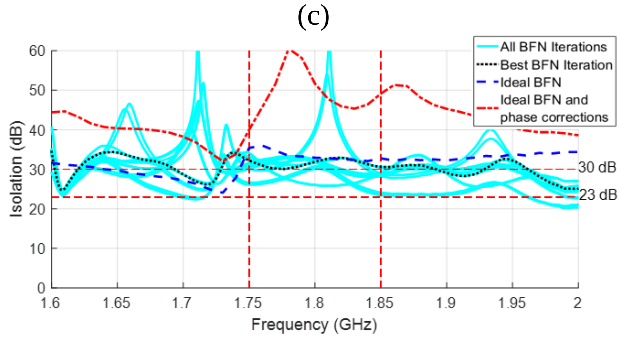

(d)

Fig. 3.9: Measurement results; (a) reflection coefficients of M1-M0, (b) reflection coefficients of MM-M0, (c) isolations of M1-M0, and (d) isolations of MM-M0.

For MM-M0 configuration, the measured isolations are close to that obtained with M1-M0. All BFN iterations demonstrate isolations more than 23 dB, and the best of them achieve isolations more than 30 dB over the operational bandwidth, as shown in Fig. 3.9(d). The reason for the limited improvement in isolation, compared with the simulation results of Fig. 3.5(c), is illustrated when applying the ideal BFN. As seen, the asymmetry in the prototype reduces the ideal isolation from 65 dB to 32 dB, which is increased to 45 dB by correcting the phase error caused by the long cables. This analysis demonstrates that MM-M0 structure is more sensitive to the asymmetry in the antenna system compared with M1-M0.

In summary, the measurement results illustrate the validity of the proposed antenna configuration to achieve system isolation of more than 30 dB. Further improvements in isolation can be achieved using MM-M0 structure, through high-precision fabrication and system integration.

3.3.3. Measurements of Radiation Patterns

Radiation pattern measurements of the system prototype were conducted in the anechoic chamber, as shown in Fig. 3.10(a), where the pattern of each antenna element is individually measured. A post-processing analysis is then performed to obtain the radiation pattern of each phase mode, by applying the necessary phase shifting between the dipoles. Measurement and simulation results of the four phase modes, i.e., M0, M1, MM1, and MM2, are shown in Fig. 3.10(b)-(e), respectively. As seen, good agreements between simulation and measurement patterns are obtained. Small discrepancies in E-plane patterns are mainly due to the asymmetry in the system prototype.

M0 demonstrates a pure omnidirectional pattern with the cross-polarized level of less than -17 dB. M1 is sensitive to the small size of the nearby ground plane, which is clear from the appearance of the back lobe in E-plane pattern and the high cross-polarization. In this prototype, the distance between the dipoles bottom edge and the ground plane (i.e., the top surface of the handheld radio) is 2 mm. Further reduction in the cross-polarization level of M1 can be obtained by increasing the height of the dipoles and/or increasing the size of the ground plane. The two mixed modes, i.e., MM1 and MM2, show two complementary omnidirectional patterns by switching between the two modes when needed. The difference between the E-plane patterns of MM1 and MM2 is due to the asymmetric shape of the handheld radio (i.e., the ground plane is a rectangle). Based on these results, the measurements validate the design performance of the proposed phase operational modes.

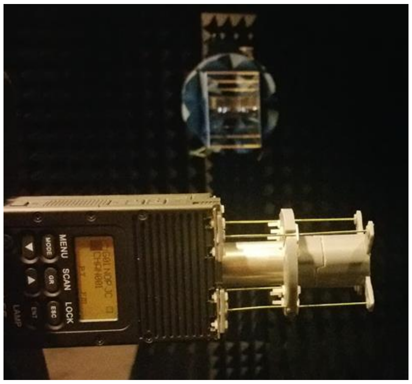

(a)

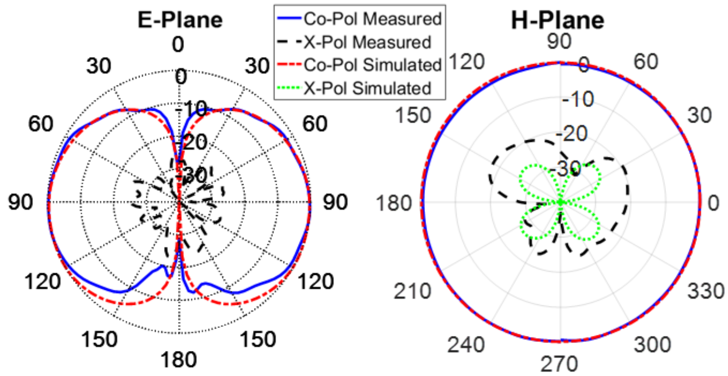

(b)

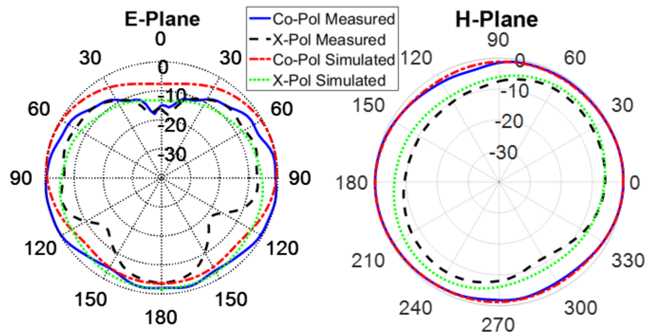

(c)

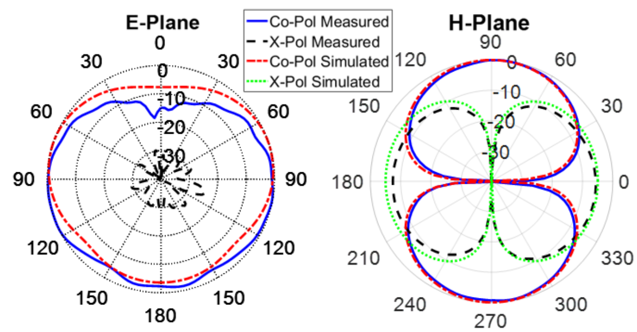

(d)

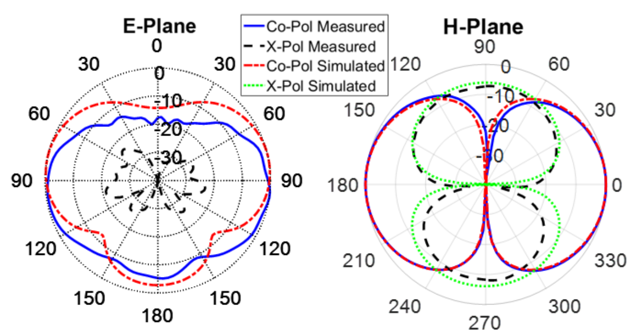

(e)

Fig. 3.10: Measured and simulated far-field radiation patterns; (a) prototype setup in the anechoic chamber, (b) M0, (c) M1, (d) MM1, and (e) MM2.

3.4. Impact of Nearby Objects

As discussed earlier, the system configuration aims to maintain symmetry between the antenna elements, therefore ensuring high isolation between the TX and RX ports. Objects close to the handheld radio can lead to strong scattering toward the antenna elements, which may affect the symmetry and reduce the isolation level. Handheld radios are used by soldiers, therefore, we have studied the impacts of the nearby human body (i.e., hand and head) and the metal helmet on the system isolation. Three common ways of handling the handheld radio close to the human hand and head are shown in Fig. 3.11(a). For each case, we conducted a parametric study on ANSYS HFSS by changing the position of the head relative to fixed locations of the handheld radio and the hand. Specifically, the position of the head changes in the three directions; (1) towards and away, (2) right and left, and (3) top and bottom, with respect to the handheld radio. Total of 64 different positions for the human head are considered in each case of these studies, (i.e., four step increments in each direction).

The simulation results are then imported in the NI AWR software, so when connected to the proposed BFNs (i.e., M1-M0 BFN and MM-M0 BFN) the isolation can be calculated. The results of these sensitivity analysis shown in Fig. 3.11(b)-(d), demonstrate high isolation levels for all the three cases under consideration. The worst-case scenario is when the handheld antenna system is very close to the head (e.g., case III), which still maintains isolation level of more than 24 dB, as shown in Fig. 3.11(d). Moreover, these results illustrate an agreement with the earlier conclusion that MM-M0 BFN is more sensitive to system asymmetry compared to M1-M0 BFN. Nevertheless, the average isolation levels confirm that MM-M0 methodology can achieve higher isolation.

Further analysis of the effect of nearby scatterers has been performed by studying the impact of soldier's metal helmet on the antenna system, as shown in Fig. 3.12(a). Nearby conductive objects can lead to strong electrical interactions with the antenna system, thereby reducing the isolation level. For a worst-case scenario, the helmet material is selected to be a perfect electrical conductor (PEC). Comparison between isolation levels, while considering soldier's head with and without a metal helmet, were performed for the three head orientations of Fig. 3.12(a). The results, shown in Fig. 3.12(b) and (c), illustrate that there is no significant change in isolation levels when the handheld radio is not directly close to the helmet (i.e., cases I and II). But in case III, the antenna system is very close to the helmet, resulting in some reduction in the isolation (> 24 dB). Based on these analyses, the proposed antenna structure illustrates high system stability to nearby objects, maintaining a high level of isolation over the operational bandwidth.

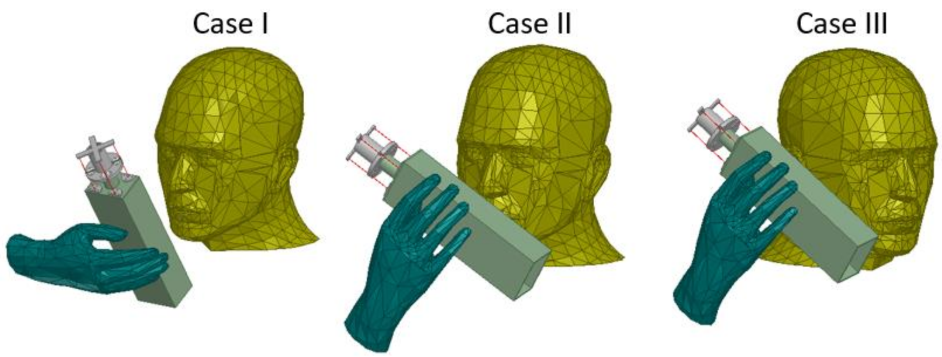

(a)

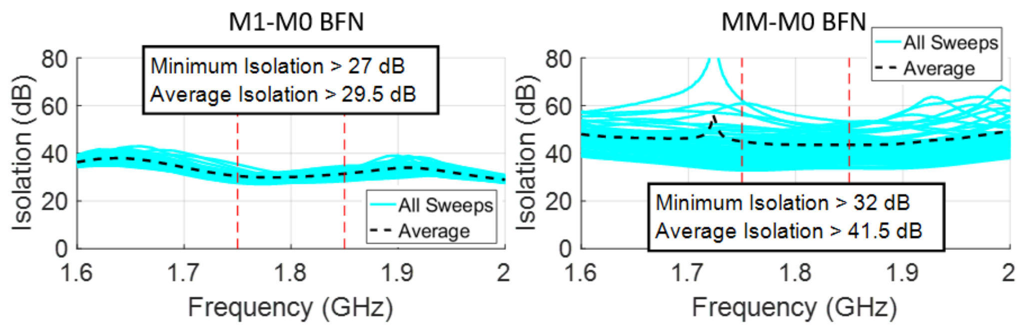

(b)

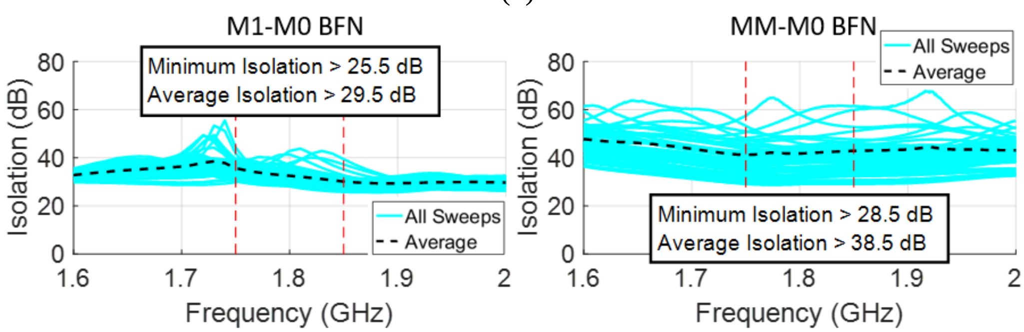

(c)

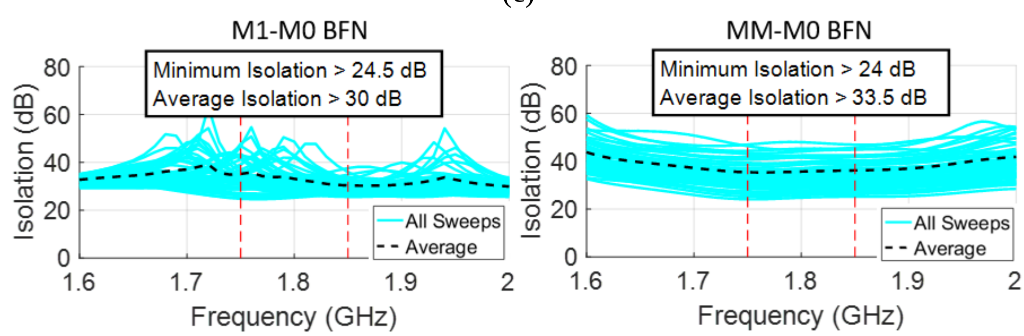

(d)

Fig. 3.11: Impact of nearby human body on system isolation; (a) Three ways of handling the radio, (b) case I, (c) case II, and (d) case III.

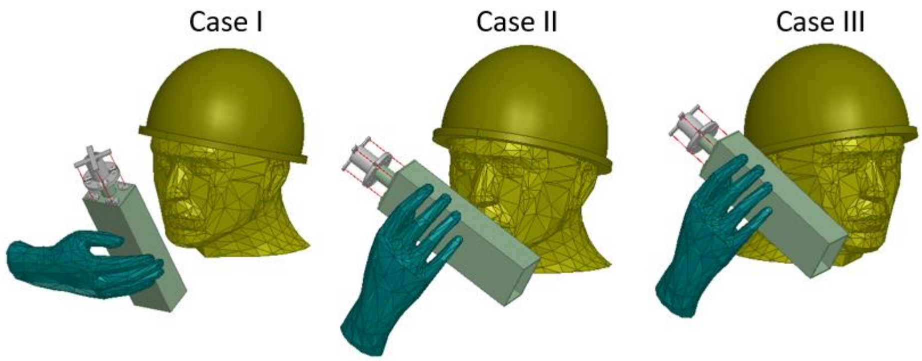

(a)

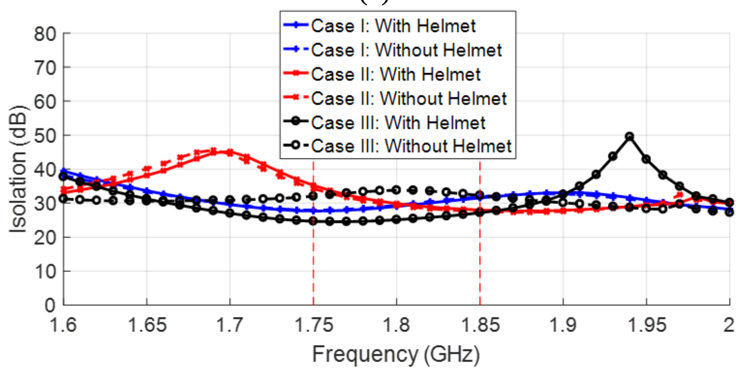

(b)

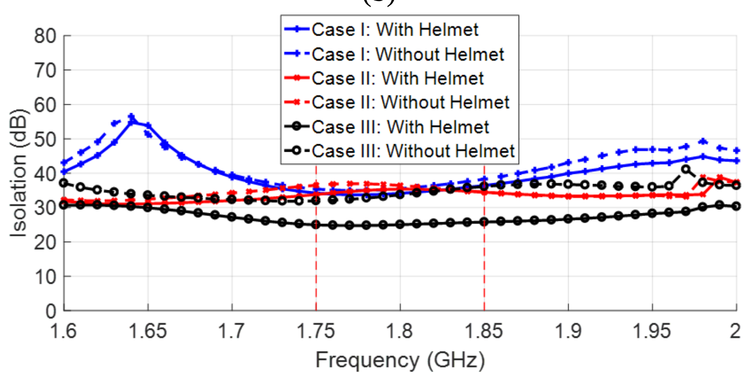

(c)

Fig. 3.12: Comparison between isolation levels with and without metal helmet; (a) Three ways of handling the radio, (b) M1-M0, and (c) MM-M0.

3.5. Feedback Cancellation for Isolation Improvements

Further improvements in the system isolation can be achieved with the feedback cancelation approach shown in Fig. 3.13(a). This method benefits from the leakage in the actual COTS 90° hybrid to cancel the coupled signal ($S_{coupled}$) at RX port. This leaked signal passes through an attenuator and a phase shifter, which are tuned so that the signal S_{leaked} has the same magnitude and opposite in phase with the coupled signal $S_{coupled}$. Consequently, these two signals are canceled at the RX port thereby increasing the system isolation. This technique is more effective in narrowband channels where the compensation of phase imbalances can be achieved relatively easily. Theoretically, this approach can achieve an infinite isolation at a single frequency.

Accordingly, a tunable attenuator and a tunable phase shifter can achieve high isolations at some discrete channels, as shown in Fig. 3.12(b). As seen, isolation of more than 60 dB is achieved at discrete channels of more than 5 MHz bandwidth, which is the RF channel bandwidth of the handheld radio under consideration [26]. This methodology is also very effective when using a dynamically tuned attenuator and phase shifter to overcome the impact of nearby scatterers.

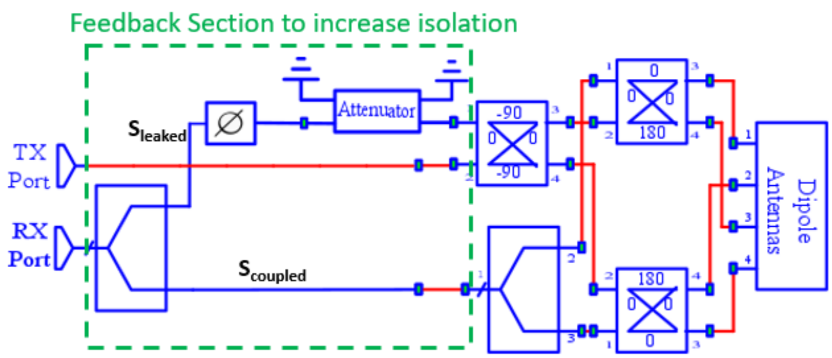

(a)

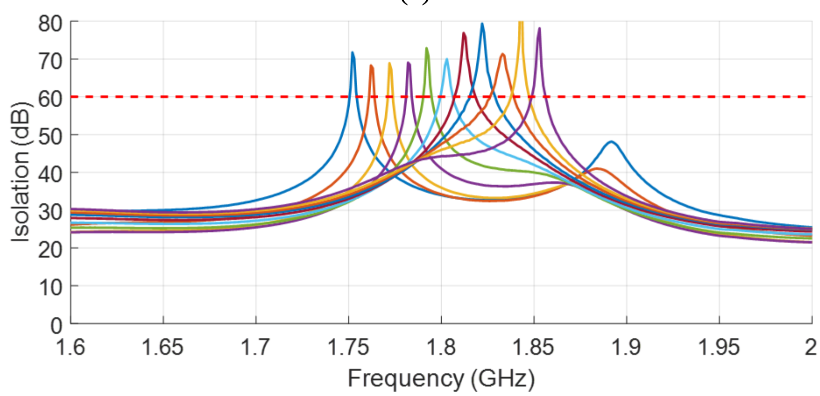

(b)

Fig. 3.13: Feedback cancelation technique, (a) M1-M0 BFN, and (b) Isolation.

3.6. Discussion

This section discusses other ideas that can be implemented using the proposed dipole array antenna system.

3.6.1. Direction Finding

The proposed antenna system that composed of a circular array of four dipoles can also be used for direction finding based on M1-M0 BFN. In this case, both ports of the BFN (M1 and M0 ports) operate in the receive mode. Fig. 3.14(a) shows the phase variation of the received signal with the change of the azimuth angle (ϕ) for both M1 and M0. As seen, the phase of M0 is almost constant, while the phase of M1 changes linearly with ϕ. As a result, computing the difference in phase between received signals of M1 and M0 can indicate the azimuth direction ϕ of the received signal, as shown in Fig. 3.14(b).

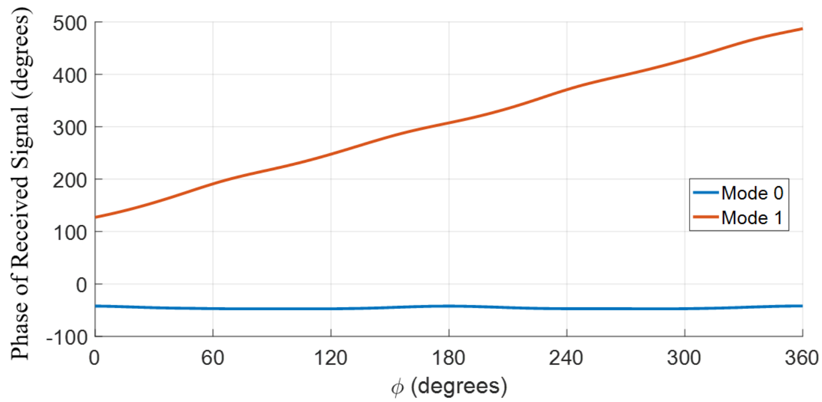

(a)

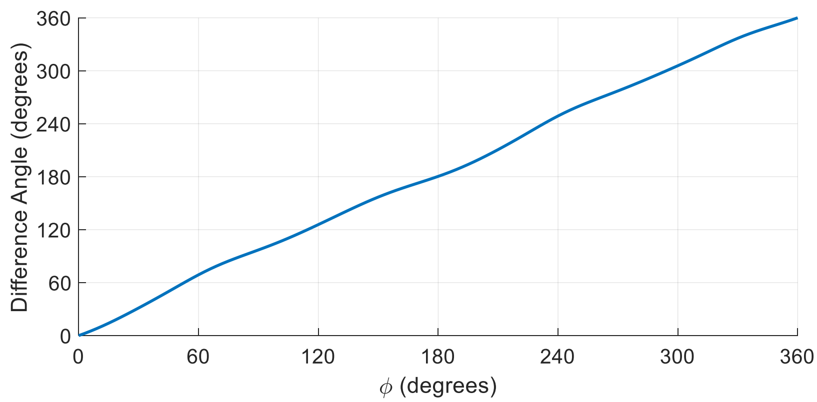

(b)

Fig. 3.14: Direction finding (a) received signal phase for M1 and M0 versus azimuth direction angle, and (b) differential phase of M1-M0.

3.6.2. Antenna Rotation Technique

As previously discussed, MM-M0 BFN topology ensures high isolation between TX and RX ports. However, one of the main limitations of this BFN configuration is the nulls located in the radiation patterns, as shown in Fig. 3.6(a) and (b). We mentioned earlier that switching between MM1-M0 and MM2-M0 can overcome this limitation. Another possibility to address this issue is to allow mechanical rotation of the four dipoles around the metallic mast, as shown in Fig. 3.15(a). Therefore, the directive beams of M1-M0 topology can be freely directed to any azimuth angle ϕ, as shown in Fig. 3.15(b), based on the direction of communication. Due to the asymmetric shape of the handheld radio, we calculated the isolation level for MM-M0 at all azimuth angles ϕ, as shown in Fig. 3.15(c), which demonstrate high isolation of > 43 dB, with considered actual COTS BFN.

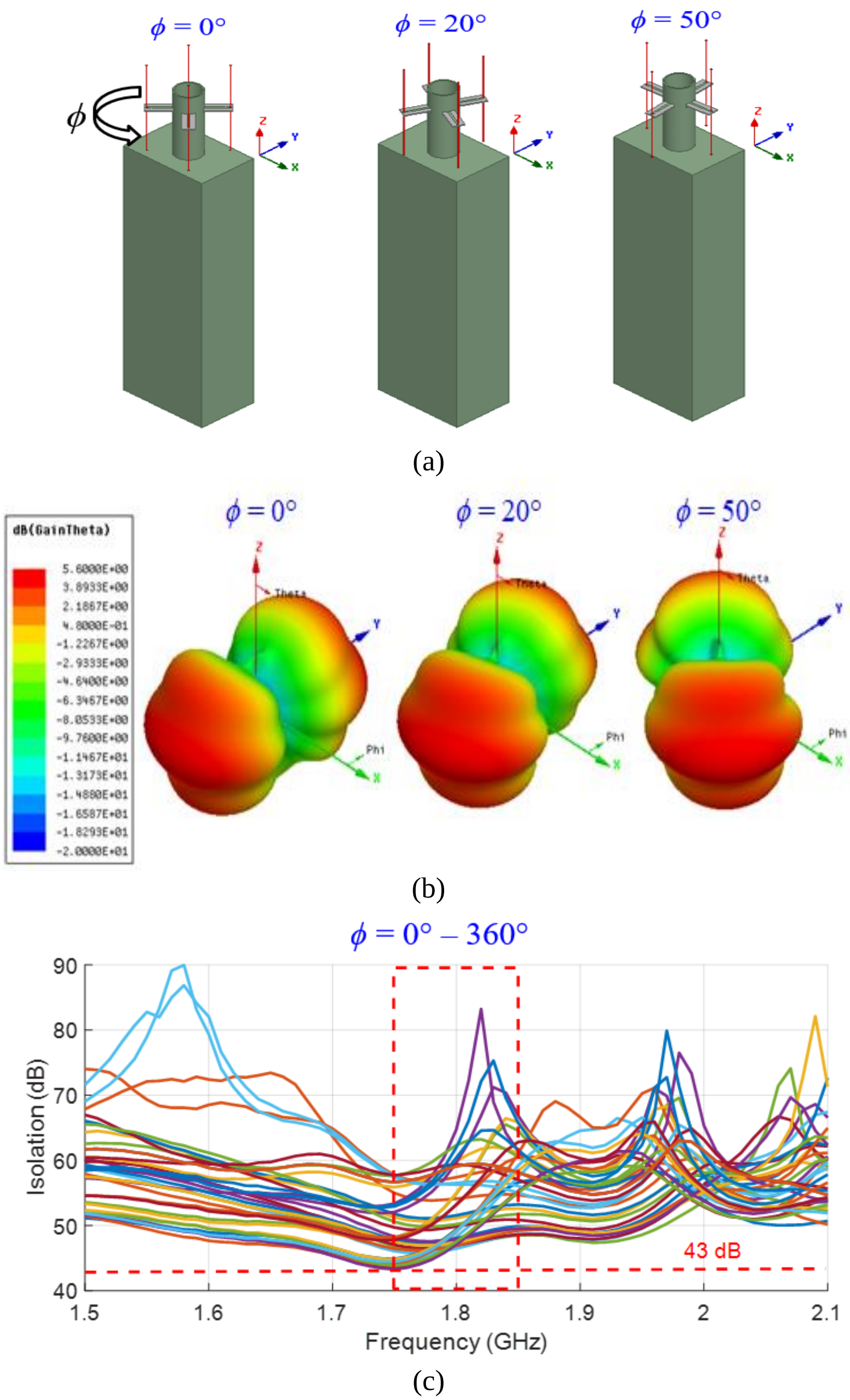

Fig. 3.15: Antenna rotation technique, (a) antenna array mechanical rotation, (b) corresponding 3D gain patterns, and (c) isolation levels.

3.6.3. Tuning Antenna to Lower Frequencies

As mentioned in Section 3.2.1, the handheld radio under consideration [26] operates over three frequency bands, 225-450 MHz, 1250-1390 MHz, and 1750-1850 MHz. We designed the antenna system to cover the highest band (i.e., 1750-1850 MHz) due to the limited space on the top of the handheld radio. Nevertheless, we studied the possibility of tuning the same antenna configuration to cover lower frequency bands while monitoring isolation levels. A matching circuit composed of four identical paths; each path has an inductor and a capacitor, is connected to the four dipole antennas. The matching circuit is tuned to a single frequency at the center of the middle frequency band (i.e., 1.32 GHz) of the handheld radio. A feedback cancelation section is added to ensure high isolation levels for both M1-M0 and MM-M0 configurations, as shown in Fig. 3.16(a) and (b), where a transmission line is used as a phase shifter. The simulation results, shown in Fig. 3.16(c) and (d), demonstrate good antenna matching and high isolation levels at the dedicated frequency for both BFN topologies. This, in turn, validates the proposed methodology for tuning the antenna system to operate at lower frequency bands.

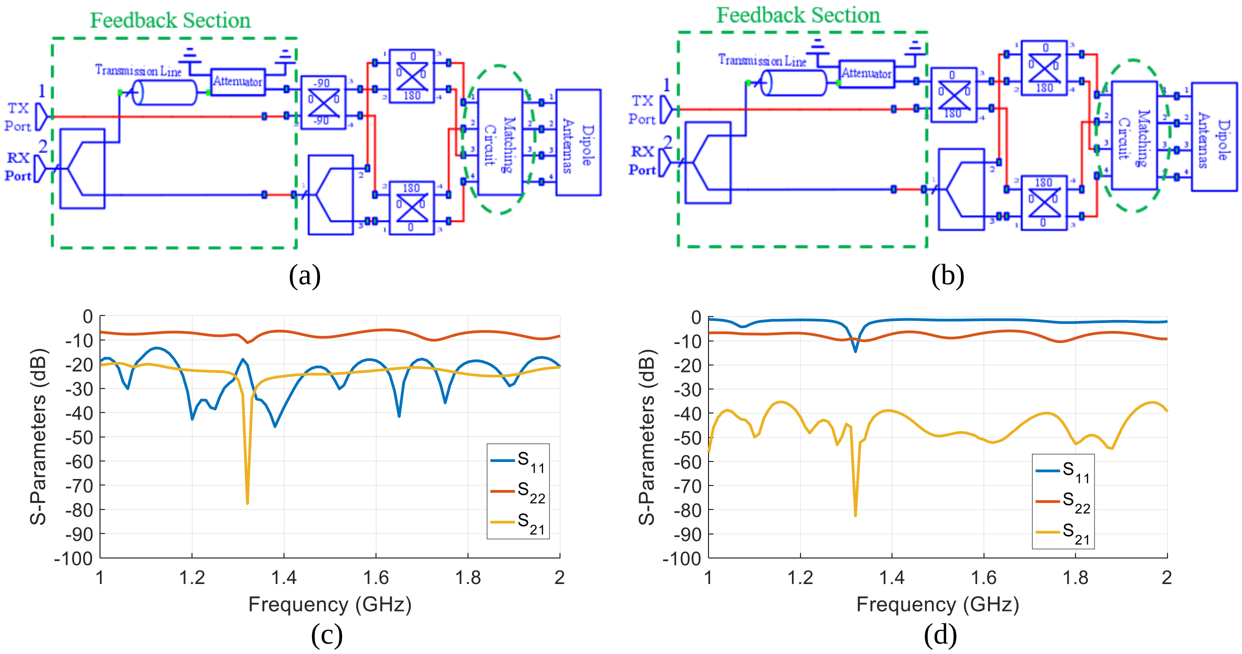

Fig. 3.16: Tuning antenna system to lower frequency band, (a) M1-M0 configuration, (b) MM-M0 configuration, (c) M1-M0 S-parameters, and (d) MM-M0 S-parameters.

3.7. Handheld Antenna System without BFN

This section presents another antenna system that can be implemented on the handheld radio platform. Two orthogonal and symmetric bifilar helix antennas, shown in Fig. 3.17(a), exhibit high isolation between the two input ports (i.e., > 45 dB) over the operational bandwidth (see Fig. 3.17(b)).

Fig. 3.17(c) shows the gain patterns of the antenna system, which illustrates circularly-polarized bidirectional radiation along the axial plane. This antenna configuration has several advantages such as, no need of a BFN, the ease of fabrication, and the availability of circularly polarized radiation patterns. For practical reasons, the handheld radio is included in the full-wave simulation to consider the impact of its asymmetric shape, as shown in Fig. 3.18(a). As seen in Fig. 3.18(b), the system isolation > 31.5 dB is maintained over the entire band in spite of reduction in isolation. The antenna gain patterns show some changes in the back lobe due to the shape of the handheld radio, as shown in Fig. 3.18(c). Further study on the impact of the soldier's body and the metal helmet is performed, as shown in Fig. 3.19, and the results demonstrate high isolation level > 26 dB over the operational bandwidth. Based on this study, the proposed quadrifilar helix antenna is a good candidate to be implemented on handheld radio platforms to enable a full-duplex operation.

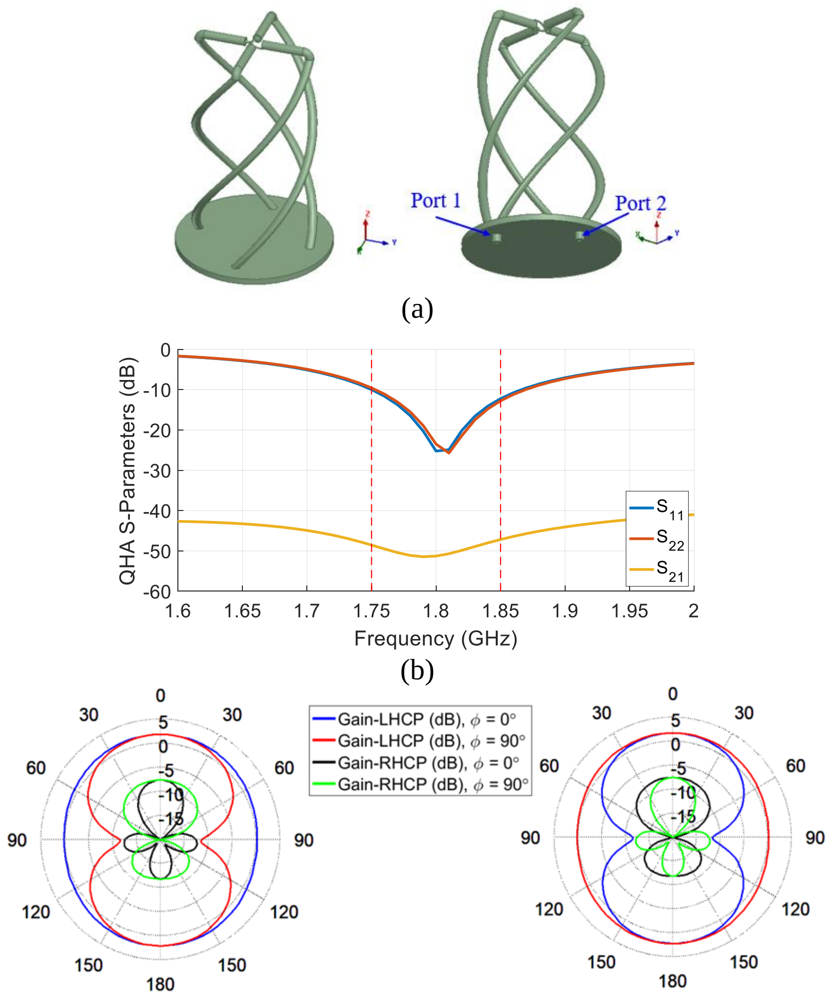

(c)

Fig. 3.17: (a) Two orthogonal bifilar helix antenna (quadrifilar helix antenna), (b) S-parameters, and (c) gain patterns.

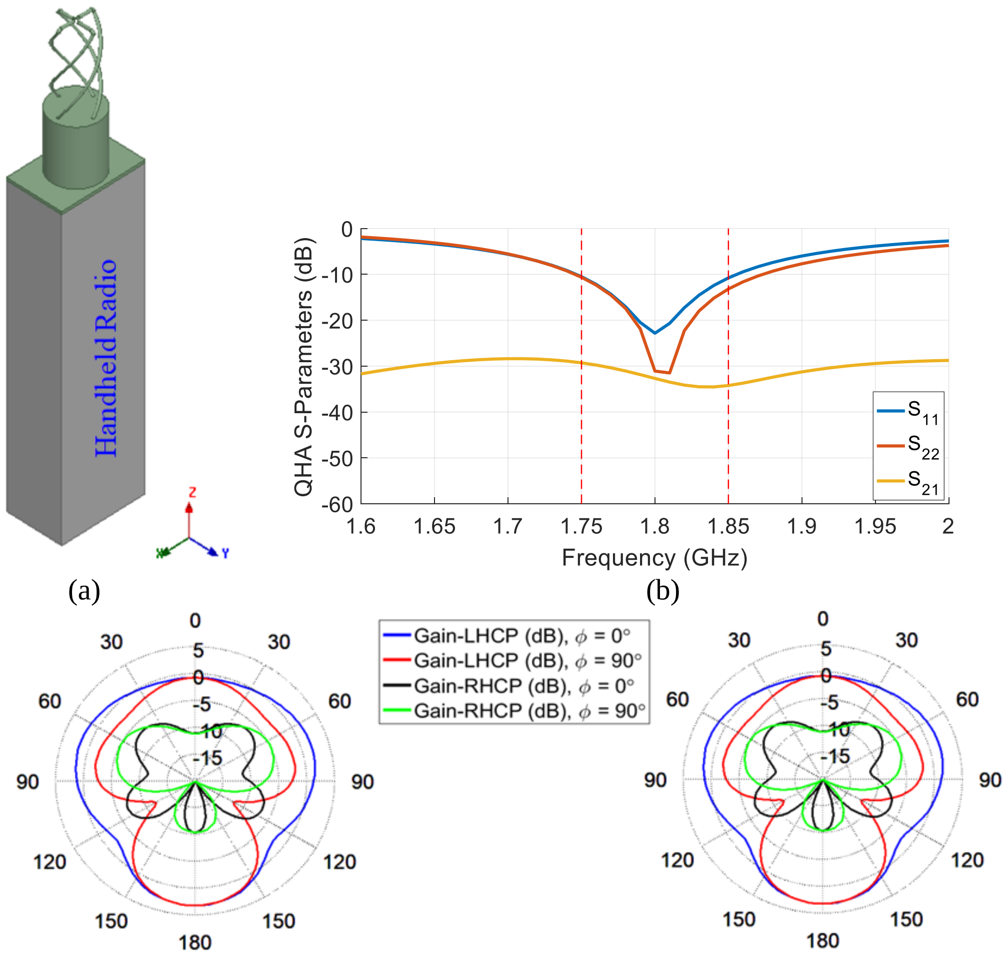

(c)

Fig. 3.18: (a) Quadrifilar helix antenna implemented on a handheld radio, (b) S-parameters, and (c) gain patterns.

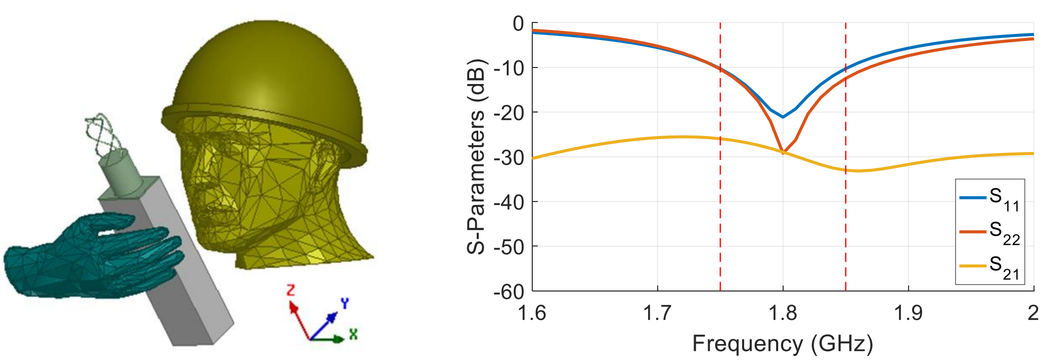

(a) (b)

Fig. 3.19: Impact of nearby soldier's body and metal helmet (a) simulation model, and (b) S-parameters.

3.8. Conclusion

This chapter discussed a monostatic STAR antenna system, designed for typical handheld radios. The antenna structure is composed of four identical half-wavelength dipole antennas, arranged in a circular array, and placed on the top of the handheld device. BFN is used to feed the dipoles in two orthogonal phase modes, thereby ensuring high isolation between TX and RX ports. The proposed antenna configuration is designed for narrowband (i.e., 1.75–1.85 GHz) radio systems. To validate the design, a system prototype is fabricated and tested using COTS BFN components. The measurement results demonstrate an isolation level of more than 30 dB, between TX and RX ports, over the operational bandwidth. Measured radiation patterns are in good agreements with the simulation results. Moreover, the impact of system imbalances, due to magnitude and phase errors in realistic BFN components and effect of nearby soldiers, are carefully studied. The sensitivity analysis shows the maintenance of high isolation levels of more than 24 dB over the entire frequency band. Further improvement in system isolation i.e., more than 60 dB, is achieved over narrow band channels, using feedback cancellation technique. Further studies on the dipole array antenna were carried out, demonstrating the antenna operation for direction finding, and the possibility of tuning the antenna to cover lower frequency bands. Furthermore, another antenna configuration, based on a quadrifilar helix antenna, can be implemented on a handheld radio platform, to achieve high isolation levels without the need for a BFN.

References

[1] D. Bharadia, E. McMilin, and S. Katti, "Full duplex radios," in *Proc. SIGCOMM'13 conf.*, 2013.

[2] J. Choi, M. Jain, K. Srinivasan, P. Levis, and S. Katti, "Achieving single channel, full duplex wireless communication," in *Proc. 16th Annual Int. Conf. on Mobile Comp. and Net.*, July 2010.

[3] A. Sabharwal, P. Schniter, D. Duo, D. W. Bliss, S. Rangarajan, and R. Wichman, "In-band full-duplex wireless: challenges and opportunities," *IEEE Trans. Selected Areas in Comm.*, Oct. 2014.

[4] J. L. Allen and B. L. Diamond, *Mutual Coupling in Array Antennas*, MIT Lincoln Lab., Cambridge, MA, EDS-66-443, 1966.

[5] O. N. Alrabadi, A. D. Tatomirescu, M. B. Knudsen, M. Pelosi, and G. F. Pederson, "Breaking the transmitter-receiver isolation barrier in mobile handsets with spatial duplexing," *IEEE Trans. Ant. Propag.*, April 2013.

[6] T. Dinc and H. Krishnaswamy, "A T/R antenna pair with polarization-based reconfigurable wideband self-interference cancellation for simultaneous transmit and receive," in *IEEE MTT-S Int. Microw. Symp. Dig.*, May 2015.

[7] F. G. Zhu, J. D.Xu, and Q. Xu, "Reduction of mutual coupling between closely-packed antenna elements using defected ground structure," in *Proc. 3rd IEEE Int. Symp. Microw., Ant., Propag. EMC Techl. Wireless Comm.*, Oct. 2009.

[8] P. V. Prasannakumar, M. A. Elmansouri, and D. S. Filipovic, "Wideband decoupling techniques for dual-polarized bi-static simultaneous transmit and receive antenna subsystem," *IEEE Trans. Ant. Propag.*, Oct. 2017.

[9] B. Chiang and M. Holdip, “Progressively phased circular arrays used in antenna isolation,” in *IEEE Ant. Propag. Soc. Int. Symp.*, Jun. 1974.
[10] K. E. Kolodziej, P. T. Hurst, A. J. Fenn, and L. I. Parad, “Ring array antenna with optimized beam former for simultaneous transmit and receive,” in *IEEE Ant. Propag. Soc. Int. Symp.*, July 2012.
[11] E. Tianang, and D. S. Filipovic, “A dipole antenna system for simultaneous transmit and receive,” in *IEEE Ant. Propag. Soc. Int. Symp.,* July 2015.
[12] B. Chiang and M. Holdip, “Progressively phased circular arrays used in antenna isolation,” in *IEEE Ant. Propag. Soc. Int. Symp.*, Jun. 1974.
[13] T. Snow, C. Fulton, and W. J. Chappell, “Multi-antenna near field cancellation duplexing for concurrent transmit and receive,” in *IEEE MTT-S Int. Microw. Symp.*, Jun. 2011.
[14] A. T. Wegener and W. J. Chappell, “Simultaneous transmit and receive with a small planar array,” in *IEEE MTT-S Int. Microw. Symp.*, June 2012.
[15] W. F. Moulder, B. T. Perry, and J. S. Her, “Wideband antenna array for simultaneous transmit and receive (STAR) applications,” in *IEEE Ant. Propag. Soc. Int. Symp.*, July 2014.
[16] C. Kalialakis, M. J. Cryan, P. S. Hall, and P. Gardner, “Analysis and design of integrated active circulator antennas,” *IEEE Trans. Microw. Theory and Tech.*, Jun. 2000.
[17] G. Lathikre, N. Jolivet, S. Nobilet, R. Gillard, and J. E. Hilard, “A novel balanced circulator for FDD MC-CDMA communications,” in *IEEE 34th Euro. Microw. Conf.*, Oct. 2004.
[18] W. Kim, M. Le, J. Kim, H. Lim, J. Yu, B. Jang, and J. Park, “A passive circulator with high isolation using a directional coupler for RFID,” in *IEEE 36th Euro. Microw. Conf.*, Sep. 2006.
[19] J. L. Young, R. S. Adams, B. O’Neil, and C. M. Johnson, “Bandwidth optimization of an integrated microstrip circulator and antenna assembly: Part 2,” *IEEE Ant. Propag. Mag.*, Jun. 2007.
[20] S. K. Cheung, T. P. Halloran, W. H. Weedon, and C. P. Caldwell, “MMIC-based quadrature hybrid quasi-circulators for simultaneous transmit and receive,” *IEEE Trans. Microw. Theory Tech.*, Mar. 2010.
[21] C. H. Cox and E. I. Ackerman, “Photonics for simultaneous transmit and receive,” in *IEEE MTT-S Int. Microw. Symp.*, Jun. 2011.
[22] S. Tang, C. Lin, and S. Hung, “Ultra-wideband quasi-circulator by cascading distributed balun with phase cancelation technique,” *IEEE Trans. Microw. Theory Tech.*, July 2016.
[23] M. E. Knox, “Single antenna full duplex communications using a common carrier,” in *IEEE Wireless Microw. Tech. Conf.*, Apr. 2016.
[24] E. A. Etellisi, M. A. Elmansouri, and D. S. Filipovic, “Wideband monostatic simultaneous transmit and receive (STAR) antenna,” *IEEE Trans. Ant. Propag.*, Jan. 2016.
[25] J. Ha, M. A. Elmansouri, P. V. Prasannakumar, and D. S. Filipovic, “Monostatic co-polarized full-duplex antenna with left- or right-hand circular polarization,” *Trans. Ant. Propag.*, Oct. 2017.
[26] *AN/PRC-148B MBITR2*, TALES Defense & Security Inc. [Online]. Available: http://www.thalescomminc.com/userimages/Documents/Data%20Sheets/Thales_PRC148B_MBITR2.pdf
[27] ANSYS® Electromagnetic Suite, version 17.2.0.
[28] E. A. Etellisi, M. A. Elmansouri, and D. S. Filipovic, “On wideband monostatic mode-multiplexed simultaneous transmit and receive circular array,” *IEEE Trans. Ant. Propag.*, Under Review.
[29] NI AWR Design Environment, version 13.0.
[30] M. P. Karaboikis, V. C. Papamichael, G. F. Tsachtsiris, and C. F. Soras, “Integrating compact printed antennas onto small diversity/MIMO terminals,” *IEEE Trans. Antennas Propag.*, July 2008.

Chapter 4: STAR Antenna Systems for UAV-Raven

4.1. Introduction

Unmanned aerial vehicles (UAVs) are used to perform tactical missions. To establish a communication link between a UAV and ground, various antennas on UAV platforms were recently proposed [1-5]. This chapter presents three configurations to implement STAR antenna system on a low-cost UAV (i.e., UAS RQ-11 Raven) platform shown in Fig. 4.1. The first configuration is a single dual-polarized patch antenna with balanced circulator feed. When a circulator is used on a monostatic antenna to isolate TX and RX channel, it is well known that the isolation is limited by the return loss of the antenna element. To overcome this, balanced circulator configuration is proposed in [6, 7]. The balanced circulator can achieve improved isolation by canceling the reflected signal from antenna port while radiation patterns of TX and RX are identical. Also, both left-handed circular polarization (LHCP) and right-handed CP (RHCP) are supported (dual-polarized). This approach is applied with a dual-polarized patch antenna element, and its flush-mounted integration on the belly of UAV is presented as the first method. The second approach is the use of a sequential rotation array (SRA) of dual-polarized antennas and two Butler matrix beamforming networks (BFN) [8]. The second approach also offers co-polarized TX and RX, dual-CP, and theoretically infinite isolation. This method is applied with the same dual-pol patch element, and its conformal integration on the tail of UAV is presented. The third considered approach is exciting two orthogonal modes on the UAV body based on the characteristics mode analysis (CMA) [9]. One characteristic mode operates for transmitting and the other mode for receiving. Due to the orthogonality of characteristic modes, high isolation between TX and RX is expected.

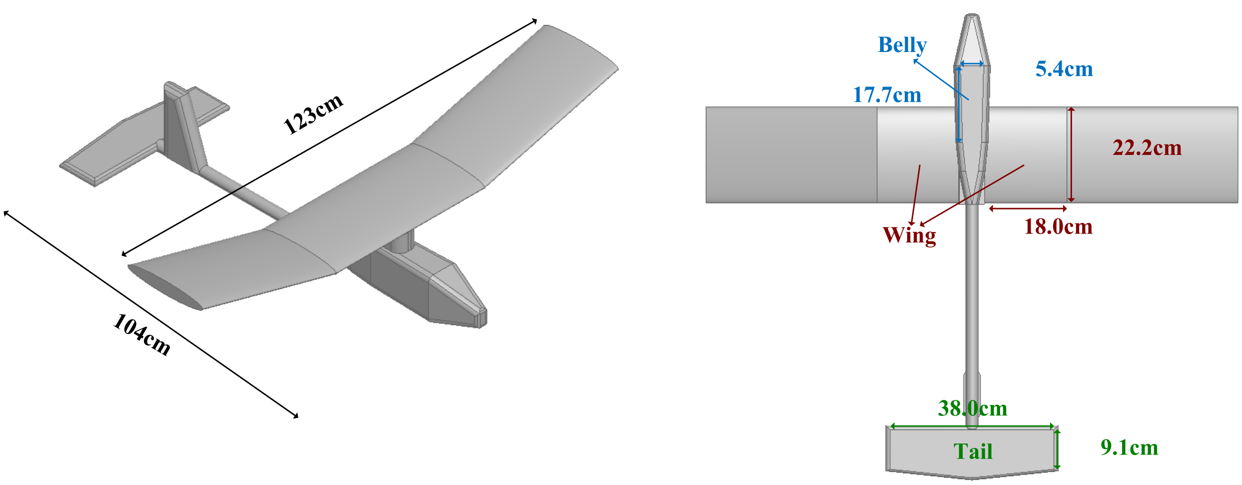

Fig. 4.1: Model of UAS RQ-11 Raven.

4.2. Balanced Circulator

Fig. 4.2 shows the balanced circulator BFN. The composed of two circulators and two 90° hybrids. Two output ports of the BFN is connected to two orthogonal ports of the antenna. With this configuration, the reflected signals from V- and H-pol ports are canceled at the RX port due to the 90° hybrids, resulting in high isolation. When $load_1$ is used as TX port and $load_2$ is used as RX port, the polarization is changed to the other sense. Detailed analysis of the balanced circulator is provided in Chapter 2.

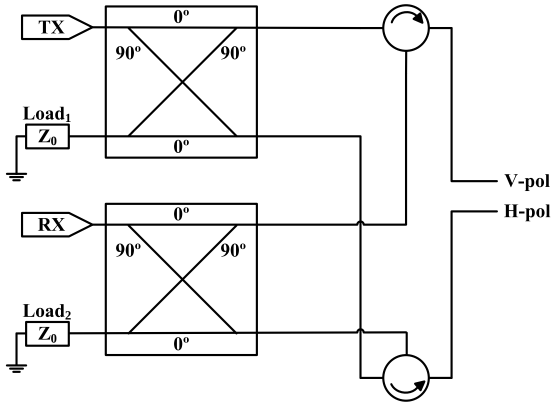

Fig. 4.2: Configuration of the balanced circulator.

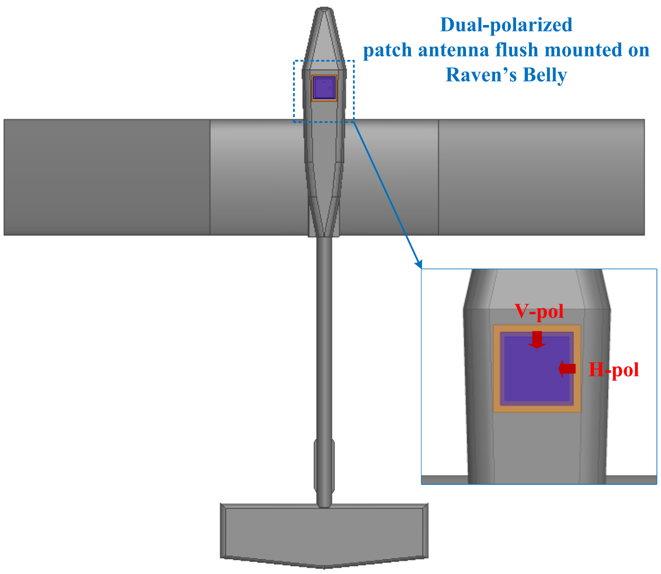

Fig. 4.3: Dual-polarized microstrip patch flush-mounted on the Raven's Belly.

A dual-polarized microstrip patch antenna is designed on Rogers TMM-4 dielectric (ε_r = 4.5, tanδ = 0.002) and is flush-mounted on the belly of UAV raven as shown in Fig. 4.3. The size of the dielectric board is 50 mm × 50 mm × 1.524 mm and that of the patch is 36.5 mm × 36.5 mm. As seen, the antenna system can be integrated with UAV Raven without causing any air drag. The isolation and return loss of the proposed STAR antenna system on UAV platform are shown in Fig. 4.4(a). Isolation higher than 20 dB is achieved over 1750–1850 MHz. Note that the isolation is limited by the coupling between V- and H-pol ports of the patch. Fig. 4.4(b) shows the radiation pattern of the antenna on the UAV. As seen, symmetric CP patterns are achieved with cross-pol rejection better than 20 dB at the boresight.

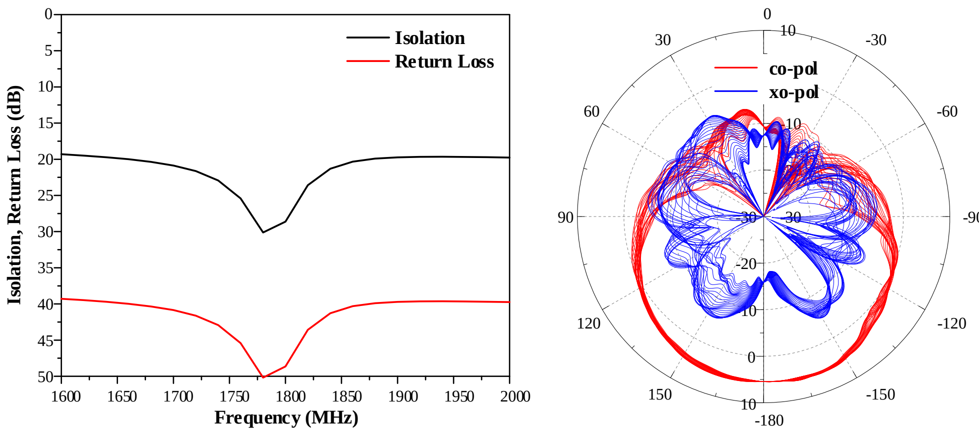

(a) (b)

Fig. 4.4: Performance of the STAR antenna system (patch with balanced circulator) on the Raven's belly. (a) Isolation and return loss. (b) Radiation pattern.

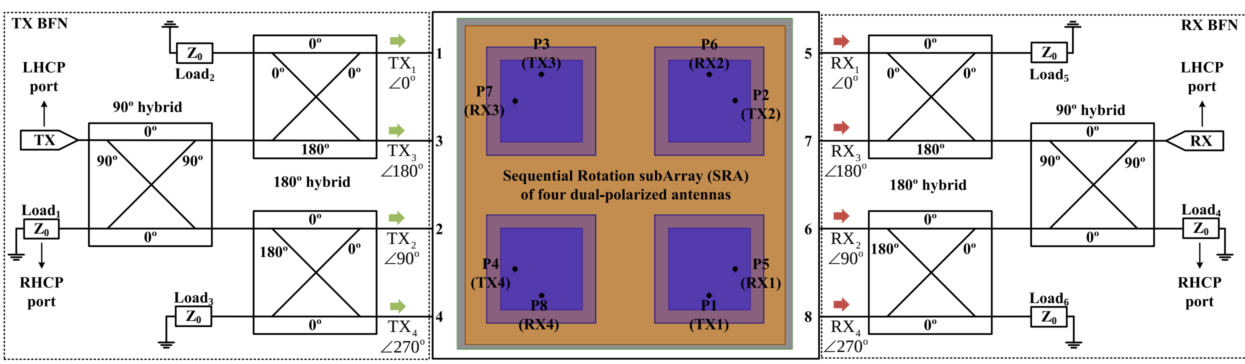

Fig. 4.5: Configuration of the proposed SRA STAR antenna system composed of four dual-polarized patch antennas and two Butler matrix BFNs.

4.3. Sequential Rotation Array (SRA) of Dual-Pol Patch Elements

Fig. 4.5 shows the configuration of the proposed STAR SRA antenna system. The system consists of SRA of four dual-polarized antenna elements and two modified Butler matrix BFNs. Each antenna has orthogonal TX and RX ports. Each set of TX and RX ports is excited with 90° phase progression by using two BFNs, one for the TX and the other for the RX channel. Since the phase progression along TX and RX SRAs are the same, the patterns of TX and RX antennas are co-polarized. The BFNs are modified Butler matrix type consisting of a 90° hybrid and two 180° hybrids interconnected to produce 90° phase progression across four output ports. When alternative TX and RX ports, denoted as load1 and load4, respectively, are excited, the phase progression is reversed and polarization becomes RHCP. In the proposed STAR antenna system, couplings from TX to RX ports are canceled with each other owing to the geometric symmetry of the SRA and phase progression of BFNs; thus, infinite isolation is achieved theoretically. In practice, the isolation is limited by asymmetry of SRA and imbalances of BFN.

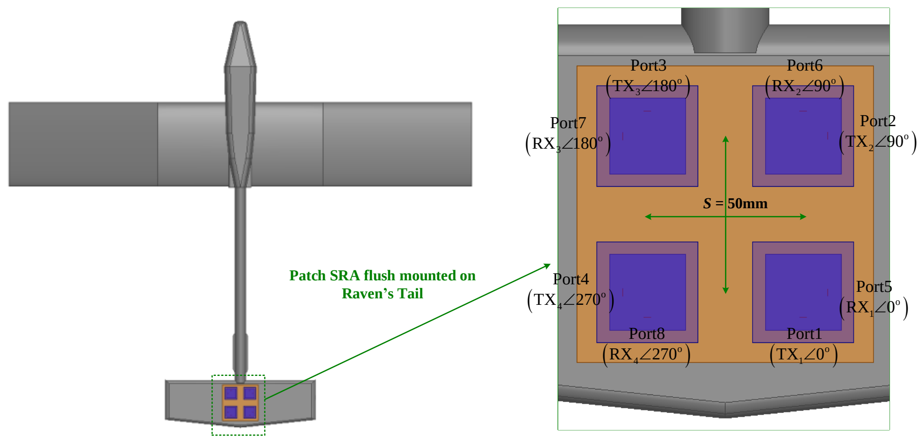

Fig. 4.6: STAR SRA flush-mounted on the tail of UAV Raven.

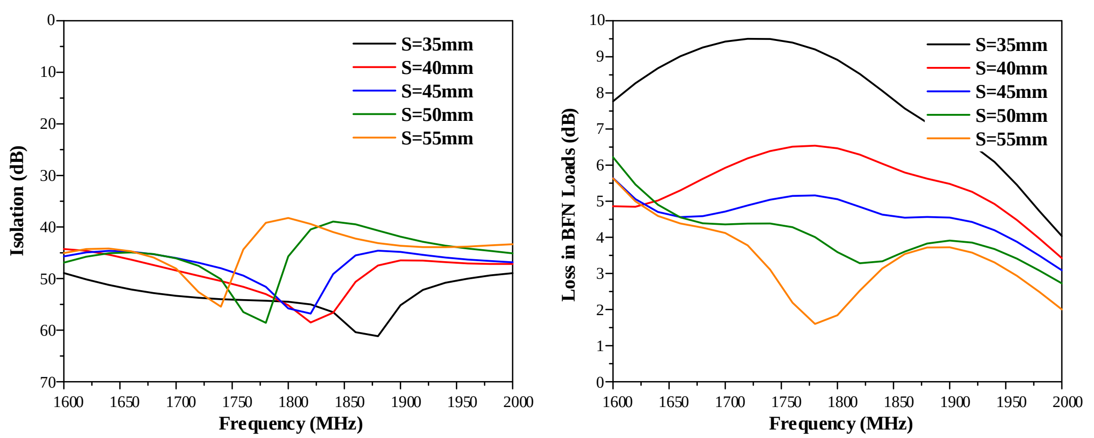

(a) (b)

Fig. 4.7: (a) Isolation and (b) loss in BFN loads for various spacing between patch elements.

Fig. 4.6 shows the proposed STAR SRA antenna system flush-mounted on the tail of UAV Raven. Due to the larger size of antenna system compared to the single patch with the balanced circulator, the tail is considered for antenna platform instead of belly. The spacing between patch elements is a critical design parameter for the proposed STAR antenna system. Fig. 4.7(a) shows the isolation for various spacing. As the spacing increases, the isolation is degraded since the geometrical symmetry is disturbed by the UAV. However, the increased spacing leads to less power loss in the BFN loads as shown in Fig. 4.7(b) due to the reduced coupling. Note the coupled power is dissipated at BFN loads. To achieve less loss and moderate isolation, the spacing is chosen to be 50 mm. The gain and radiation pattern of the STAR antenna on the tail of Raven are shown in Fig. 4.8(a) and (b), respectively. Gain higher than 7dBic is achieved over 1750–1850 MHz with symmetric CP patterns.

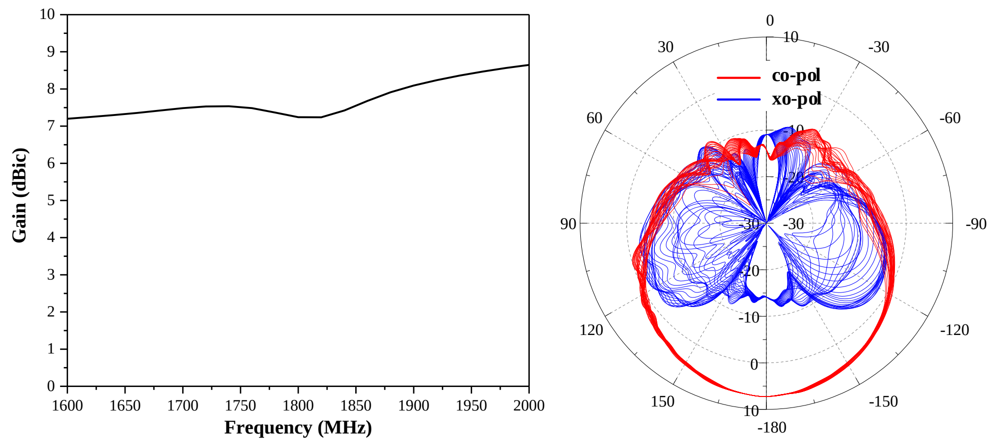

(a) (b)

Fig. 4.8: (a) Gain and (b) radiation pattern of the STAR antenna on Raven with S = 50mm.

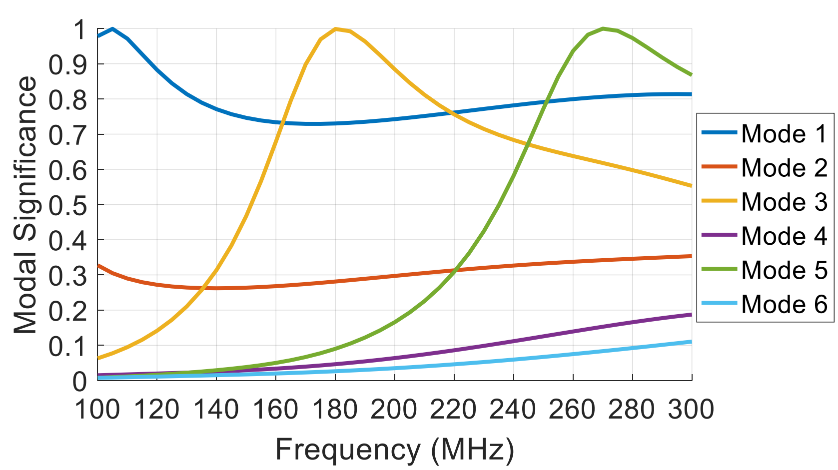

Fig. 4.9: Modal significance of UAV-Raven.

4.4. Characteristic Mode Analysis (CMA) Based Approach

Characteristic mode analysis (CMA) is carried out using FEKO software. Model significance results, shown in Fig. 4.9, indicate that the modes “mode 1 – mode 3” at 180 MHz and “mode 1 – mode

5” at 270 MHz are orthogonal. If we successively excite any of these orthogonal modes for TX and RX, high isolation could be achieved. The surface current distributions and radiation patterns, based on CMA, of modes 1 and 3 at 180 MHz are plotted in Fig. 4.10. The objective is to excite these modes using antenna elements. This is an interesting theoretical approach; however, more studies are needed to assess its practical significance.

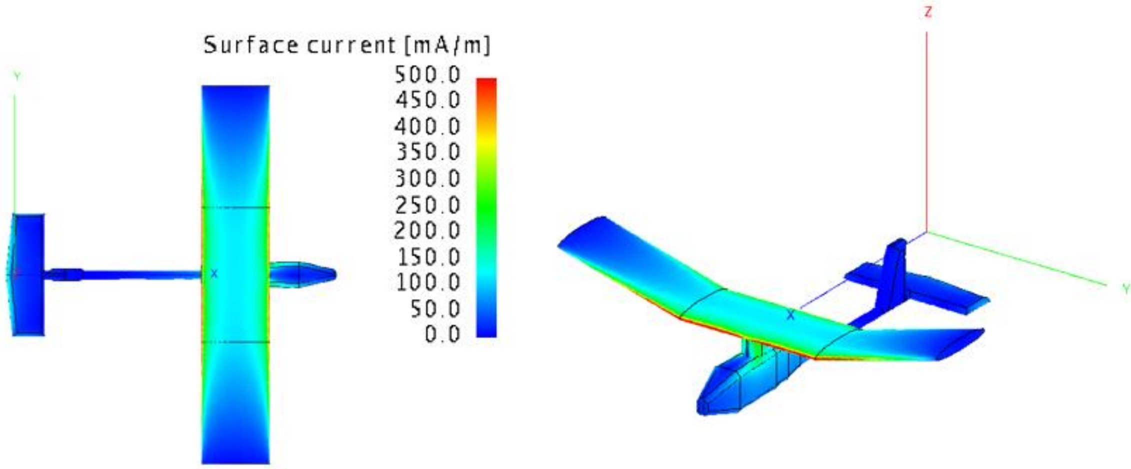

(a)

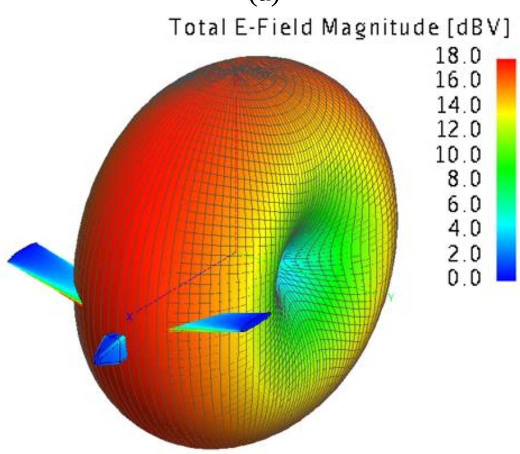

(b)

Fig. 4.10: Mode 1 based on CMA, (a) current distribution, and (b) 3D radiation pattern.

4.4.1. Mode 1 Excitation

Based on CMA results of Fig. 4.10(a), mode 1 can be generated using two dipole antennas parallel to the front and back edges of the UAV wings, as shown in Fig. 4.11(a). Surface current distributions and radiation patterns obtained by the proposed antenna design using ANSYS HFSS, as shown in Fig. 4.11, demonstrate good agreements with those obtained by CMA in Fig. 4.10. Based on these results, mode 1 is successfully generated.

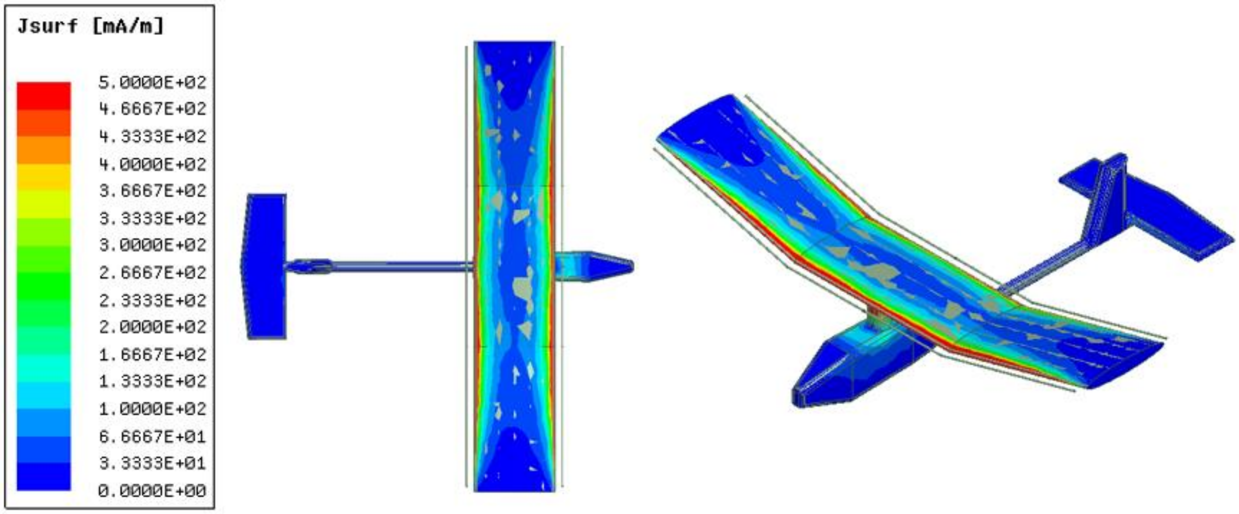

(a)

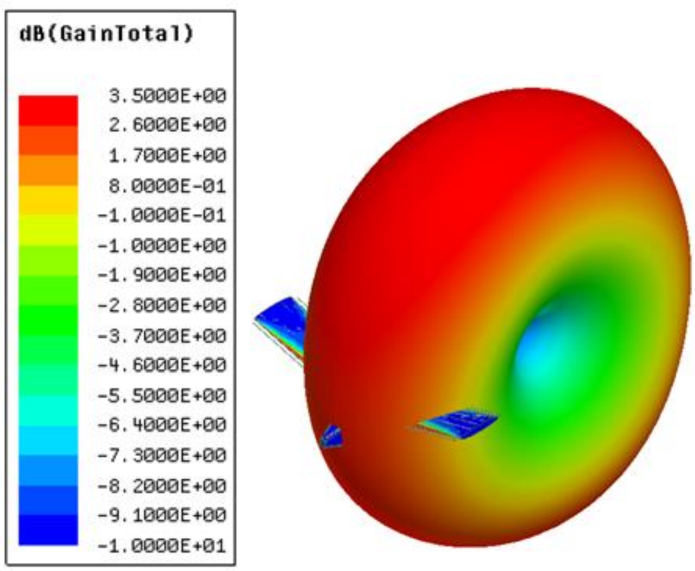

(b)

Fig. 4.11: Mode 1 excitation using two dipole antennas, (a) current distribution, and (b) 3D radiation pattern.

4.4.2. Mode 3 Excitation

Excitation of mode 3 is considerably more challenging, as shown in the surface current distribution and radiation patterns of Fig. 4.12(a). To generate the required surface currents on the wings, we aim to use the same antenna elements that generate mode 1, but for different locations of the ports.

The surface current distribution and radiation patterns obtained from this design are still unsatisfactory, and further effort is still required.

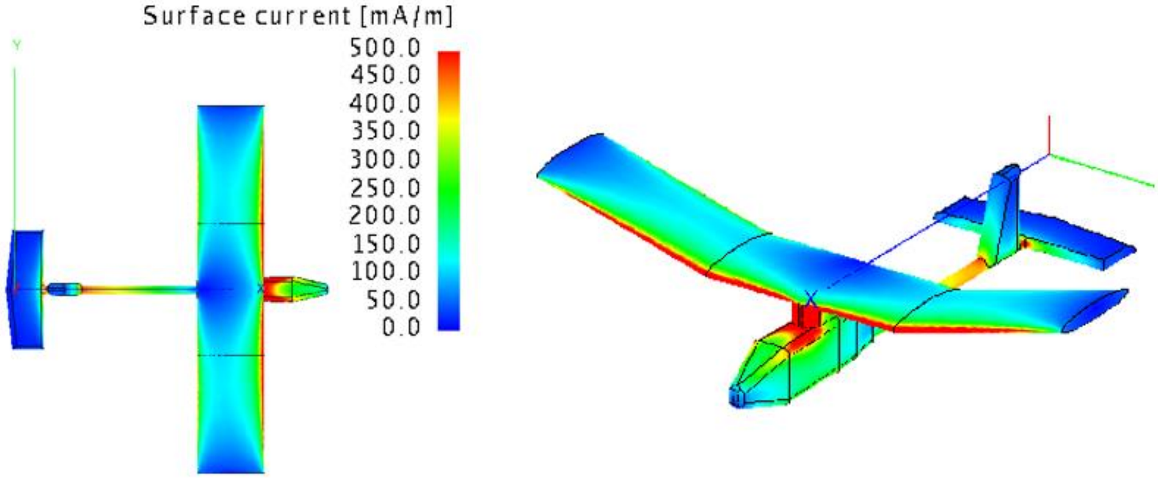

(a)

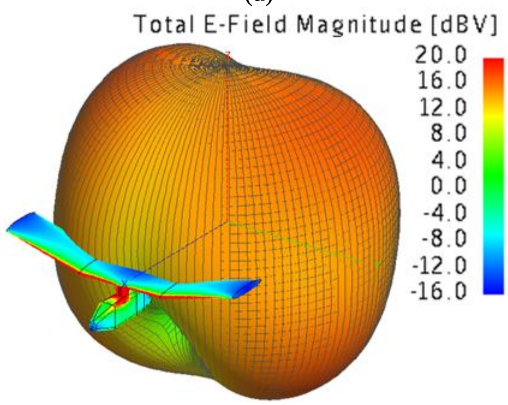

(b)

Fig. 4.12: Mode 3 based on CMA, (a) current distribution, and (b) 3D radiation pattern.

4.5. Summary

Three approaches to realize STAR antenna system on the UAV Raven are considered. Balanced circulator BFN with a single patch antenna can be installed on the belly of Raven conformal. The achieved isolation is higher than 20 dB over 1750–1850 MHz bandwidth and dual-CP performance can be obtained. Further improvement can be obtained with a patch antenna designed for higher cross-polarized isolation. The SRA of four patch antennas integrated on the body of the UAV is also proposed. Two Butler matrix BFNs are used to produce 90° phase progression and therefore achieve high isolation of > 38 dB between the TX and RX channels, whilst identical radiation patterns and polarization are obtained for both channels. Lastly, the CMA of UAV body is conducted and two orthogonal modes are excited by dipole elements. High isolation can be achieved due to the modal orthogonality.

References

[1] M. Sharawi, D. Aloi, and O. Rawashdeh, “Design and implementation of embedded printed antenna arrays in small UAV wing structures,” *IEEE Trans. Ant. Propag.,* 2010.

[2] Y. Yohandri, V. Wissan, I. Firmansyah, P. Rizki Akbar, J. T. Sri Sumantyo, and H. Kuze, “Development of circularly polarized array antenna for synthetic aperture radar sensor installed on UAV,” *Progress In Electromag. Research C,* 2011.

[3] A. Patrovsky and R. Sekora, “Structural integration of a thin conformal annular slot antenna for UAV applications,” *Loughborough Ant. Propag. Conf., LAPC,* 2010.

[4] P. Park, S. Choi, D. Lee, B. Lee, “Performance of UAV (unmanned aerial vehicle) communication system adapting WiBro with array antenna,” *Int. Conf. Adv. Comm. Tech., 2009.*

[5] C. Cheng, P. Hsiao, H. T. Kung, and D. Vlah, “Performance measurement of 802.11a wireless links from UAV to ground nodes with various antenna orientations, *Proc. Int. Conf. Comp. Comm. Network, ICCCN,* 2006.

[6] W. Kim and J. Yu, “Balanced circulator structure with enhanced isolation characteristics,” *Micrw. Opt. Tech. Lett.,* pp.2389-2391, 2008.

[7] M. Knox, “Single antenna full duplex communications using a common carrier,” *WAMICON,*

[8] J. Ha, M. A. Elmansouri, P. V. Prasannakumar, and D. S. Filipovic, “Monostatic co-polarized full-duplex antenna with left- or right-hand circular polarization,” *IEEE Trans. Ant. Propag*., pp. 5103-5111, Oct. 2017.

[9] Y. Chen, C.-F. Wang, “Electrically small UAV antenna design using characteristic modes,” *IEEE Trans. Ant. Propag.,* pp. 535-545, Feb. 2014.

Chapter 5: Conclusion

5.1. Summary

In-band full duplex or simultaneous transmit and receive (STAR) antenna systems for selected tactical platforms are studied on this program. The proposed antenna systems demonstrate high isolation between TX and RX channels without space, frequency, time, or polarization multiplexing; therefore, they may facilitate the future realization of US Army's wireless systems with STAR capability. Three different platforms are considered in this study: line-of-sight (LOS) microwave relay dish antenna, handheld radio, and unmanned aerial vehicle (UAV). For each platform, several approaches to implement STAR antenna are proposed. Most of the considered approaches are experimentally verified with the relevant mockup models.

5.1.1. Line-of-Sight STAR System

A wideband monostatic high gain, high isolation reflector based STAR approach is proposed for a point-to-point microwave link. The configuration relies on a balanced circulator beamforming network (BFN) to achieve high isolation between TX and RX. Using commercial-off-the-shelf (COTS) components with noticeable imbalances in amplitude and phase, average isolation of >30 dB is demonstrated with the fabricated system. Additionally, it is shown that the asymmetry in the antenna geometry and the BFN can significantly influence the isolation of the system. To minimize the dependency of system isolation on imbalances and asymmetries, a novel quasi-monostatic high gain reflector based STAR antenna configuration is proposed. High isolation between TX feed and RX is achieved by using high front-to-back ratio (FBR), low cross-pol level coaxial cavity antennas, and by operating the feeds in circularly polarization (CP). System isolation >70 dB is achieved with ideal BFN and average measured isolation of 61 dB is achieved with COTS BFN components. Moreover, it is shown that the quasi-monostatic approach described herein is more robust to imbalances and asymmetries in the BFN and antenna geometry, respectively.

5.1.2. Handheld Radio Antenna System

A monostatic STAR antenna system is proposed for handheld radio platforms. The radiating element is a circular array of four dipole antennas on top of the radio device. The BFN is designed to provide two orthogonal phase modes for TX and RX, therefore ensuring high (theoretically infinite) isolation. The BFN is composed of one 90° hybrid, two 180° hybrids, and one power divider. Mode 1 (M1) used for TX has quadrature phase progression along the dipoles, whereas Mode 0 (M0) used for RX has an in-phase feed for all dipole elements. Both modes have omnidirectional, vertically polarized radiation patterns. A prototype is fabricated and tested to validate the theory. The measured isolation is higher than 30dB over 1750–1850 MHz range. The isolation is limited by imbalances in the BFN and imperfect symmetry due to nearby objects. A sensitivity study is performed to understand the impact of these imperfections including soldier's presence. To compensate for the imperfections, feedback cancelation layer can be added. It is demonstrated that the feedback cancelation layer can improve isolation to >60dB over a narrow instantaneous bandwidth. Other possible applications of the proposed antenna system are discussed including direction finding. Finally, a simple and novel configuration without BFN based on quadrifilar helix antenna is also considered.

5.1.3. STAR Antenna Systems for UAV Raven

Three STAR antenna systems for UAV Raven platform are also researched. Balanced circulator BFN used for LOS STAR reflector antenna system in Chapter 2 is used here to feed a dual-polarized patch antenna element, and the conformal antenna system is integrated on the belly of the Raven. The isolation >20dB is achieved from 1750 MHz to 1850 MHz. TX and RX have the same polarization, which can be either left-handed CP (LHCP) or right-handed CP (RHCP) depending on which input port is used. To achieve higher isolation with wider beamwidth, sequential rotation array (SRA) of four dual-polarized patch elements is installed on the tail of Raven, and two Butler matrix BFNs are used to feed the antenna system. Each BFN is composed of a 90° hybrid and two 180° hybrids to provide 90° phase shift along the clockwise or counterclockwise direction, therefore supporting both, LHCP, and RHCP. The four patch SRA configuration can achieve >38dB of isolation and gain >7dBic from 1750 MHz to 1850 MHz. Characteristic mode analysis (CMA) technique is also considered to design a STAR antenna system on a UAV. Based the CMA, orthogonal mode currents are excited on the UAV body using dipole elements, one for TX and one for RX. Due to the orthogonality, high isolation can be theoretically achieved.

5.2. Research Accomplishments

In this research, different design approaches for achieving monostatic STAR antenna functionality on platforms of interest for US Army are investigated. Theoretical and computational studies are conducted to bridge the gap between the proposed technical approaches and the fundamental antenna theory. Based on the herein developed systematic antenna/array design approach, several antenna and array prototypes are built and theoretical findings are fully validated with experiments. This research project has clearly demonstrated that the fundamental research on STAR antenna systems is now ready to move into the next step, specifically, practical demonstration of a fully-integrated full-duplex system. The main accomplishments of this work can be summarized as follows:

- Monostatic STAR antenna system with a highly directive reflector antennas of interest for microwave links is ***demonstrated for the first time***. Some specific technical contributions include:
    - A coaxial cavity antenna is designed to have an octave bandwidth with VSWR < 2, which is higher than the bandwidth reported in the open literature.
    - The influence of geometry, configuration, and roughness of the reflector on the system's gold STAR isolation are demonstrated.
    - *New* quasi-monostatic configuration for reflector based STAR is proposed in which system isolation is less sensitive to the imbalances and asymmetries and much wider instantaneous bandwidth is achievable.
    - Average measured system isolation of 61 dB is achieved with quasi-monostatic STAR configuration, using COTS BFN components.
- Gold STAR antenna system for handheld device platform is proposed. Some selected technical contributions include:
    - Prototype of handheld radio antenna system is fabricated and tested. Isolation of more than 30 dB is measured.
    - Omnidirectional patterns with highly correlated beams are measured for M0 and M1.
    - Extensive sensitivity study that takes into account impact of the soldier's head and the helmet is performed.
    - Simple feedback cancelation layer is seen to achieve even high isolation over a narrow channel bandwidth.
- Gold STAR antenna systems on a UAV are studied, which includes:
    - Balanced circulator BFN with dual-polarized patch antenna.
    - SRA of four dual-polarized patch elements with two Butler matrix BFNs.

5.3. Publications (at the time of the report submission)

The list of journal papers:

- Prathap Valale Prasannakumar, Mohamed A. Elmansouri, and D. S. Filipovic, "Broadband reflector antenna with high isolation feed for full duplex applications," *IEEE Trans. Ant. Propag.*, Online ISSN: 1558-2221, Digital Object Identifier: 10.1109/TAP.2018.2814224.

- Prathap Valale Prasannakumar, Mohamed A. Elmansouri, and D. S. Filipovic, “High directivity wideband full duplex reflector antenna system,” *IEEE Trans. Ant. Propag.*, in preparation.
- Ahmed Abdelrahman, and D.S. Filipovic, “Antenna System for Full-Duplex Operation of Handheld Radios”, *IEEE Trans. Ant. Propag.*, in preparation.

The list of conference proceedings:

- Prathap V Prasannakumar, M. A. Elmansouri, and D. S. Filipovic, "High-directivity broadband simultaneous transmit and receive (STAR) antenna systems," *IEEE Int. Symp. Ant. Propag, (APSURSI)*, 2018, Accepted.
- Prathap V Prasannakumar, A. H. Abdelrahman, M. Elmansouri, and D. Filipovic, "Simultaneous transmit and receive systems for advanced wireless services," *GOMACTech Conf.*, Mar. 2018.
- Prathap V Prasannakumar, M. A. Elmansouri, and D. S. Filipovic, "Broadband reflector antenna for simultaneous transmit and receive (STAR) applications," *2017 XXXII^{e} URSI General Assembly and Sci. Symp. (URSI GASS)*, 2017. (Honorable Mention)
- A. H. Abdelrahman and D. S. Filipovic, "Full duplex antenna subsystem for handheld radios," *IEEE Int. Symp. Ant. Propag. (APSURSI)*, 2017.
- Prathap V Prasannakumar, M. A. Elmansouri and D. S. Filipovic, "Broadband monostatic simultaneous transmit and receive reflector antenna system," *IEEE Int. Symp. Ant. Propag. (APSURSI)*, 2017.

Patents:

- The quasi bi-static reflector based high directive STAR antenna system proposed herein is currently going through the UCB’s system for near-future disclosure.